論文 / 著書情報
Article / Book Information

題目(和文)	鉱物に含まれる流体包有物の研究-熱水性石英の冷却速度
Title(English)	A study on fluid inclusions in mineral - Cooling rate of hydrothermal quartz
著者(和文)	大場武
Author(English)	Takeshi OHBA
出典(和文)	学位:理学博士, 学位授与機関:東京工業大学, 報告番号:甲第1884号, 授与年月日:1988年3月26日, 学位の種別:課程博士, 審査員:
Citation(English)	Degree:Doctor of Science, Conferring organization: Tokyo Institute of Technology, Report number:甲第1884号, Conferred date:1988/3/26, Degree Type:Course doctor, Examiner:
学位種別(和文)	博士論文
Type(English)	Doctoral Thesis

A Study on Fluid Inclusions in Minerals
- Cooling Rate of Hydrothermal Quartz

by Takeshi Ohba

A Dissertation Submitted in Partial Fulfillment of the Requirements for the Doctor of Science

Department of Chemistry, Tokyo Institute of Technology
O-okayama, Meguro-ku, Tokyo, Japan, 152

1988

Acknowledgments

I wish to express my sincere thanks to Professor S.Matsuo of Tokyo Institute of Technology, who showed me the true pleasure through the scientific research, i.e., any phenomena we encounter should be explained by some simple laws. I am greatly indebted especially to his idea for the discussion in Chapter-Ⅱ, where a complicated experimental result is clearly explained.

I also thank to Dr.K.Kazahaya of Geological Survey of Japan for his generous permission to use his analytical data, and for his useful suggestions on the diffusion model and the information on the Kaneuchi quartz.

I am grateful to Prof.S.Takenouchi of Tokyo University for his guidance of the sampling in the Kuga deposit and for supplying us the quartz samples from the Takemori deposit.

My thanks are extended to Mr.Tajima who is a glasswork specialist of Andoh Glass Processing Technique Research Institute, Limited, for the glass work of the vacuum ball mill.

The measurement of the $\delta^{18}O$ value on the Kaneuchi quartz by Dr.N.Yoshida of Toyama University is greatly acknowledged.

At the last, I express my thanks to the members of Matsuo Laboratory for their suggestions and encouragements throughout my study.

CONTENTS

Chapter I

A Diffusion model for the fluid inclusion

Chapter-II

Influence of adsorption on the isotope ratios of inclusion fluid extracted using a vacuum ball mill

Chapter-Ⅲ

$^{18}O/^{16}O$ and D/H ratio determinations for water samples of several micro moles

Chapter I

A Diffusion model for the fluid inclusion

< 1-1 > Introduction

In the field of earth science, the time dependent phenomena other than radioactive decay such as the cooling rate of mineral are the essential information in relation to the description of geological process. In this study, the cooling rate of a hydrothermal vein quartz was estimated on the basis of a relation between the diameter of fluid inclusion contained in quartz and the $^{18}O/^{16}O$ ratios of the water in fluid inclusions.

The fluid inclusions contained in a mineral grown under hydrothermal conditions can be considered as a fossil hydrothermal solution. Hattori and Sakai (1980) measured D/H ratio of the inclusion water contained in vein quartz after extracting the water by step-wise heating to know the D/H ratio of hydrothermal solution.

Rye and O'Neil (1968) extracted the water by crushing the mineral under vacuum and analyzed the water of fluid inclusions in quartz for the oxygen isotope ratio. The measured oxygen isotope ratios indicated the oxygen isotope exchange with the host quartz during the cooling process of the host quartz.

Kazahaya (1986) measured both D/H and $^{18}O/^{16}O$ ratios of the inclusion water contained in vein quartz collected from the Kaneuchi tungsten deposit, and obtained the same trend for the $^{18}O/^{16}O$ ratios as that found by Rye and O'Niel (1967).

Kazahaya also measured the diameter of the fluid inclusions and found a systematic relation between the diameter and the $^{18}O/^{16}O$ ratio of inclusion water, where a smaller inclusion had a lower $^{18}O/^{16}O$ ratio.

Provided that the oxygen isotope exchange equilibrium is established between the host quartz and the inclusion water at the

time when the hydrothermal solution is entrapped in the quartz, the fact that a lower $^{18}O/^{16}O$ ratio of water is found in smaller inclusions should be a reflection of the lower temperature, since the $^{18}O/^{16}O$ ratio of the overwhelming quartz is preserved and the $^{18}O/^{16}O$ fractionation factor becames larger when the temperature falls. Therefore, the $^{18}O/^{16}O$ ratio of inclusion water is expected to reflect the cooling history of quartz.

For the evaluation of the influence of cooling rate on the $^{18}O/^{16}O$ ratio of the inclusion water, a diffusion model is presented in this study. The basic idea of the diffusion model is that the $^{18}O/^{16}O$ ratio of inclusion water is controlled by the diffusion of ^{18}O in the quartz crystal. Based on the diffusion model a relation between the diameter of fluid inclusions and the $^{18}O/^{16}O$ ratio of the inclusion water can be calculated. The results of calculation are compared with the trend found by Kazahaya (1986). As a result of the comparison, the cooling rate of quartz formed in the Kaneuchi deposit can be estimated.

< 1-2 > Sample description

The Kaneuchi ore deposit locates at 35 ° 14′ - 15′ N, 135° 23′ - 24 ˆ , in the Kyoto Prefecture, central Japan. An intrusive granitic body called the Miyazu granite is outcropped 20km distant from the Kaneuchi ore deposit in the direction of north west (Imai, et al.,1972).

The Kaneuchi ore deposit are believed to be formed with a close genetic relation with an undiscovered granitic body related to the Miyazu granite. The undiscovered granitic body is supposed to lie underground with a shape of cupola under the ore deposit.

Shibata and Ishihara (1974) dated the major tungsten and molybdenum deposits in Japan by the K-Ar method. According to their results, the age of the Kaneuchi deposit is 91×10^6 years.

Scheelite, $CaWO_4$ and wolframite $(Mg,Fe)WO_4$ which are found in the quartz vein are the major tungsten minerals in the Kaneuchi deposit. A representative cross section view of the quartz vein are shown in Fig.1-1. The average width of quartz veins was 30cm (Watanabe, 1956). About five hundred veins are recognized in the region of the Kaneuchi ore deposit.

The location of Kaneuchi deposit belongs to the Tanba zone consistsing mainly of slate, sand stone, chert and green rock. The sedimentary rock adjacent to the quartz vein are suffered from a week hornfelsnazation (Watanabe, 1956). Tourmaline and sericite with microscopic scale are found in the sedimentary rock (Imai, et al., 1972).

Kim et al.(1972) measured the filling temperature of fluid inclusions in the vein quartz, which ranged from 250 to 320 ℃. No appreciable difference among the filling temperatures of samples

collected at different levels in the pits is found.

The average air temperature in the Kaneuchi deposit is 16 ℃ (Komura et al., 1984).

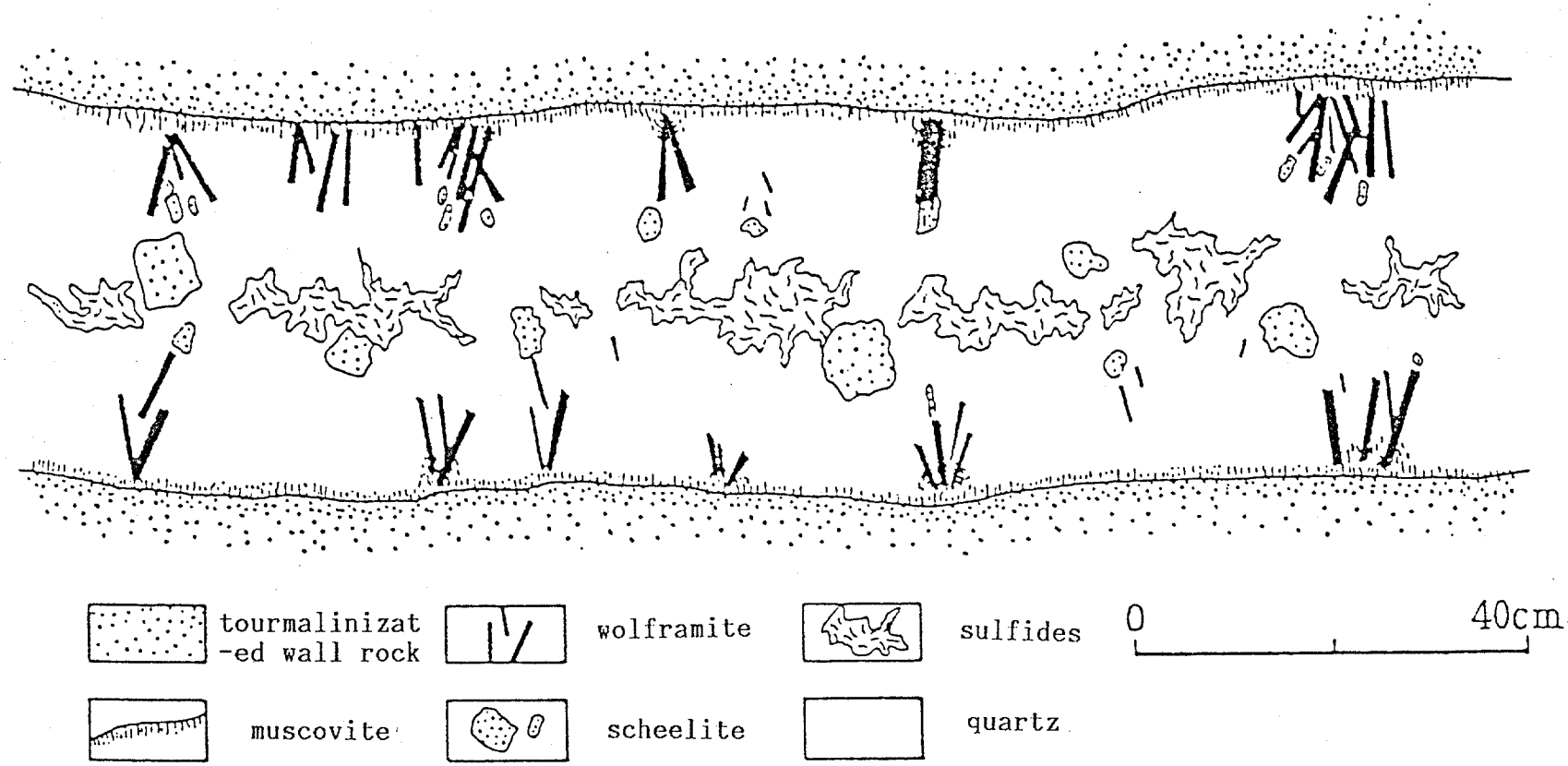

Fig. 1-1 A representative cross section veiw of the quartz vein in the Kaneuchi deposit (reproduced from Watanabe, T., 1956).

< 1-3 > Analyses of fluid inclusions

<1-3-1> $\delta^{18}O$ of the inclusion water

For the $\delta^{18}O$ measurement of the inclusion water, the inclusion water must be extracted from the quartz crystal. The inclusion water was extracted using a vacuum ball mill devised by Kita (1981). The results on measured $\delta^{18}O$ values of the Kaneuchi quartz given by Kazahaya (1986) are listed in Table 1-1. The details of extraction procedure and the method for isotope ratio measurment are referred to Kazahaya (1985).

During the crushing process by the Kita's mill, a part of the liberated water vapor from the fluid inclusions is adsorbed on the surface of quartz powder. The adsorbed water was recovered by the heating after the crushing (post-heating). The $\delta^{18}O$ value of the recovered water in this manner is biased through the interaction with the fresh surface of quartz powder, which will be described in detail in Chapter- Ⅱ. According to a result in Chapter- Ⅱ, in order to estimate the original $\delta^{18}O$ value of inclusion water, amounts and isotope ratios of four kinds of water components are necessary. The four kinds of water are main- and sub-component obtained respectively by procedure-1 and -2 of which definitions are given in Chapter- Ⅱ. The $\delta^{18}O$ value measured by Kazahaya (1986) was that of mixture of the water in main- and sub-component obtained by procedure-2.

Using the isotope values on the adsorbed water and the desorbed water obtained for a quartz sample, the following equation is obtained for the estimation of the original $\delta^{18}O$ value,

Table 1-1 $\delta^{18}O$ value of inclusion water of the Kaneuchi quartz

sample	measured $\delta^{18}O$ (‰)	corrected $\delta^{18}O$ (‰)	Amount of extracted water (μmol)
-90mL			
7054	-0.7	-15.0	32.8
7071	+0.1	-13.3	35.1
7053	+0.1	- 3.8	119.5
7052	-0.5	- 2.8	207.9
-150mL#1			
KA(150)-1	-6.3	- 9.2	161.4
KA(150)-2	-6.3	- 9.1	168.7
KA(150)-3	-5.4	- 8.6	147.9
KA(150)-4	-5.8	- 9.0	147.9
KA(150)-5	-5.2	- 9.0	123.6
-150mL#2			
150-13	-0.9	- 3.4	190.2
150-1920	-1.6	- 3.0	336.2
150-1718	-1.0	- 2.4	326.3
150-1516	-1.0	- 2.3	348.9
QU-2	-0.9	- 9.0	57.5
-420mL#2			
-420#2-3	-11.3	-16.9	82.2
-420#2-1	-11.1	-20.3	50.4
-420#2QE-3	-11.3	-29.6	25.4

The amount of quartz sample is about 6g for each run.

$$\delta^{18}O_o = \delta^{18}O_{WM}(2)[\,1 - \{0.469/Wt(2)\}\,] - 469/Wt(2) \quad (1),$$

where $\delta^{18}O_o$, $\delta^{18}O_{WM}(2)$ and $Wt(2)$ are the $\delta^{18}O$ value of the original inclusion water, the measured and the amount of extracted water, respectively. The derivation of (1) refer to Appendix-2. The corrected $\delta^{18}O$ ($\delta^{18}O_o$) is listed in Table 1-1, where a large deviation from the measured value is noted for samples especially with small amount of water.

As seen in the result of Table 1-1, the dependence of $\delta^{18}O$ value on the amount of water is not found, which suggests that the adsorption-desorption effect on the $\delta^{18}O$ value was much smaller than that of Q-6 sample used for the derivation of equation (1). Therefore the correction goes too far for the sample with small amount of water. Hence, the corrected value with the largest amount of water is taken as the lower limit of representative $\delta^{18}O$ range for each group (in Table 1-2).

<1-3-2> Diameter of fluid inclusions in the Kaneuchi quartz

Kazahaya (1986) measured the diameter of inclusions in the Kaneuchi quartz. However, since the diameter of inclusion was not the main interest in his work, the details of measuring method have not been described. Hence, the procedure for measuring the diameter and the results are described in this section.

Several quartz grain with a flat shape were selected from the grains prepared for the $\delta^{18}O$ analysis of the inclusion water. The photographs of the fluid inclusions contained in such grains were taken with a 100 times magnification. A thin section of quartz

Table 1-2 Corrected range of $\delta^{18}O$ values for the inclusion water in the Kaneuchi quartz

sample	corrected $\delta^{18}O_{(SMOW)}$ (‰)
- 90mL	- 2.8 ～ + 0.1
-150mL#1	- 9.1 ～ - 5.2
-150mL#2	- 2.3 ～ - 0.9
-420mL#2	-16.9 ～ -11.1

sample was not prepared for the purpose of photograph because the sample quartz grains were enough transparent. About ten photographs for representative parts in respect of a distribution of fluid inclusions were taken. The fluid inclusions on the photographs were classified according to the diameters. Arithmetic mean length of the major and minor axis of a fluid inclusion was used for the representative diameter of fluid inclusion.

The results of the counting are listed in Table.1-3a, 1-3b, 1-3c and 1-3d, and are shown in Fig.1-2a, 1-2b, 1-2c and 1-2d as histograms. Histograms in Fig.1-3a, 1-3b,1-3c and 1-3d show the occupying volume ratio of fluid inclusions in each diameter range to the total volume of fluid inclusions. A representative range of diameter for each sample are defined to be the diameter range covering at least 80% of the total volume of fluid inclusions, which are listed in Table 1-4.

Size distribution of inclusions in the Kaneuchi quartz

Table 1-3a

-90mL diameter (μm)	number of counts	volume occupation(%)
0 ~ 1.0	156	0.00
1.0 ~ 3.1	199	0.13
3.1 ~ 5.0	113	0.31
5.0 ~ 7.4	57	0.51
7.4 ~10.6	70	1.85
10.6 ~13.1	30	1.50
13.1 ~16.0	130	11.81
16.0 ~19.0	60	9.13
19.0 ~23.1	56	15.32
23.1 ~27.7	42	19.81
27.7 ~32.1	54	39.63
sum	967	100.00

Table 1-3b

-150mL#1 diameter (μm)	number of counts	volume occupation(%)
0 ~ 0.6	67	0.01
0.6~ 1.4	49	0.13
1.4~ 2.6	77	1.23
2.6~ 3.6	60	2.56
3.6~ 4.6	55	4.93
4.6~ 5.7	6	1.05
5.7~ 6.6	26	6.93
6.6~ 7.6	68	27.71
7.6~ 8.7	35	21.73
8.7~ 9.7	10	8.60
9.7~12.1	6	10.08
12.1~20.0	2	15.03
sum	461	99.99

Table 1-3c

-150mL#2 diameter (μm)	number of counts	volume occupation(%)
0 ~ 1.0	156	0.01
1.0 ~ 3.0	114	0.18
3.0 ~ 5.0	139	1.04
5.0 ~ 7.6	45	1.17
7.6 ~10.6	106	7.53
10.6 ~13.1	89	11.95
13.1 ~16.0	38	9.29
16.0 ~19.0	38	15.56
19.0 ~23.1	37	27.23
23.1 ~27.7	11	13.96
27.7 ~32.3	6	12.07
sum	779	99.99

Table 1-3d

-420mL#2 diameter (μm)	number of counts	volume occupation(%)
0 ~ 0.6	356	1.03
0.6 ~ 1.6	118	7.13
1.6 ~ 2.7	31	9.64
2.7 ~ 3.9	15	13.48
3.9 ~ 5.0	5	9.76
5.0 ~ 6.9	2	10.09
6.9 ~10.0	3	48.87
sum	530	100.00

Table 1-4 Representative range of diameter of fluid inclusions in the Kaneuchi quartz

sample	diameter (μm)	volume occupation (%)
-90mL	16.0 ~ 32.1	83.9
-150mL#1	6.6 ~ 20.0	83.2
-150mL#2	10.6 ~ 32.3	90.1
-420mL#2	2.7 ~ 10.0	82.2

The representative range covers more than 80 % of the total volume in the fluid inclusions.

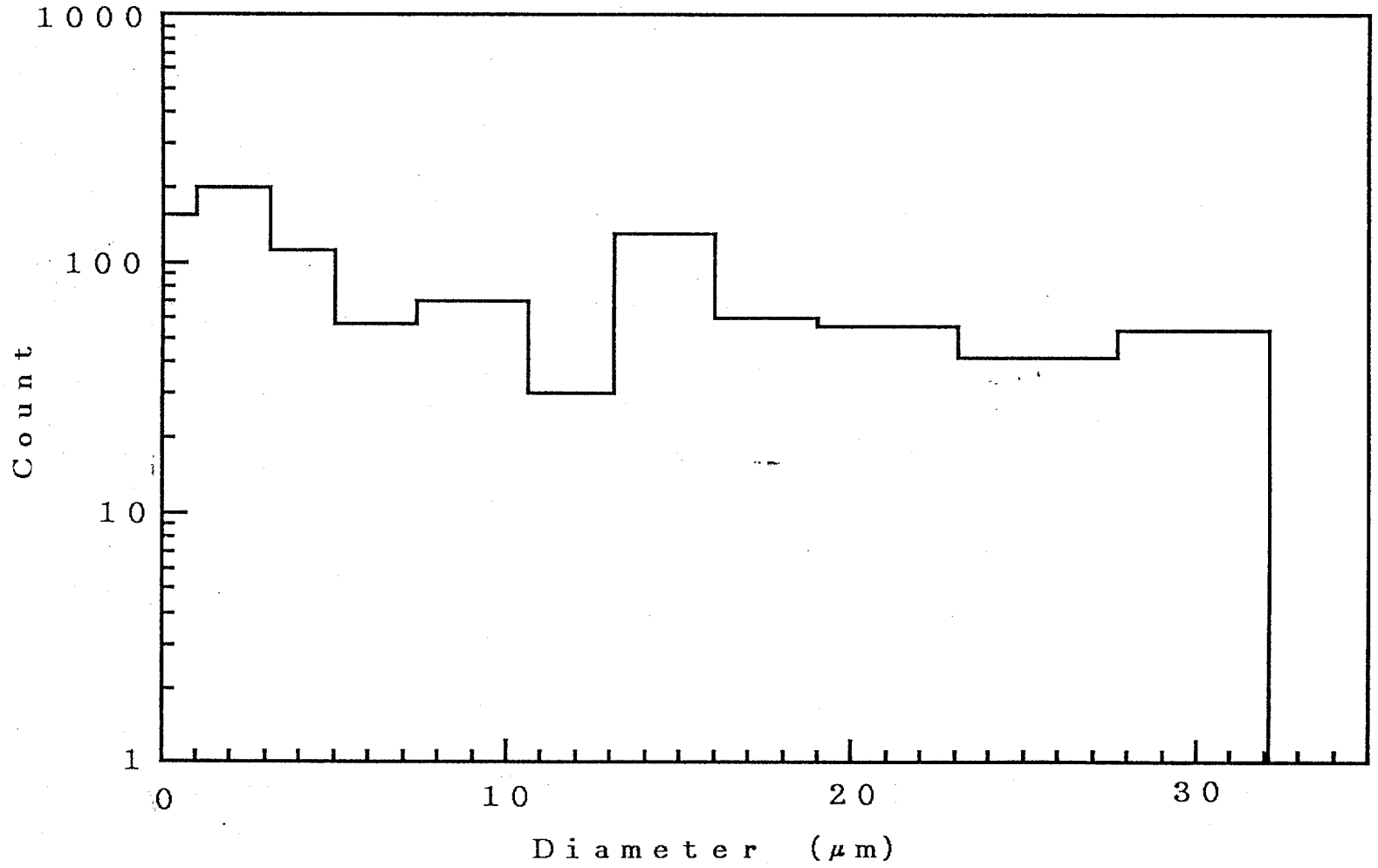

Fig.1-2a Histogram of the size distribution of fluid inclusions (-90mL)

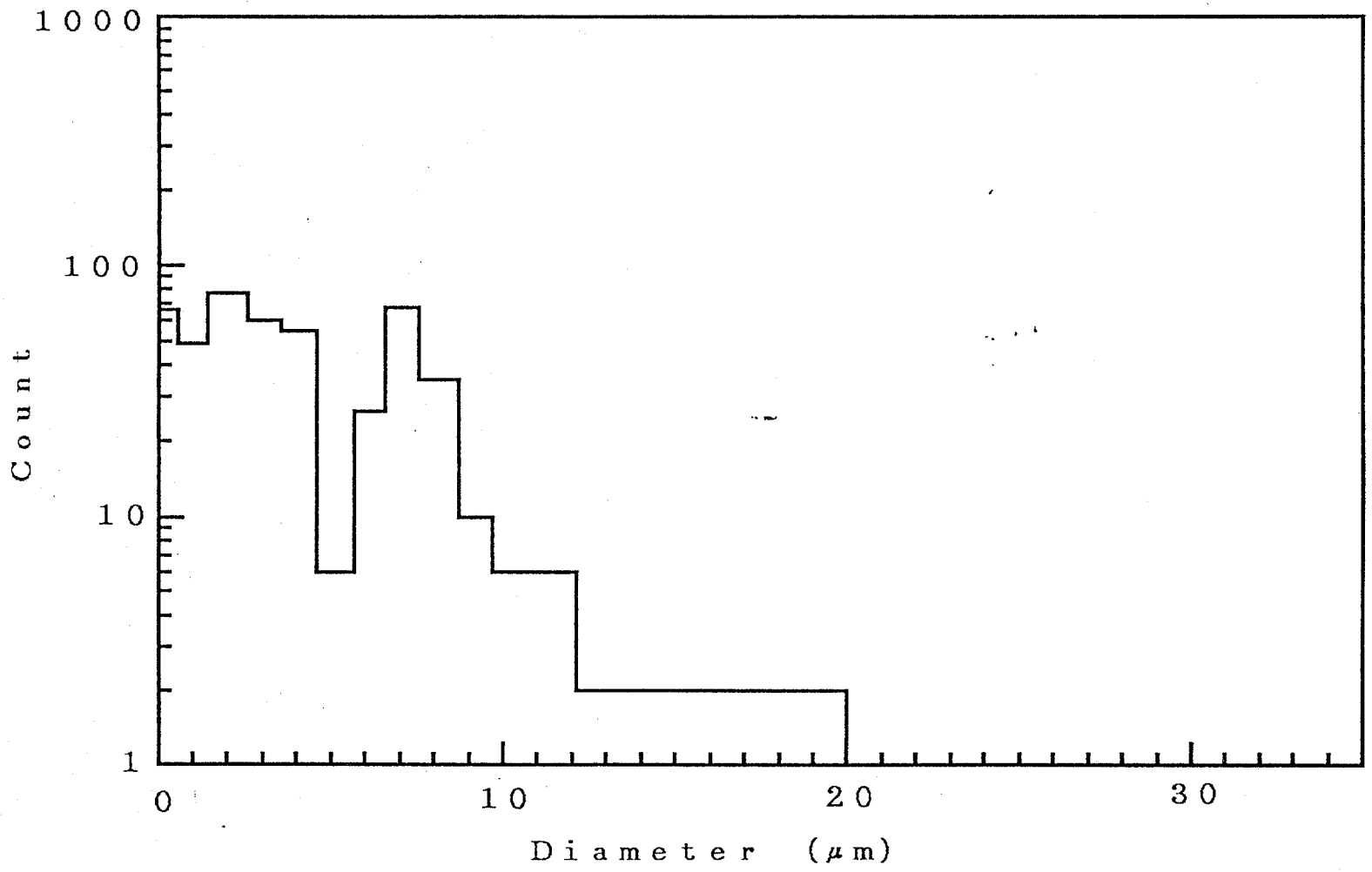

Fig.1-2b Histogram of the size distribution of fluid inclusions (-150mL#1)

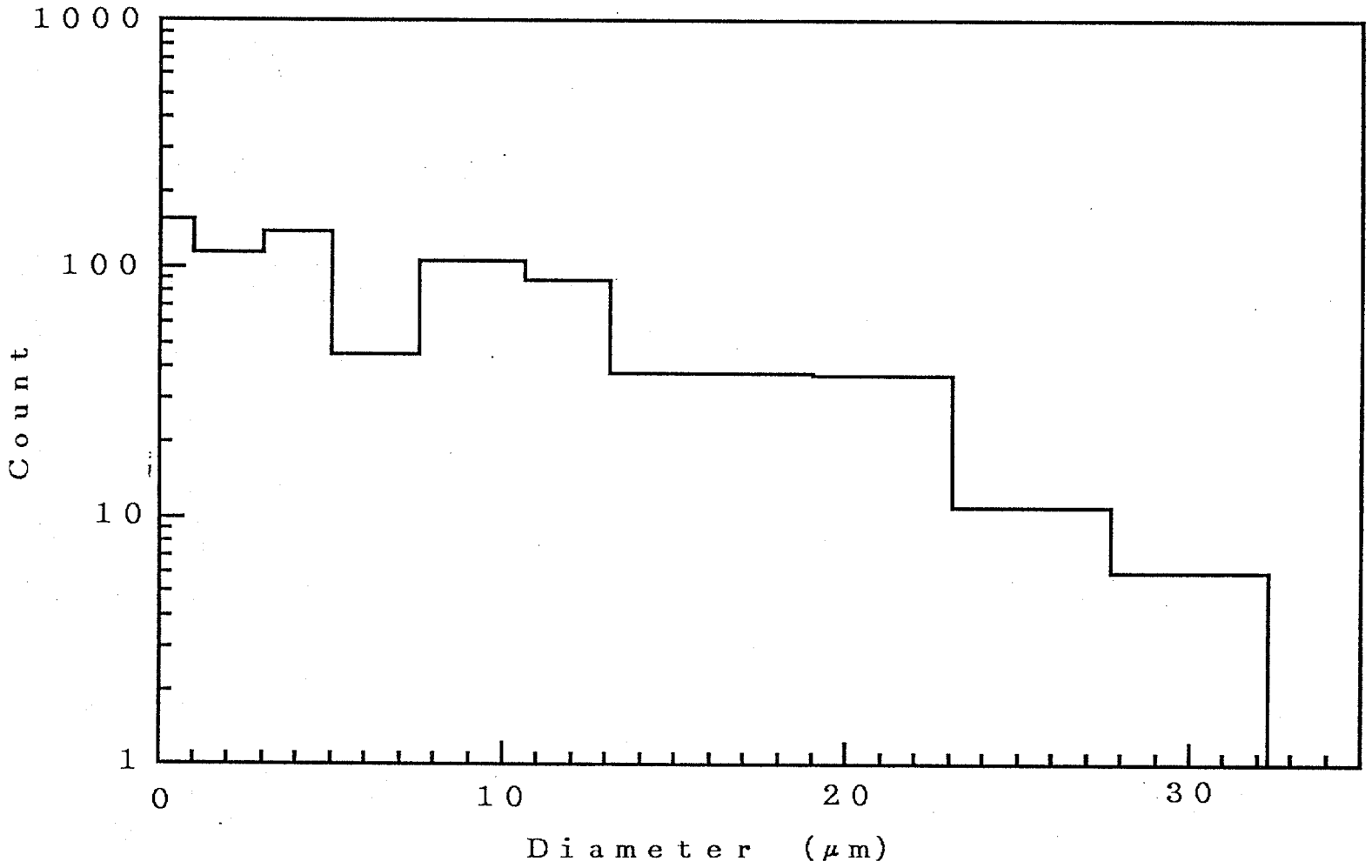

Fig.1-2c Histogram of the size distribution of fluid inclusions (-150mL#2)

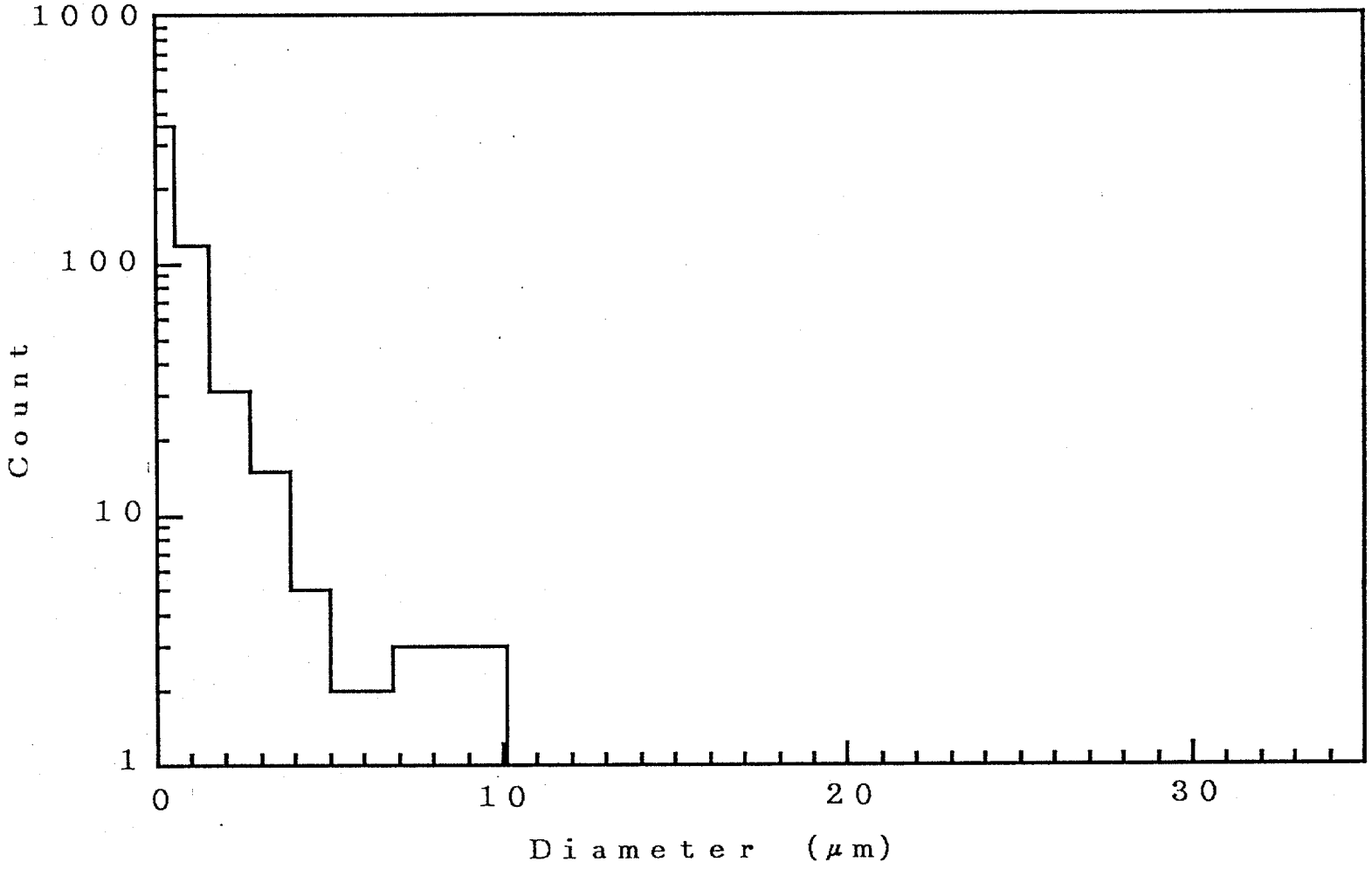

Fig.1-2d Histogram of the size distribution of fluid inclusions (-420mL#2)

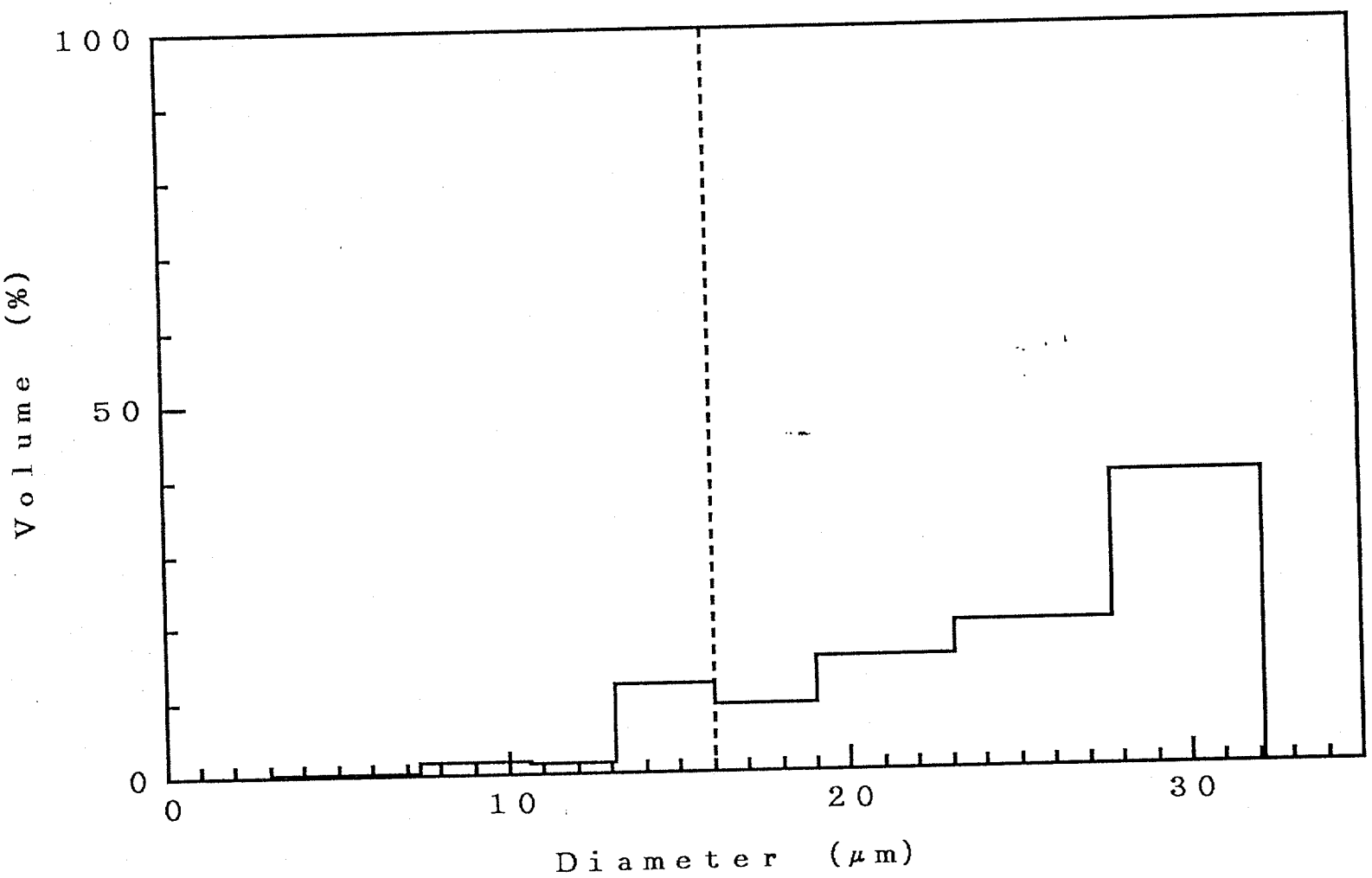

Fig.1-3a Histogram of the volume occupation by each range of inclusion diameter (-90mL). (The broken line shows the lower limit of the representative range of inclusion diameter.)

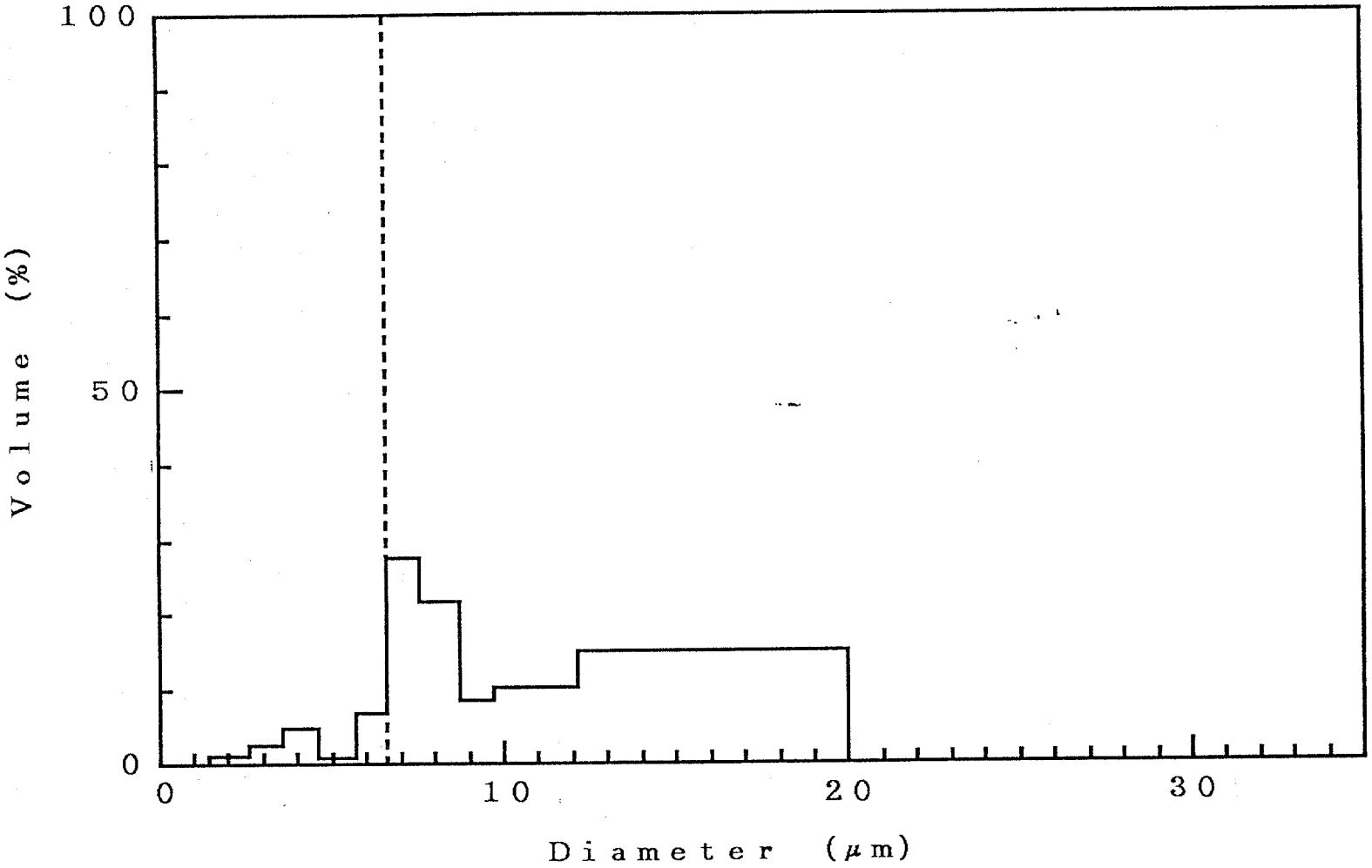

Fig.1-3b Histogram of the volume occupation by each range of inclusion diameter (-150mL#1). (The broken line shows the lower limit of the representative range of inclusion diameter.)

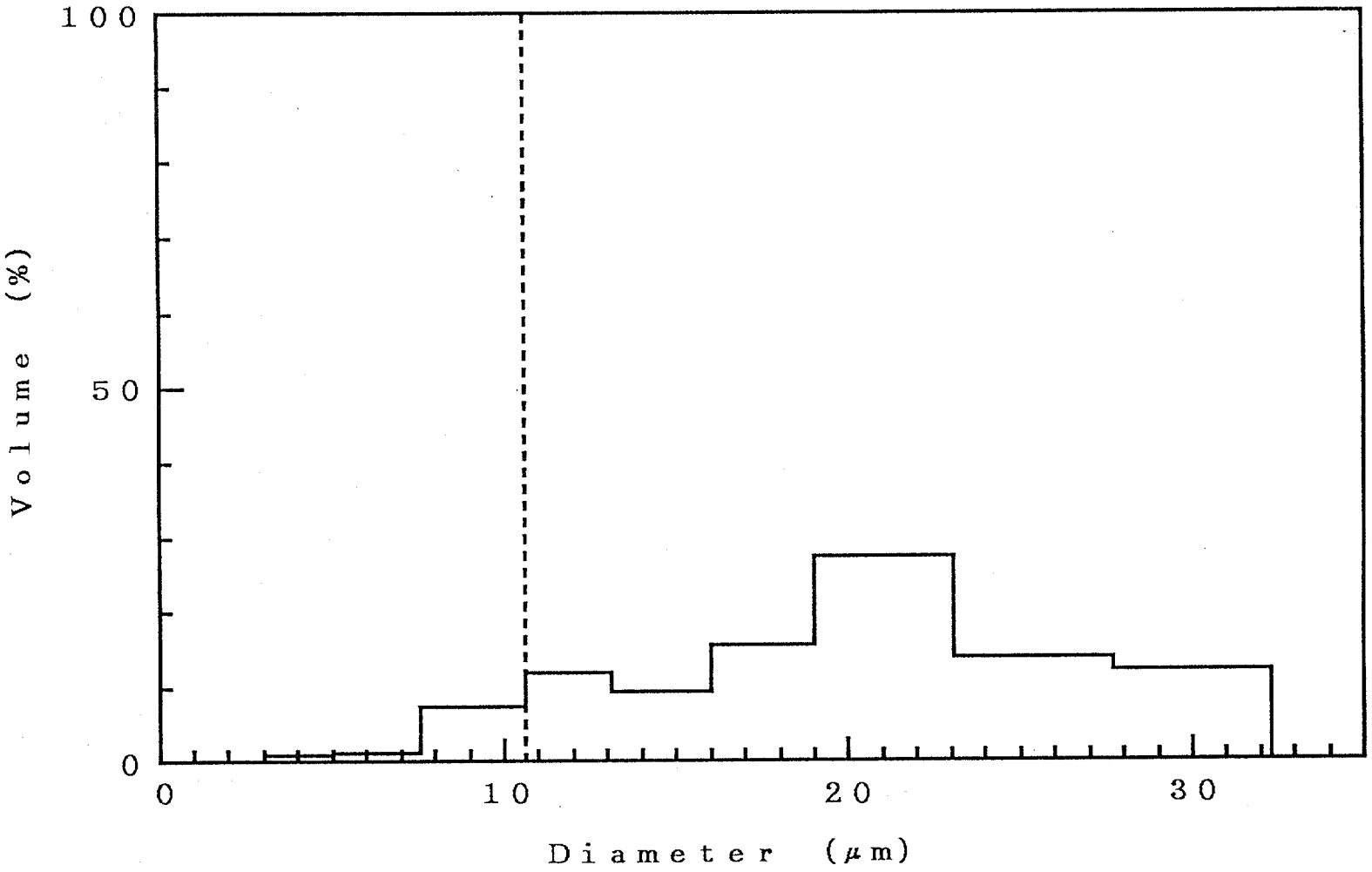

Fig.1-3c Histogram of the volume occupation by each range of inclusion diameter (-150mL#2). (The broken line shows the lower limit of the representative range of inclusion diameter.)

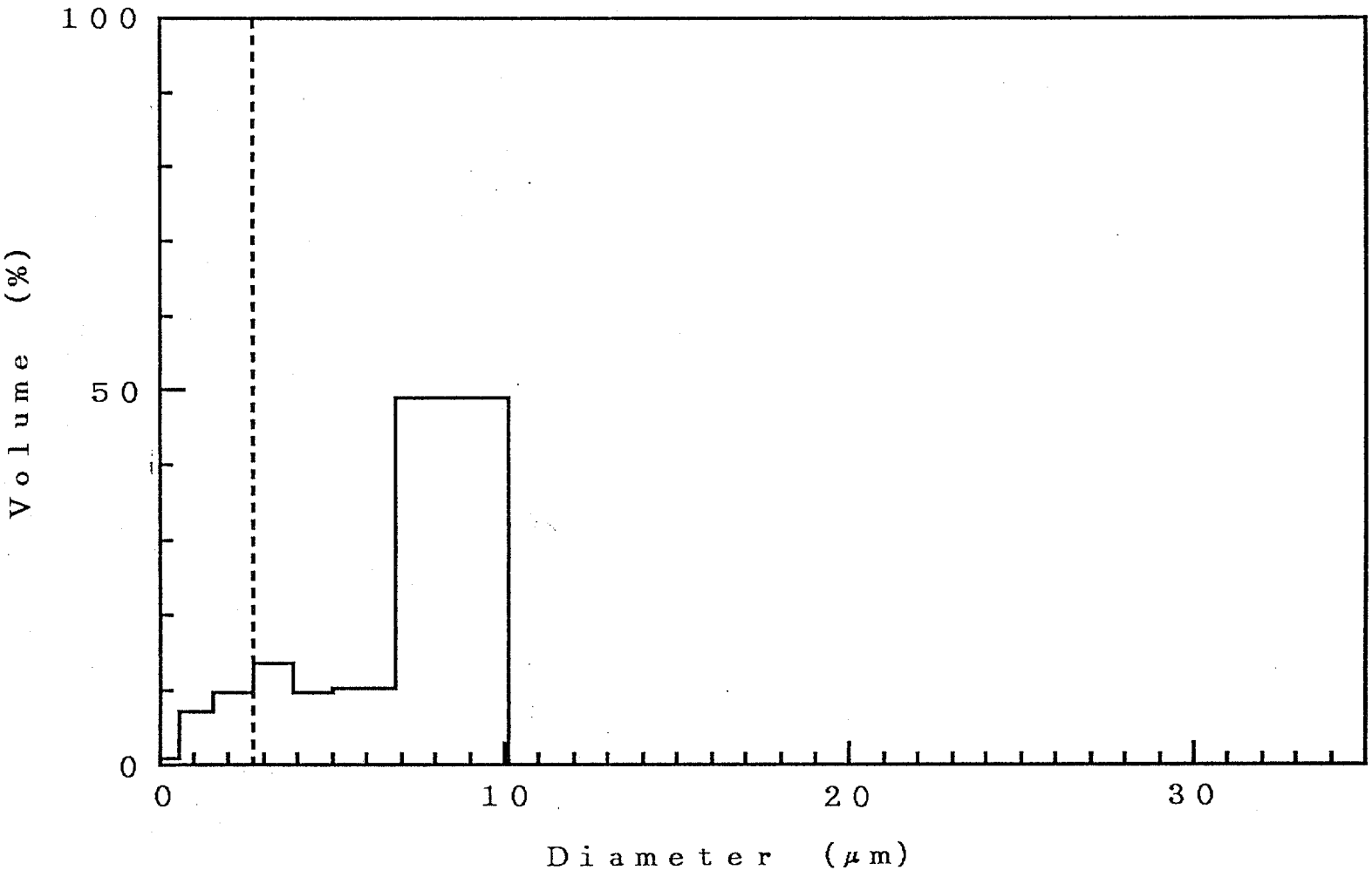

Fig.1-3d Histogram of the volume occupation by each range of inclusion diameter (-420mL#2). (The broken line shows the lower limit of the representative range of inclusion diameter.)

< 1-4 > The model for fluid inclusion

<1-4-1> Shape of fluid inclusion

The fluid inclusions found in the Kaneuchi quartz showed a variety of shapes. Their shape is usually out of complete sphere. To collect 10μmol of water for the $\delta^{18}O$ measurement, 4×10^4 of inclusions must be crushed when the average diameter of fluid inclusions is 30μm. Since it is impossible to take account of the individual shape of inclusions and the mathematical expression for the shape out of sphere is troublesome, the shape of fluid inclusions is assumed to be a sphere in the following discussion.

<1-4-2> Two kinds of diffusion model

Choudhury et al.,(1965) found an anisotropic oxygen diffusion in quartz crystal under a hydrothermal condition. Gilletti and Yund (1984) showed that the diffusivity of oxygen atoms in β-quartz at 700℃ in the direction parallel to the C-axis was 100 times faster than that perpendicular to the C-axis. However, the corresponding measurements on α-quartz have not been done. Hence, two kinds of diffusion model are considered in this study, one is that the oxygen atoms in quartz diffuse isotropically, another is that the oxygen atoms diffuse anisotropically in the direction parallel to the C-axis.

<1-4-3> Anisotropic diffusion model

The model of fluid inclusion is shown in Fig.1-4. Since the oxygen atoms diffuse one dimensionally, the shape of fluid inclusion can be converted into that shown in Fig.1-5. The converted shape of fluid inclusion in Fig.1-5 is a column with the radius of a and with the length of (4/3)a. The volume of hypothetical column-shaped fluid inclusion is $(4/3)\pi a^3$ which is the same as the original spherical volume. The oxygen atoms diffuse in the quartz column for a finite distance of γa.

Some symbols are defined as follow.

r; the distance in the direction parallel to C-axis from the boundary between the inclusion water and quartz column to the end of quartz.

C(r,t); the $^{18}O/(^{16}O+^{18}O)$ ratio in quartz at r when the time is t. ($0 \leqq r \leqq \gamma a$).

Co; C(r,0) ($0 < r \leqq \gamma a$).

W(t); $^{18}O/(^{16}O+^{18}O)$ ratio in the inclusion water.

Wo; W(t) at t=0.

β_{fu}; the volume ratio of inclusion water to the total volume of a fluid inclusion.

Dw; the oxygen atom density of inclusion water (number of atoms $/m^3$).

Dq; the oxygen atom density of quartz (number of atoms $/m^3$).

$\alpha(T)$; the oxygen isotope fractionation factor between quartz and water at temperature T(K).

$\alpha(T) = [\ ^{18}O/\ ^{16}O\ ]_{quartz}/[\ ^{18}O/\ ^{16}O\ ]_{water}$

In this study the value obtained by Matsuhisa, et al.,(1979) is used for $\alpha(T)$, where $10^3 \ln \alpha(T)_{quartz\text{-}water} = 3.34 \times 10^6/T^2 - 3.31$.

$\beta(T)$; = $\beta_{fu} Dw/[Dq\,\alpha(T)]$

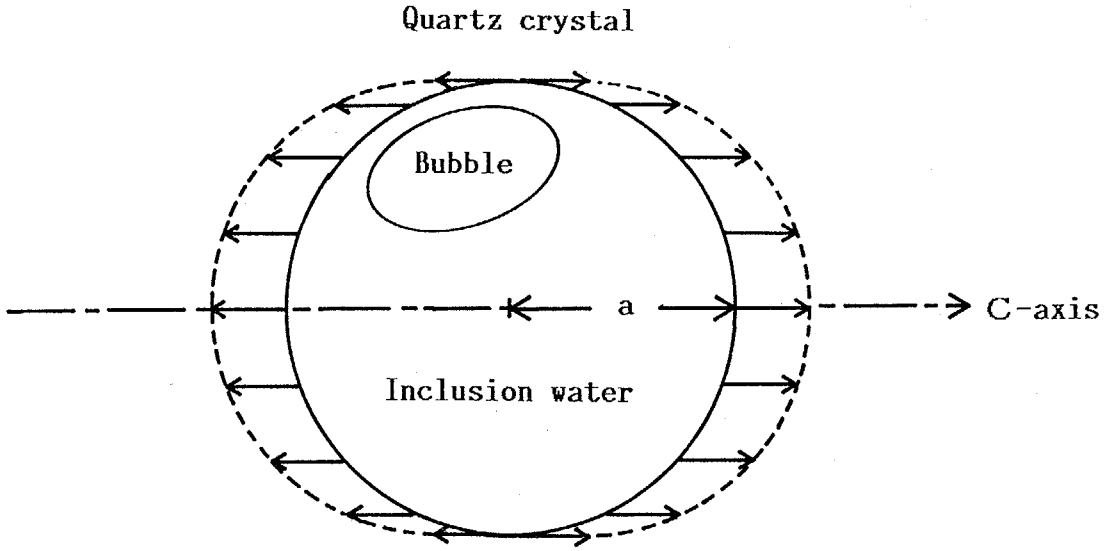

Fig.1-4 Model of fluid inclusion employed in the anisotropic diffusion model. ("→" in the figure indicates the diffusion direction of ^{18}O atoms.)

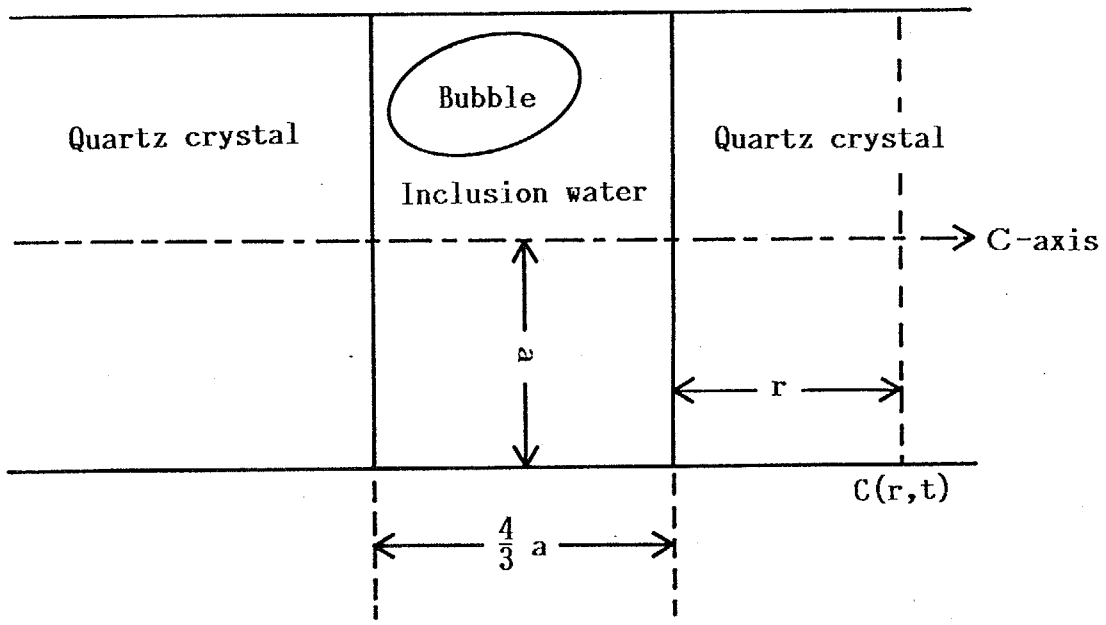

Fig.1-5 Converted fluid inclusion for the anisotropic diffusion model.

<1-4-4> Isotropic diffusion model

The model of fluid inclusion is shown in Fig.1-6. A spherical inclusion water with the radius of a is surrounded by spherical quartz with the radius of γa.

Some symbols are defined as follow.

r; the distance from the center of fluid inclusion.

C(r,t); the $^{18}O/(^{16}O+^{18}O)$ ratio in quartz at r when the time is t. ($a \leqq r \leqq \gamma a$).

Co; C(r,0) ($a < r \leqq \gamma a$).

The definitions of β_{ru}, Dw, Dq, β, W(t) are the same as those in the anisotropic diffusion model.

<1-4-5> Some assumptions on the diffusion model

In this section the reason for the adoption of diffusion model to interpret the $\delta^{18}O$ change in the inclusion water and some assumptions associated with the diffusion model are described.

At first, it is assumed that the inclusion water is in oxygen isotope exchange equilibrium with the surrounding quartz at the temperature when the fluid inclusion is formed, Ti(K). If Ti is 600K and $\delta^{18}O$ of the surrounding quartz is put to 0 ‰, the equilibrated $\delta^{18}O$ of inclusion water is -6.0 ‰, according to the oxygen isotope fractionation factor between quartz and water.

When the temperature of fluid inclusion falls from Ti to Tf, the following behavior of the ^{18}O atoms is expected. As a result of cooling, the fractionation factor becomes larger, then an isotope exchange disequilibrium between the inclusion water and the surrounding quartz could occur. However, even at the environmental

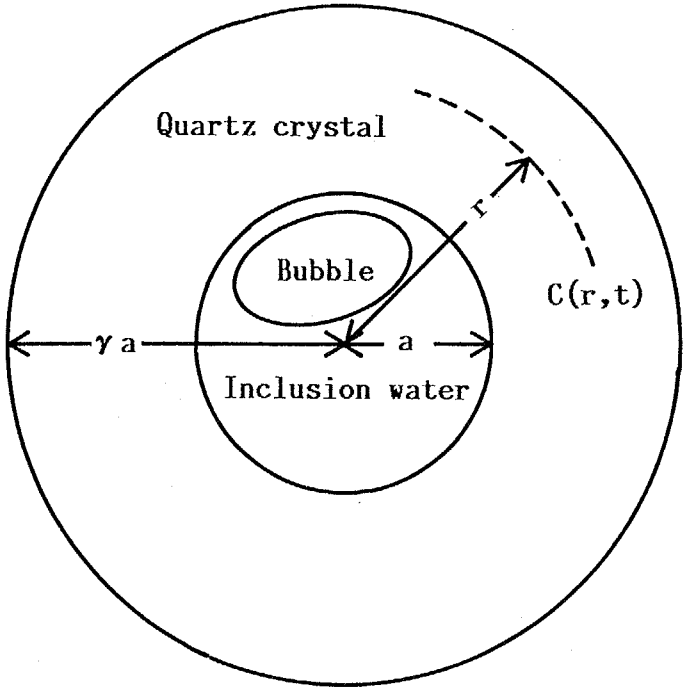

Fig.1-6 Model of fluid inclusion employed in the isotropic diffusion model.

(final) temperature, Tf, of 300K, let us assume here that the oxygen isotope exchange is still established between the inclusion water and the inner wall of the surrounding quartz. Then the $\delta^{18}O$ value of the inclusion water should decrease to -33.8 ‰. In this process, a part of ^{18}O atoms in the inclusion water must be transferred to the surrounding quartz.

It is supposed that the oxygen atoms on the surface of inner quartz wall of crystal have a higher mobility compared to those in the substantial part of the quartz crystal. Then the exchange rate of oxygen atoms between the water being in contact with the quartz surface is expected to be much faster than that between the quartz surface and the internal quartz. Therefore, it is assumed that the oxygen atoms on the quartz surface are always equilibrated with the inclusion water.

According to the assumption when the temperature of fluid inclusion falls from Ti to Tf, the inner surface of surrounding quartz are enriched in ^{18}O and equilibrated with the inclusion water. By the ^{18}O enrichment, the gradient of ^{18}O concentration between the inner surface of quartz and the internal quartz is produced. Along the gradient ^{18}O atoms diffuse into the internal quartz area.

In this study, ^{18}O atoms from inclusion water is considered to be transferred to the surrounding quartz according to the above mentioned diffusion mechanism.

<1-4-6> "Rapid cooling" and "Slow cooling"

As mentioned already, the $\delta^{18}O$ value of the inclusion water can be controlled by the cooling rate of fluid inclusion. For

example, when the temperature of fluid inclusion falls from Ti to Tf much faster than the diffusing speed of ^{18}O in the quartz crystal, diffusion will proceed almost at temperature Tf and the diffusion during the cooling process is negligible, which corresponds to the negligible change in the ^{18}O value of the inclusion water. Such a fast cooling is called as "**rapid cooling**" hereafter.

On the other hand, when the cooling rate is comparable to the diffusion speed of ^{18}O in the quartz crystal, the change in $\delta^{18}O$ of inclusion water is more complicated than that for the rapid cooling. In other words, while the temperature is high enough, the diffusion speed is higher than that of the cooling rate, and the inclusion water can be assumed to be always equilibrated with the surrounding quartz. However, the diffusion speed of ^{18}O decreases drastically, when the temperature falls and eventually the cooling rate exceeds the diffusing speed. Such a cooling is called as "**slow cooling**" hereafter.

< 1-5 > Change in the $^{18}O/(^{16}O+^{18}O)$ ratio of inclusion water.

<1-5-1> Rapid-cooling

<1-5-1-1> The anisotropic diffusion model

In this section the change in the $^{18}O/(^{16}O+^{18}O)$ ratio of inclusion water produced by the rapid cooling of fluid inclusion is presented using the anisotropic diffusion model.

At the initial temperature of Ti, the inclusion water is assumed to be isotopically in equilibrium with the surrounding quartz. Here the $^{18}O/(^{16}O+^{18}O)$ ratio of the inclusion water (= Wo) is $Co/\alpha(Ti)$. Let us take an extreme case where the temperature of fluid inclusion drops to Tf instantaneously. Since the inner surface of quartz being in contact with the inclusion water has been assumed to be always in equilibrium with the inclusion water, the $^{18}O/(^{16}O+^{18}O)$ ratio of inner surface of quartz is, $Wo \times \alpha(Tf) = Co\,\alpha(Tf)/\alpha(Ti)$.

Here the following partial differential equation are introduced.

$$D(Tf)\ \frac{\partial^2 C}{\partial r^2} = \frac{\partial C}{\partial t} \qquad ,(\ t>0,\ 0<r<\gamma a) \qquad (2)$$

(2) represents the Fick's law of diffusion.

$$\beta_{ru} Dw (4/3)\pi a^3 \left[\frac{\partial W}{\partial t}\right] = D(Tf) Dq 2\pi a^2 \left[\frac{\partial C}{\partial r}\right], (\ t>0, r=0) \quad (3)$$

The left side of (3) represents the decreasing amount of ^{18}O in the inclusion water per unit time. On other hand the right side of (3) represents the flux of ^{18}O through the surface of quartz being in contact with the inclusion water. Therefore (3) describes the conservation of ^{18}O in a fluid inclusion.

$$\frac{\partial C}{\partial r} = 0 \qquad ,(\ t \geqq 0,\ r = \gamma a) \qquad (4)$$

(4) is the boundary condition at the end of quartz column.

$$C = Co\,\alpha(Tf)/\alpha(Ti) \qquad ,(\ t = 0,\ r = 0) \qquad (5)$$

$$C = Co \qquad ,(\ t = 0,\ 0 < r \leqq \gamma a) \qquad (6)$$

(5) and (6) are the initial conditions mentioned already.

In order to eliminate the dimensions in the equations (2) $\sim$(6), the following dimensionless variables τ and X, and function F are introduced.

$$\tau = D(Tf)t/a^2 \qquad (7)$$

$$X = r/a \qquad (8)$$

$$F = [\ (C/Co) - 1\ ]/[\ \alpha(Tf)/\alpha(Ti) - 1\ ] \qquad (9)$$

Using the variables τ and X and the function F, equations (2)$\sim$(6) are transformed into the following forms.

$$\frac{\partial^2 F}{\partial X^2} = \frac{\partial F}{\partial \tau} \qquad ,(\tau>0,\ 0<X<\gamma) \qquad (10)$$

$$\beta(Tf)\left[\frac{\partial F}{\partial \tau}\right] = \left[\frac{\partial F}{\partial X}\right] \qquad ,(\tau>0,\ X=0) \qquad (11)$$

where $\beta(Tf) = \beta_{ru} Dw(2/3)/[\,D(Tf)Dq\,]$. (12)

$$\frac{\partial F}{\partial X} = 0 \qquad ,(\tau \geqq 0,\ X=\gamma) \qquad (13)$$

$$F = 1 \qquad ,(\tau=0,\ X=0) \qquad (14)$$

$$F = 0 \qquad ,(\tau=0,\ 0<X \leqq \gamma) \qquad (15)$$

The equations (10)～(15) can be solved analytically (Crank (1956) p52 -56).

A result of calculation shows that,

$$F(X,\infty) = (3/2)\beta(Tf)/[(3/2)\beta(Tf)+\gamma\,]. \qquad (16)$$

For the convenience of the later discussion, a function ξ is introduced.

$$\xi(\tau) = [\,1 - F(X=0,\tau)\,]/[\,1 - F(X,\infty)\,]$$
$$= [\,1 - F(X=0,\tau)\,]/[\,1 - (3/2)\beta(Tf)/[(3/2)\beta(Tf) + \gamma\,] \qquad (17)$$

At $t = 0$, $\xi = 0$ and at $t = \infty$, $\xi = 1$.

The ξ function represents the degree of advancement of the oxygen isotope exchange reaction.

<1-5-1-2> The isotropic diffusion model

The following equations correspond to the isotropic diffusion model.

$$D(Tf)\left[\frac{\partial^2 C}{\partial r^2} + \frac{2}{r}\frac{\partial C}{\partial r}\right] = \frac{\partial C}{\partial t} \qquad ,(\,t>0,\ a<r<\gamma a) \qquad (18)$$

(18) represents the Fick's law of diffusion holding in the radial diffusion in a sphere (Crank, 1956, p84).

$$\beta_{fu} Dw (4/3)\pi a^3 \left[\frac{\partial W}{\partial t}\right] = D(Tf) Dq 4\pi a^2 \left[\frac{\partial C}{\partial r}\right] \qquad (19)$$

$,(\,t>0,\ r=a\,)$

(19) describes the conservation of ^{18}O in a fluid inclusion.

$$\frac{\partial C}{\partial r} = 0 \qquad ,(\ t \geqq 0,\ r = \gamma a) \tag{20}$$

(20) is the boundary condition at the outer surface of surrounding quartz.

$$C = Co\,\alpha(Tf)/\alpha(Ti) \qquad ,(\ t = 0,\ r = a) \tag{21}$$

$$C = Co \qquad ,(\ t = 0,\ a < r \leqq \gamma a) \tag{22}$$

(21) and (22) are the initial conditions.

In order to eliminate the dimension in the equation (17)～(22), the following dimensionless variables τ and X, and function F are introduced.

$$\tau = D(Tf)t/a^2 \tag{23}$$

$$X = (\ r - a\ )/a \tag{24}$$

$$F = (\ r/a\ )[\ (C/Co) - 1\ ]/[\ \alpha(Tf)/\alpha(Ti) - 1\ ] \tag{25}$$

Using the above variables and function, (17)～(22) are rewritten into the following forms.

$$\frac{\partial^2 F}{\partial X^2} = \frac{\partial F}{\partial \tau} \qquad ,(\tau > 0,\ 0 < X < \gamma - 1\ ) \tag{26}$$

$$\beta(Tf)\left[\frac{\partial F}{\partial \tau}\right] + F = \left[\frac{\partial F}{\partial X}\right] \quad ,(\tau>0,\ X=0) \tag{27}$$

where $\beta(Tf) = \beta_{ru}Dw(1/3)/[\,D(Tf)Dq\,]$. (28)

$$\frac{\partial F}{\partial X} - \frac{F}{\gamma} = 0 \quad ,(\tau \geqq 0,\ X=\gamma-1) \tag{29}$$

$$F = 1 \quad ,(\tau=0,\ X=0) \tag{30}$$

$$F = 0 \quad ,(\tau=0,\ 0<X\leqq\gamma-1) \tag{31}$$

Since the analytical solution for (25)～(29) have not ever been obtained, the analytical solution was calculated using the Laplace transformation. For the details of calculation, refer to Appendix-1.

The obtained analytical solution is,

$$F(X,\tau) = 2\beta\sum_{n=1}^{\infty}\left[\frac{q_n\sin\{q_n(X-\gamma+1)\} + \gamma q_n^2\cos\{q_n(X-\gamma+1)\}}{A_n\sin\{q_n(\gamma-1)\} + B_n\sin\{q_n(\gamma-1)\}}\right]$$

$$\times\exp(-q_n^2\tau) + [\,3(X+1)\beta(Tf)\,]/[\,\gamma^3 + 3\beta(Tf) - 1\,] \tag{32}$$

,where q_n (n=1,2,3...) is the solution of the following equation.

$$\tan\{q_n(\gamma-1)\} = [(\gamma-1-\gamma\beta q_n^2)q_n]/[1+(\gamma-\beta)q_n^2] \quad (33)$$

A_n and B_n are,

$$A_n = -\beta\gamma(\gamma-1)q_n^3 + (\gamma^2-\gamma+1-\beta)q_n \quad (34)$$

$$B_n = -\{\gamma^2 + (\beta-1)\gamma+\beta\}q_n^2 + (\gamma-1) \quad (35)$$

In the extreme case when τ is ∞, (32) turns out to be,

$$F(X,\infty) = 3\beta(Tf)/[3\beta(Tf)+\gamma^3-1]. \quad (36)$$

For the convenience in the later discussion, a function ξ is introduced.

$$\xi(\tau) = [1 - F(X=0,\tau)]/[1 - F(X,\infty)]$$
$$= [1 - F(X=0,\tau)]/[1 - 3\beta(Tf)/\{3\beta(Tf)+\gamma^3-1\}] \quad (37)$$

At t = 0, ξ = 0 and at t = ∞, ξ = 1.

The ξ function represents the degree of advancement of the oxygen isotope exchange reaction.

<1-5-1-3> Numerical solution

The partial differential equations presented in the preceding sections can be solved also by a numerical method. In this section, the procedure of calculation for the numerical solution and the results are presented.

The explicit finite difference method (EFDM) was used for the numerical solution. The EFDM is the simplest method to obtain a numerical solution of parabolic partial differential equation. In the EFDM it is not necessary to handle a matrix, then the calculation can be carried out easily by a microcomputer using BASIC for the programming language.

A procedure for the EFDM will be shown in the case of the isotropic diffusion model. For the calculation of EFDM, a grid shown in Fig.1-6 is put on the x- τ rectangular coordinate plane, where x and τ are dimensionless variables defined in the preceding section for space and time, respectively. In Fig.1-6, x and τ are put on the horizontal and vertical axes, respectively. On the x-axis the region of quartz on the x axis is $0 \leqq x \leqq (\gamma - 1)$. This region is divided into n sections from x=0 to x= γ -1 and the address is put on the points at the boundary between each adjacent sections as 00, 01, 02,..., 0(n-1), 0n. Likewise points are put at regular intervals on the τ-axis. The parameters h and k are assigned to the intervals on x and τ axes. Drawing lines parallel to x and τ axes passing the points on both axes, an address ij is assigned to the cross point at coordinate (ih,jk). In the calculation for EFDM, it is impossible to select an arbitrary value for k. The deviation of numerical solution from the analytical solution is reduced to a minimum when the intervals h and k are

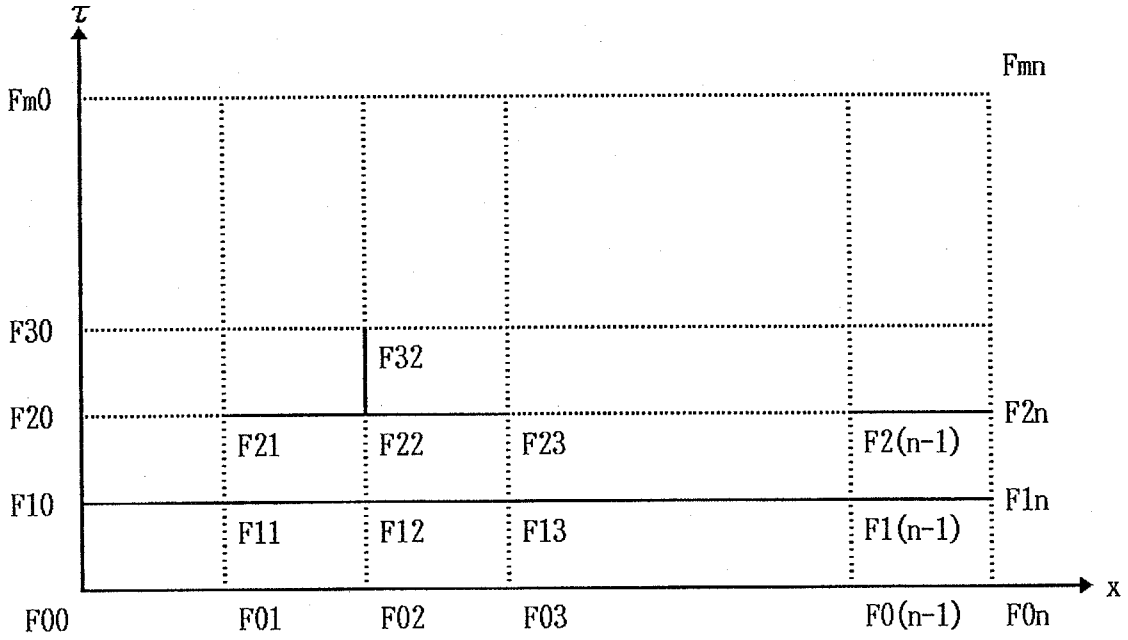

Fig. 1-6

Grid for calculation by explicit finite difference method.

For example, F32 is calculated from F21, F22 and F23.

F2n is calculated from F2(n-1).

F10 is calculated from F11, F12, F13,..,F1(n-1) and F1n.

connected by the following relation,

$$k/h^2 = 1/6 \qquad (38).$$

This k/h^2 ratio is used in the numerical calculation in this study throughout. In EFDM, $F(x, \tau)$ is defined only at the grid point ij. The calculation in EFDM is carried out among the values on the grid point. A symbol "Fij" is defined to be the value of $F(x, \tau)$ at point ij, hereafter. Fij means the value of $F(x, \tau)$ in quartz at the place where x=ih at the time when $\tau = jk$. To solve the partial differential equation, it is nothing else but to calculate F0(j+1) ~Fn(j+1) from F0j~Fnj. A feature of EFDM will appear in the procedure of the calculation.

In EFDM, $[\partial^2 F/\partial X^2]$ is approximated as,

$$\frac{\partial^2 F}{\partial X^2} = \frac{F(i-1)j - 2Fij + F(i+1)j}{h^2} \qquad (39)$$

$[\partial F/\partial \tau]$ is approximated as,

$$\frac{\partial F}{\partial \tau} = \frac{Fi(j+1) - Fij}{k} \qquad (40)$$

$[\partial F/\partial X, (X = \gamma - 1)]$ is approximated as,

$$\frac{\partial F}{\partial X} = \frac{Fnj - F(n-1)j}{h} \qquad (41)$$

Substituting (39) and (40) into the equation of,

$$\frac{\partial^2 F}{\partial X^2} = \frac{\partial F}{\partial \tau} \qquad ,(\tau > 0,\ 0 < X < \gamma - 1) \qquad (42)$$

$$\frac{F(i-1)j - 2Fij + F(i+1)j}{h^2} = \frac{Fi(j+1) - Fij}{k} \qquad (43)$$

$$,\{\ i=1,2,\ldots,(n-1),\ j \geqq 0\ \}$$

is obtained.

Solving for Fi(j+1),

$$Fi(j+1) = Fij + (k/h^2)(\ F(i-1)j + F(i+1)j - 2Fij\ ) \qquad (44)$$

is obtained.

For example, F23 is calculated using (44) from F21, F22 and F23 (see Fig.1-6).

Substituting (41) into the equation of,

$$\frac{\partial F}{\partial X} - \frac{F}{\gamma} = 0 \qquad ,(\tau \geqq 0,\ X = \gamma - 1) \qquad (41.1)$$

$$\frac{Fnj - F(n-1)j}{h} - \frac{Fnj}{\gamma} = 0 \qquad ,(\ i=n,\ j \geqq 0\ ) \qquad (41.2)$$

Solving on Fnj,

$$Fnj = \{ \gamma/(\gamma - 1) \}F(n-1)j \qquad (45),$$

is obtained.
For example, Fn2 is calculated using (45) from F(n-1)2 (see Fig.1-6). Using an approximated equation for,

$$\beta(Tf)\left[\frac{\partial F}{\partial \tau} \right] + F = \left[\frac{\partial F}{\partial X} \right] \quad ,(\tau > 0,\ X = 0) \qquad (46),$$

it is possible to calculate F0(j+1), however, a large error by the approximation will be produced. Equation (46) represents the conservation of ^{18}O atoms in a fluid inclusion. The same physical meaning can be expressed by the following integral equation.

$$\beta_{fu} Dw (4/3)\pi a^3 W(t) + \int_a^{\gamma a} Dq 4\pi a^2 C(r,t)dr$$

$$= \beta_{fu} Dw (4/3)\pi a^3 W(0) + \int_a^{\gamma a} Dq 4\pi a^2 C_o dr \qquad (47)$$

The first and second terms in both sides of (47) represent the

amount of ^{18}O atoms in the inclusion water and the surrounding quartz, respectively. The left and right sides represent the total amount of ^{18}O atoms when the time is t and 0, respectively. Using the variables τ , X and the function $F(X, \tau)$ defined in the isotropic diffusion model, equation (47) is rewritten as,

$$\beta(Tf)[\, F(0,\tau) - 1 \,] + \int_0^{\gamma-1} F(X,\tau)(X + 1)dX = 0 \qquad (48).$$

Approximating the integral term in left side of (48) based on the trapezium rule,

$$\beta(Tf)[\, F0(j+1) - 1 \,] + (1/2)h[\, F0(j+1) + Fn(j+1) \,] + h\sum_{i=1}^{n-1}[\, Fi(j+1)(ih + 1) \,] = 0 \qquad (49)$$

is obtained.

Solving (49) for F0(j+1),

$$F0(j+1) = \frac{\beta(Tf) + (1/2)h[Fn(j+1)] + h\sum_{i=1}^{n-1}[Fi(j+1)(ih+1)]}{\beta(Tf) + (1/2)h} \quad (50)$$

is obtained.

Using (13), F0(j+1) is calculated from F1(j+1)～Fn(j+1) which were calculated from F0j ～Fnj using (44) and (45) in advance.

The initial data set F00～Fn0 are,

$$F00 = 1,\ F01 \sim F0n = 0 \quad (51).$$

From F00～F0n, the following F0j～Fnj ($j \geqq 0$) are calculated in sequence.

In Fig.1-7a and 1-7b, the change of ξ calculated by EFDM for the anisotropic and isotropic diffusion model, respectively, are shown. The numerical values used for the parameters, γ and $\beta_{ru}Dw/Dq$, are 10 and 0.5, respectively, for both of the diffusion models.

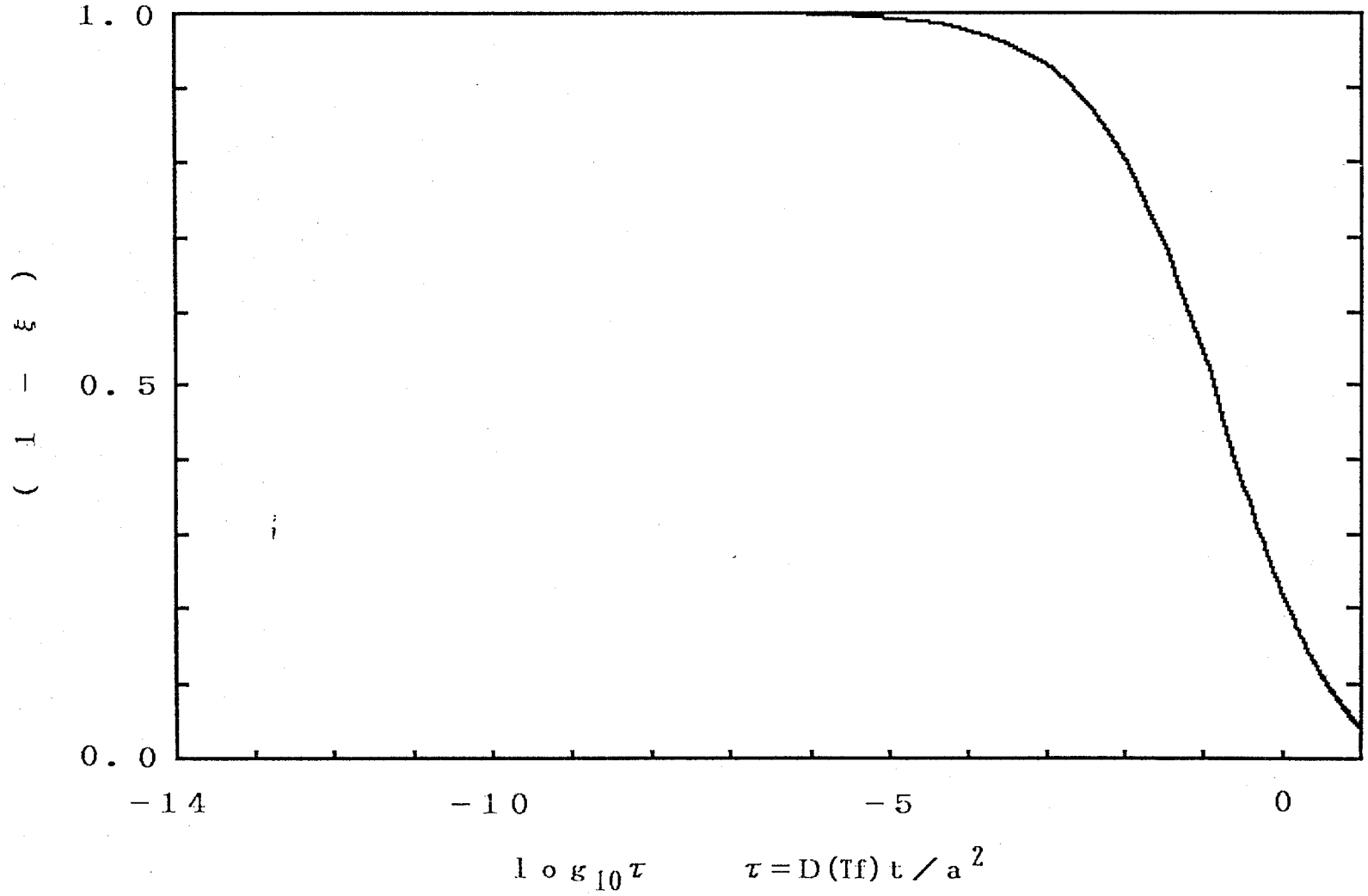

Fig.1-7a Change in ξ when the fluid inclusion is cooled very fast (rapid-cooling) for the anisotropic diffusion model.

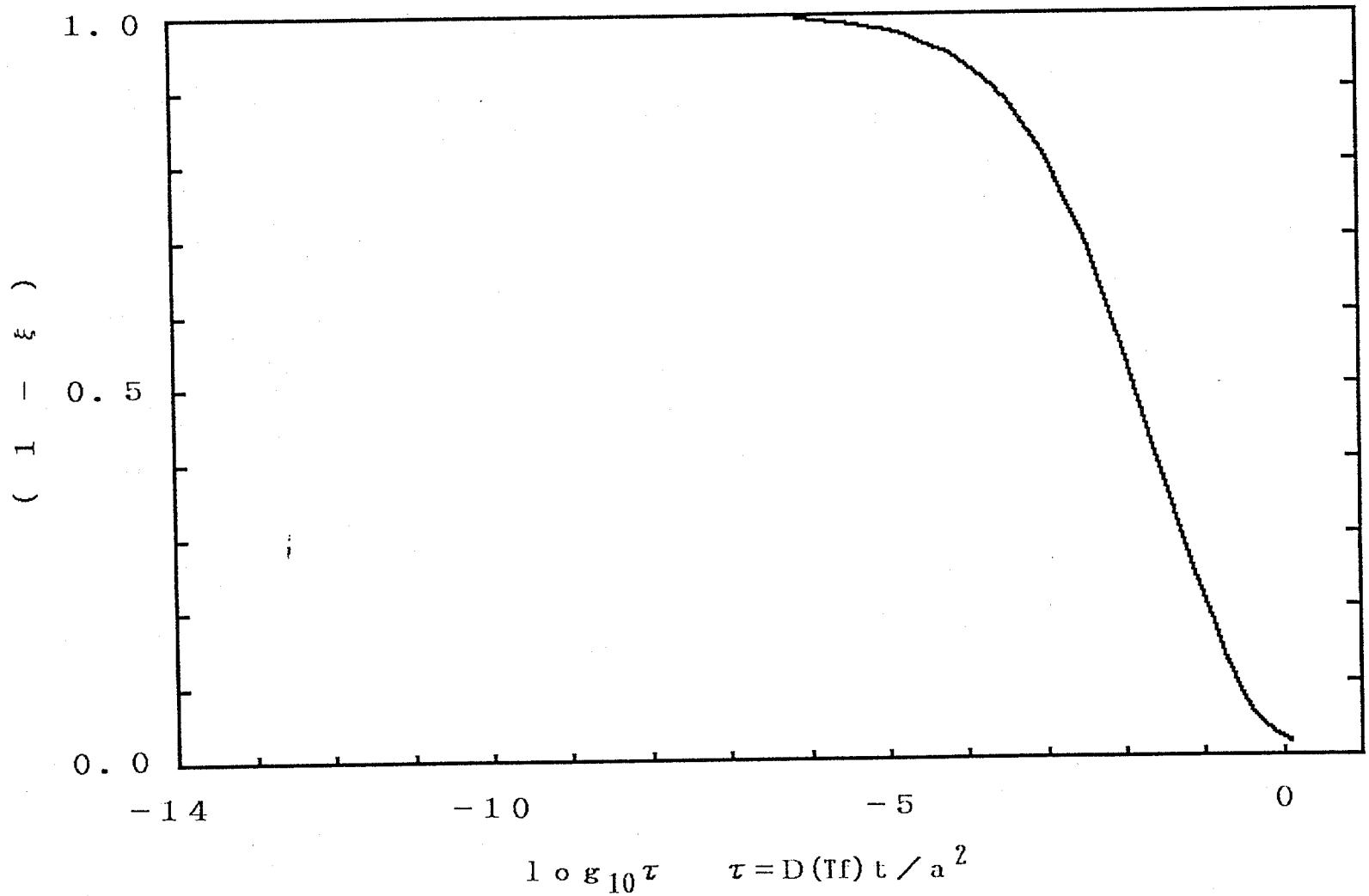

Fig.1-7b Change in ξ when the fluid inclusion is cooled very fast (rapid-cooling) for the isotropic diffusion model.

<1-5-2> Slow cooling

<1-5-2-1> Cooling pattern

The vein quartz is believed to be formed from a hydrothermal water which had filled the cleavage in a stratum. A distribution of temperature around the vein quartz is postulated as shown in Fig.1-8. In the figure, the vein quartz is assumed to be a plate extending infinitely with a thickness of 2h. The X-axis is perpendicular to the plate plane. The initial temperatures of quartz vein and the surrounding stratum are taken to be Ti and Tf, respectively for simplicity. The change of temperature at X=0 is expressed by the following formula (Crank, 1956, p13-14),

$$(T - Tf)/(Ti - Tf) = \mathrm{erf}(4\kappa t/h^2)^{-1/2} \quad (52),$$

where κ is the thermal diffusivity of quartz vein and the stratum, which are assumed to be the same.

For the convenience of the later discussion, the half time of temperature drop, t_h will be employed, instead of the constant in (52), $4\kappa/h^2$. The half time is defined by the following equation.

$$1/2 = \mathrm{erf}(4\kappa t_h/h^2)^{-1/2} \quad (53).$$

Since $1/2 = \mathrm{erf}(0.47723)$ (54), then

$$(T - Tf)/(Ti - Tf) = \mathrm{erf}(kt/t_h)^{-1/2} \quad (55),$$

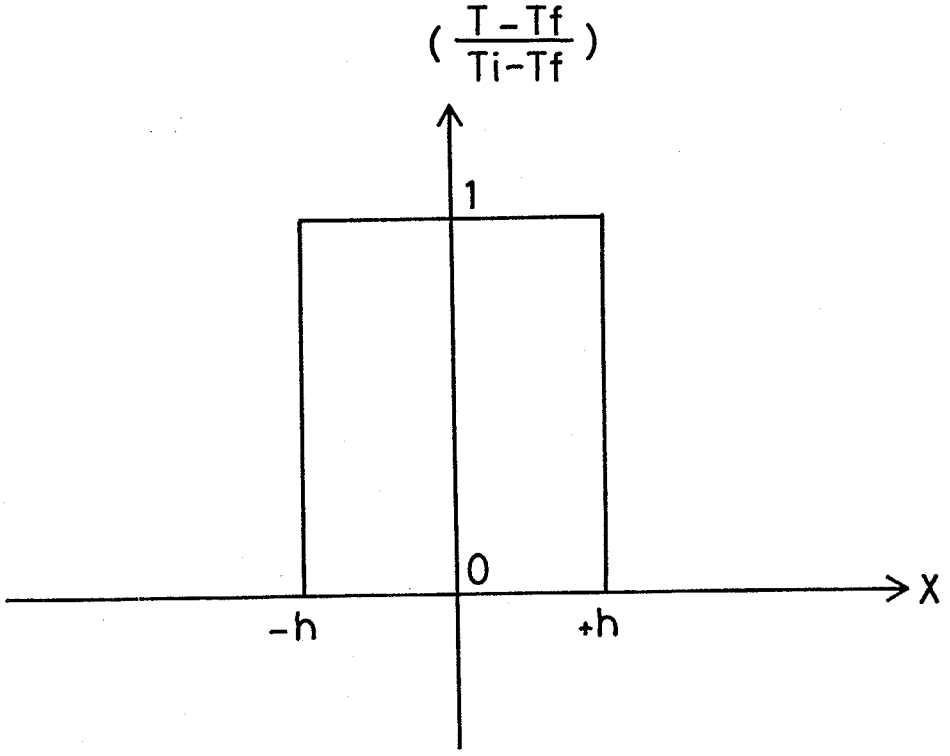

Fig.1-8 Initial distribution of temperature around the quartz vein.

where k = 4.3908, because $(4.3908)^{-1/2} = 0.47723$.
The change in (T-Tf)/(Ti-Tf) represented by the equation (55) is shown in Fig.1-9.

Using the cooling pattern considered here, a quantitative cooling history of vein quartz is expressed by two parameters.
One is t_h , the half time of temperature drop.
Another is t_n , the time elapsed from the start of cooling.
The ratio, t_n / t_h can be used as an index expressing the relative cooling speed.

Hereafter let us express the cooling pattern of fluid inclusion (vein quartz) by equation (53).

<1-5-2-2> Procedure for the calculation in the case of slow-cooling

As described in the preceding section, it is assumed that the cooling of fluid inclusions takes place according to the following equation,

$$(T - Tn)/(T0 - Tn) = \mathrm{erf}(kt/t_h)^{-1/2} \qquad (54),$$

where T0 and Tn are the initial and final temperature (K) of fluid inclusion. As mentioned in the case of rapid cooling, the variable t is converted to the dimensionless variable τ in the partial differential equation. Hereafter the dimensionless variable τ is called as "reduced time". Whereas t is called as "actual time".

As the cooling of fluid inclusion is expressed using the actual time in (54), it must be converted so as to be expressed by

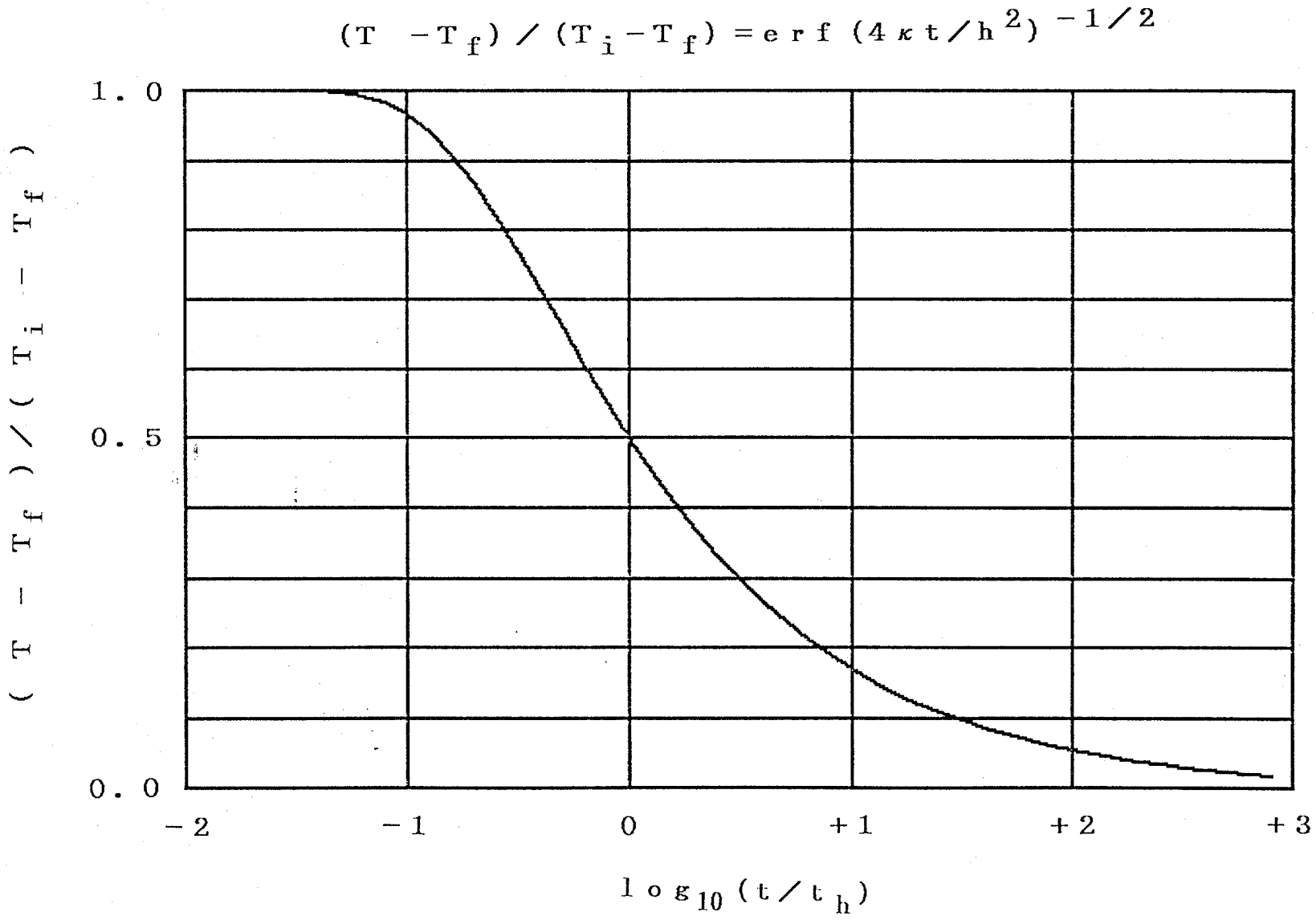

Fig.1-9 Cooling patern of vein quartz

the reduced time.

$$(T - Tn)/(T0 - Tn) = \mathrm{erf}[k\tau(Tn)/\tau_h(Tn)]^{-1/2} \quad (55),$$

where $\tau(T)$ is the reduced time defined as $\tau = D(T)t/a^2$,

and $\tau(Tn) = D(Tn)t/a^2$ and $\tau_h(Tn) = D(Tn)t_h/a^2$.

In Fig.1-10, the relation between the temperature and reduced time calculated by equation (55) is shown.

For the purpose of calculation, the step-wise temperature drop shown in Fig.1-10 is used for an approximation to the smooth curve of cooling. In the step-wise cooling, the temperature range to be covered,[T0-Tn], is divided into N (=10 in Figure). The temperature of each step is denoted to be T1, T2,..,T(n-1), Tn in order of high to low temperature. The reduced time at which the temperature of fluid inclusion reaches T1, T2,...,T(n-1) on the curve in Fig.1-10 corresponds to $\tau 1(Tn)$, $\tau 2(Tn),\ldots,\tau n\text{-}1(Tn)$, respectively. Using the anisotropic diffusion model as an example, the procedure for calculation of the change in the $^{18}O/(^{16}O+^{18}O)$ ratio of inclusion water will be described.

At $\tau(Tn) = 0$, the temperature of fluid inclusion drops from T0 to T1.

In $[\ 0 \leqq \tau(Tn) < \tau 1(Tn)]$, the following equations hold,

$$\frac{\partial^2 F}{\partial X^2} = \frac{\partial F}{\partial \tau} \qquad ,(\tau > 0,\ 0 < X < \gamma\ ) \qquad (56)$$

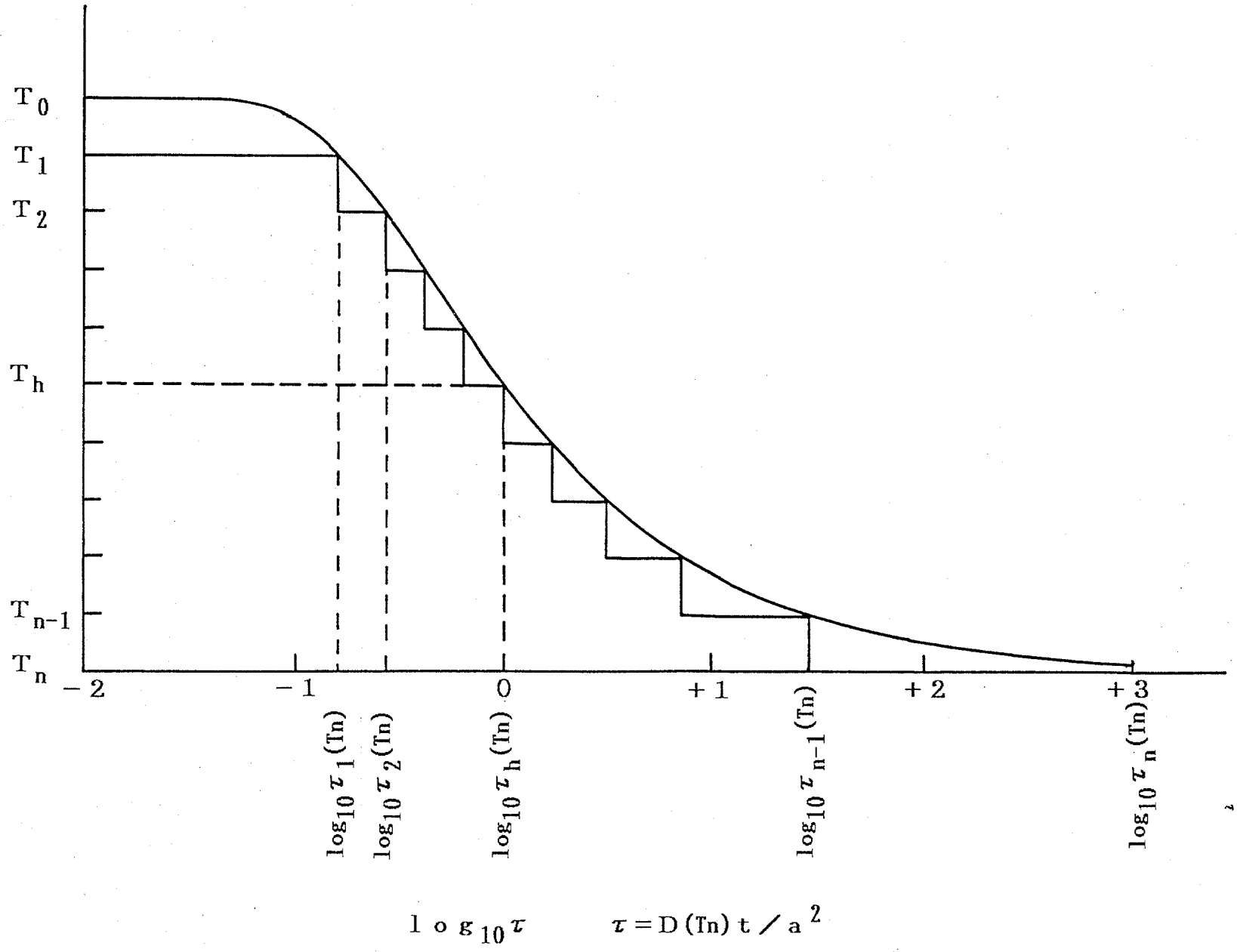

Fig.1-10 A step-wise approximation to the cooling pattern of vein quartz. (The calibration on the horizontal axis referred to the case of $\tau_h(Tn) = 1$.)

$$\beta(T1)\left[\frac{\partial F}{\partial \tau}\right] = \left[\frac{\partial F}{\partial X}\right] \quad ,(\tau>0,\ X=0) \qquad (57)$$

where $\beta(T1) = \beta_{ru} Dw(2/3)/[\,D(T1)Dq\,]$ (58)

$$\frac{\partial F}{\partial X} = 0 \quad ,(\tau \geqq 0,\ X=\gamma) \qquad (59)$$

$$F = [\,\alpha(T1)/\alpha(T0) - 1\,]/[\,\alpha(Tn)/\alpha(T0) - 1\,] \quad (\tau=0,\ X=0) \qquad (60)$$

$$F = 0 \quad ,(\tau=0,\ 0<X \leqq \gamma-1) \qquad (61)$$

The definitions for $F(X,\tau)$ and X are the same as those in the case of fast cooling of the anisotropic diffusion model, however, τ is defined as $\tau = D(T1)t/a^2$. Except for (60), the equations (56)~(61) are the same as those of the isotropic diffusion model. The initial and final temperature T0 and Tn correspond to Ti and Tf, respectively in the rapid cooling. The diffusion coefficient depends strongly on the temperature. The length of $\tau(Tn)$ is different from that of $\tau(T1)$ for the same actual time t. The reduced time in the equation (56) ~(61) contains D at temperature T1. On the other hand the reduced time in the expression of the range $[\,0 \leqq \tau(Tn) < \tau 1(Tn)]$ includes D at temperature Tn. Then $\tau(Tn)$ must be converted to $\tau(T1)$.
Since $\tau(Tn)$ and $\tau(T1)$ are defined as,

$$\tau(Tn) = D(Tn)t/a^2 \ , \ \tau(T1) = D(T1)t/a^2 \ ,$$

then $\tau(T1) = D(T1/Tn)\,\tau(Tn)$ (62),

is obtained,
where D(T1/Tn) is the abbreviation for D(T1)/D(Tn). Based on the experimental measurements, the diffusion coefficient D is expressed as a function of temperature T(K) in the Arrehenius' equation,

$D(T) = Do \exp(-E/RT)$ (63),

where Do, E and R are respectively the pre-exponential factor, activation energy and the gas constant.

Then, $D(T1/Tn) = \exp[-E(T1^{-1} - Tn^{-1})]$ (64).

It should be noted that the activation energy of diffusion is needed only for the calculation of D(T1/Tn).

$0 \leqq \tau(Tn) < \tau 1(Tn)$ is converted to $0 \leqq \tau(T1) < D(T/Tn)\,\tau 1(Tn)$.

The change of $^{18}O/(^{16}O+^{18}O)$ ratio of inclusion water is calculated by EFDM in this range.

When $\tau(T1)$ reaches $D(T1/Tn)\,\tau 1(Tn)$, the temperature of fluid inclusion drops from T1 to T2. The $^{18}O/(^{16}O+^{18}O)$ ratio of the inner surface of quartz just before the drop of temperature is C1. C1 increases to $\alpha(T2/T1)C1$ by the drop of temperature, where $\alpha(T2/T1)$ is the abbreviation for $\alpha(T2)/\alpha(T1)$.

$\tau 1(Tn) \leqq \tau(Tn) < \tau 2(Tn)$ is converted to

$$\tau 1(Tn)D(T2/Tn) \leqq \tau(T2) < \tau 2(Tn)D(T2/Tn).$$

The following equation for the subsequent steps are written.

$$\frac{\partial^2 F}{\partial X^2} = \frac{\partial F}{\partial \tau(T2)} \tag{65}$$

$$\tau 1(Tn)D(T2/Tn) < \tau(T2) < \tau 2(Tn)D(T2/Tn), \quad 0 < X < \gamma .$$

$$\beta(T2)\left[\frac{\partial F}{\partial \tau(T2)}\right] = \left[\frac{\partial F}{\partial X}\right] \tag{66}$$

$$\tau 1(Tn)D(T2/Tn) < \tau(T2) < \tau 2(Tn)D(T2/Tn), \quad X=0$$

$$\frac{\partial F}{\partial X} = 0 \tag{67}$$

$$\tau 1(Tn)D(T2/Tn) \leqq \tau(T2) < \tau 2(Tn)D(T2/Tn), \quad X = \gamma$$

$$F = [\,(C1/Co)\,\alpha(T2/T1) - 1\,]/[\,\alpha(Tn/T0) - 1\,] \tag{68}$$

$$\tau(T2) = \tau 1(Tn)D(T2/Tn), \quad X=0$$

$$F[X, \tau(T2)] = F1(X) \tag{69}$$

$$\tau 1(Tn)\{D(T2)/D(Tn)\} \leqq \tau(T2) < \tau 2(Tn)\{D(T2)/D(Tn)\}, \quad 0 < X \leqq \gamma - 1$$

where F1(X) is the F(X) just before the drop of temperature from T1 to T2.

Generally the following equations are written in the range, $\tau i\text{-}1(Tn) \leqq \tau(Tn) < \tau i(Tn)$.

$$\frac{\partial^2 F}{\partial X^2} = \frac{\partial F}{\partial \tau(\mathrm{Ti})} \tag{70}$$

τ i-1(Tn)D(Ti/Tn) $< \tau$ (Ti) $< \tau$ i(Tn)D(Ti/Tn), $0 < X < \gamma$

$$\beta(\mathrm{Ti})\left[\frac{\partial F}{\partial \tau(\mathrm{Ti})}\right] = \left[\frac{\partial F}{\partial X}\right] \tag{71}$$

τ i-1(Tn)D(Ti/Tn) $< \tau$ (Ti) $< \tau$ i(Tn)D(Ti/Tn), X=0

$$\frac{\partial F}{\partial X} = 0 \tag{72}$$

τ i-1(Tn)D(Ti/Tn) $\leqq \tau$ (Ti) $< \tau$ i(Tn)D(Ti/Tn), X= γ

$$F = [\{C(i-1)/Co\}\{\alpha(Ti/Ti-1) - 1\}]/[\alpha(Tn/T0) - 1] \tag{73}$$

τ (Ti) = τ i-1(Tn)D(Ti/Tn), X=0

where C(i-1) is C(a,t) just before the decreasing of temperature from T(i-1) to Ti.

$$F[X, \tau(\mathrm{Ti})] = F(i-1)(X) \tag{74}$$

τ i-1(Tn)D(Ti/Tn) $\leqq \tau$ (Ti) $< \tau$ i(Tn)D(Ti/Tn), $0 < X \leqq \gamma$

where F(i-1)(X) is the F(X) just before the drop of temperature from T(i-1) to Ti.

Like in the case of rapid cooling, a function ξ is introduced, which represents the advancement of the decrease in the $^{18}O/(^{16}O+^{18}O)$ ratio of inclusion water.

For the anisotropic diffusion model,

$$\xi = \frac{[\ F(X=0)\{\alpha(Tn/T0)-1\}\alpha(T0/T) + \alpha(T0/T) - 1\ ]}{[\ \gamma/\{\gamma+(2/3)\beta(Tn)\ \}][\alpha(T0/T) - 1\ \}} \qquad (75)$$

Substituting T=Tn into (75),

$$\xi = [\ 1 - F(X=0)\ ]/[\ \gamma/\{\gamma+(2/3)\beta(Tn)\ \}\ ] \qquad (77),$$

is obtained, which is identical to the ξ of (17) defined in the rapid cooling for anisotropic diffusion model.

For the isotropic diffusion model ξ is defined as,

$$\xi = \frac{[\ F(X=0)\{\alpha(Tn/T0)-1\}\alpha(T0/T) + \alpha(T0/T) - 1\ ]}{\{(\gamma^3-1)/(\gamma^3+3\beta(Tn)-1)\}\{\alpha(T0/T) - 1\ \}} \qquad (78)$$

Substituting T=Tn into (78),

$$\xi = [\ 1 - F(X=0)\ ]/[(\gamma^3-1)/\{\gamma^3+3\beta(Tn)-1\ \}\ ] \qquad (80),$$

is obtained, which is identical to the ξ of (37) defined in the rapid cooling for isotropic diffusion model.

Calculation in each step was carried out from the first step with temperature T1 to the last step with temperature Tn in sequence.

<1-5-2-3> Result of calculation for the slow cooling

A result of calculation for the slow cooling based on the anisotropic diffusion model is shown in Fig.1-11a. The numerical values used for the parameters are listed, below,

γ = 10

$\beta_{fu}Dw/Dq$ = 0.5

The number of steps in the cooling process = 10

T0 = 300K

Tn = 600K

The activation energy of diffusion, E = 155.5 (kJ/mol)

(Elphick et al.1986)

In the Figure, both the (1- ξ) value and "apparent temperature" are taken on the vertical axis and $\log_{10}\tau$ (Tn) is on the horizontal axis.

The apparent temperature is defined as follow. The $^{18}O/(^{16}O+^{18}O)$ ratio of the surrounding quartz equilibrated completely with the inclusion water at temperature T(K) is C_T , and the initial and final (at t=∞) $^{18}O/(^{16}O+^{18}O)$ ratio of the surrounding quartz are Ci and Cf, respectively. The $^{18}O/(^{16}O+^{18}O)$ ratio of the inclusion water, W, can be expressed using ξ function as,

$$W = [Ci/\alpha(T0)] - [\{Ci/\alpha(T0)\} - \{Cf/\alpha(Tn)\}]\xi \qquad (81).$$

$C_T/\alpha(T)$, which is the $^{18}O/(^{16}O+^{18}O)$ ratio of inclusion water equilibrated with the quartz at T(K), is substituted into (81), then

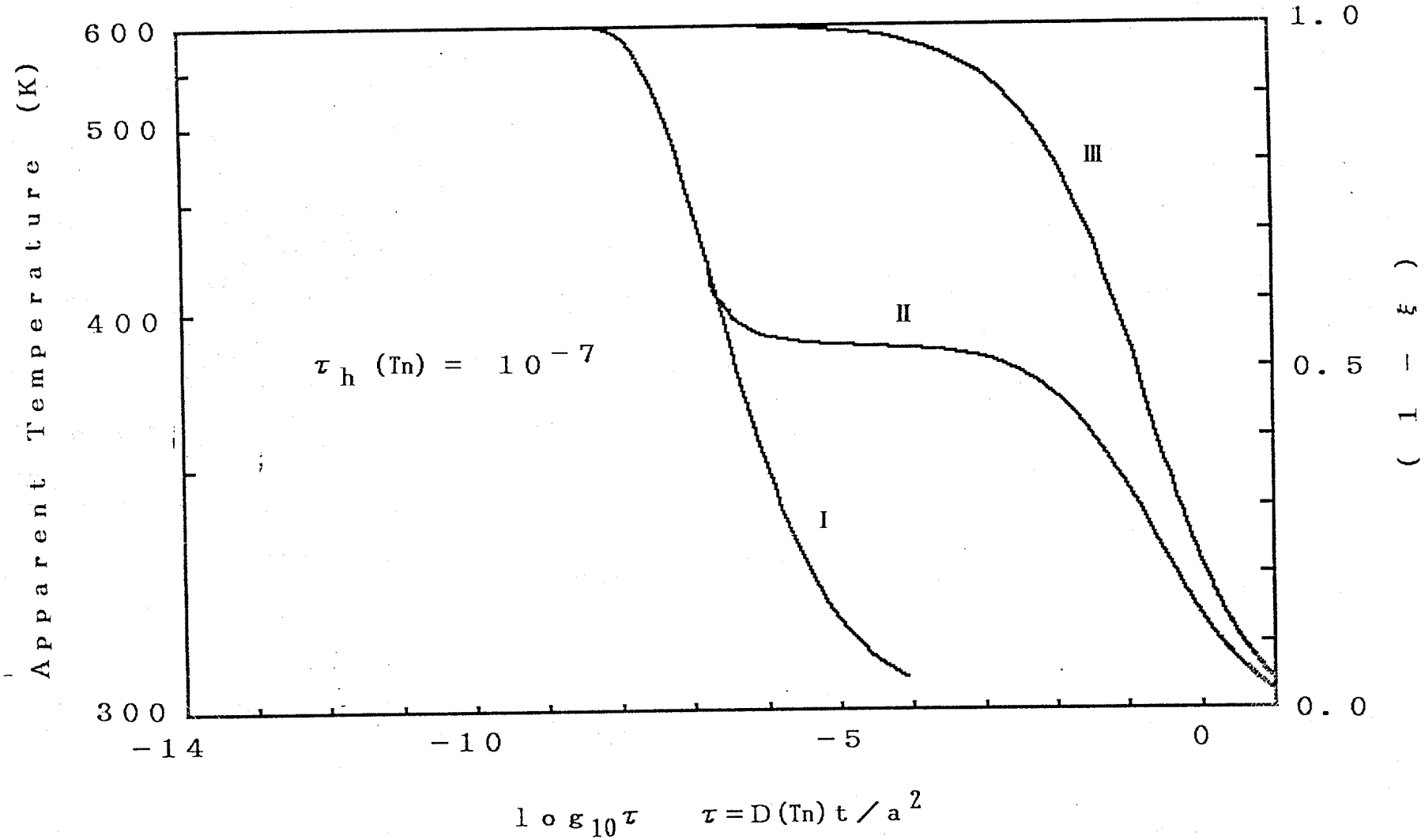

Fig.1-11a Change in ξ by the slow cooling for the anisotropic diffusion model. (The reduced half time, τ_h(Tn) is 10^{-7}.)

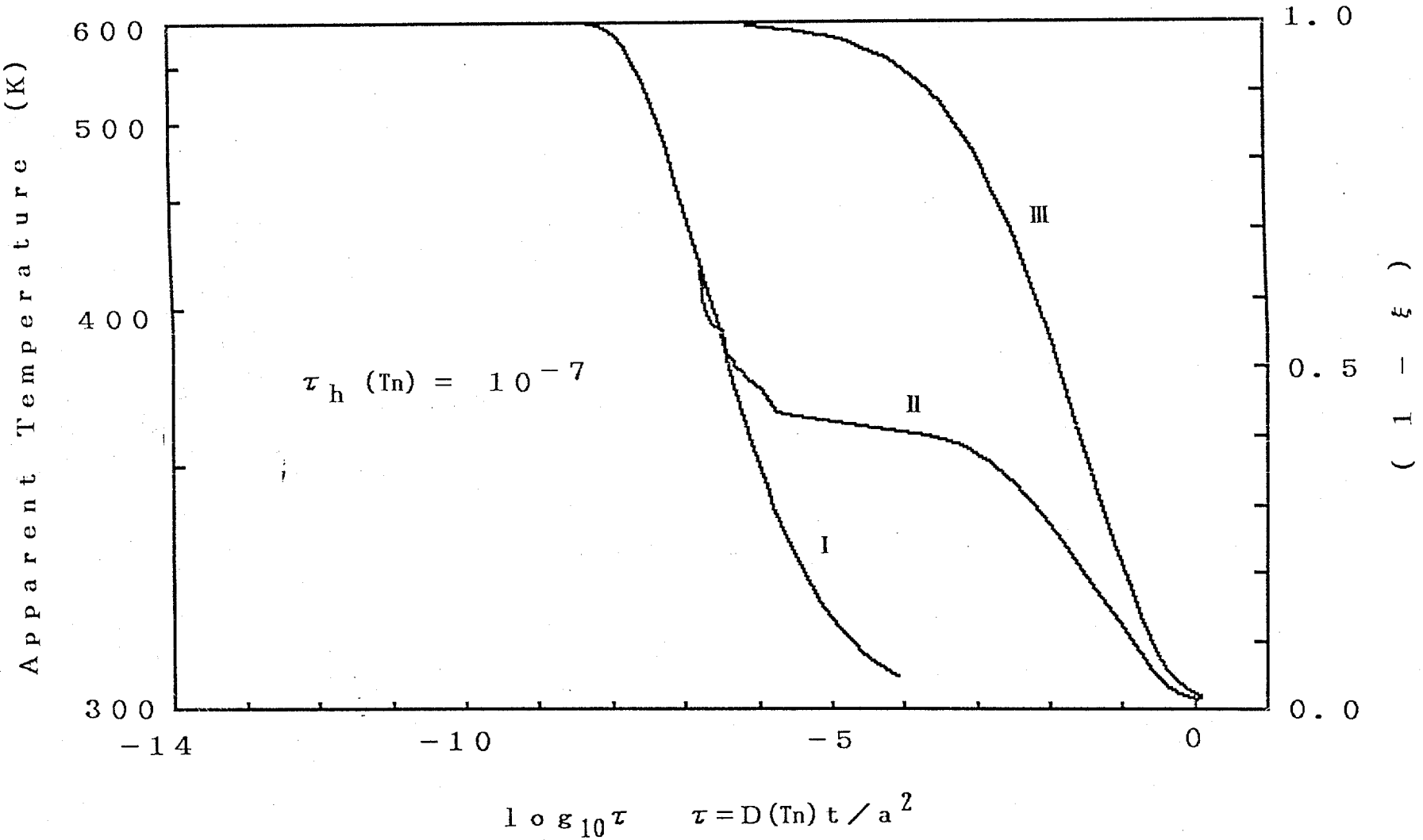

Fig.1-11b Change in ξ by the slow cooling for the isotropic diffusion model. (The reduced half time, τ_h(Tn) is 10^{-7}.)

$$C_T/\alpha(T) = [Ci/\alpha(T0)] - [\{Ci/\alpha(T0)\} - \{Cf/\alpha(Tn)\}]\xi \quad (82),$$

is obtained.

Dividing both sides by Ci,

$$(C_T/Ci)\,\alpha(T) = [1/\alpha(T0)] - [\{1/\alpha(T0)\} - \{(Cf/Ci)\,\alpha(Tn)\}]\xi \quad (83)$$

is obtained.

In (83), the one-to-one correspondence is found between T and ξ. The apparent temperature is the T in (83) calculated for arbitrary ξ. When the inclusion water is in equilibrium with the quartz completely, the temperature of fluid inclusion and the apparent temperature is identical, on the other hand when the inclusion water and the quartz is in disequilibrium, the temperature of fluid inclusion is lower than the apparent temperature.

(C_T/Ci) and (Cf/Ci) are given for the isotropic diffusion model to be,

$$(C_T/Ci) = [\{\beta^*/\alpha(T0)\} + \gamma^3 - 1]/[\{\beta^*/\alpha(T)\} + \gamma^3 - 1] \quad (84),$$

$$(Cf/Ci) = [\{\beta^*/\alpha(T0)\} + \gamma^3 - 1]/[\{\beta^*/\alpha(Tn)\} + \gamma^3 - 1] \quad (85),$$

and for the anisotropic diffusion model to be,

$$(C_T/Ci) = [\{\beta^*/\alpha(T0)\} + \gamma]/[\{\beta^*/\alpha(T)\} + \gamma] \quad (86),$$

$$(Cf/Ci) = [\{\beta^*/\alpha(T0)\} + \gamma]/[\{\beta^*/\alpha(Tn)\} + \gamma] \quad (87),$$

where $\beta^* = \beta_{fu} Dw/Dq$ (88).

In Fig.1-11a, curve I show the temperature of fluid inclusion. Curve II represents the change in ξ or apparent temperature of inclusion water when the fluid inclusion is cooled step-wise as described in the preceding section with the reduced half time, $\tau_h(Tn)$, of 10^{-7}. Comparing the two curves, it is found that the apparent temperature of inclusion water is identical to the temperature of fluid inclusion until the temperature of fluid inclusion drops to about 400K, which means that the diffusion coefficient is high enough to bear the equilibrium between the inclusion water and the surrounding quartz. However, the rate of decrease of the curve II is restrained when the temperature of fluid inclusion drops lower than 400K, which means that the diffusion coefficient is too small to bear the equilibrium between the inclusion water and the surrounding quartz. Hereafter such a state where the change in ξ or apparent temperature of inclusion water is restrained is called as the "quenched state".

The quenched temperature depends on the cooling speed of fluid inclusion. The more the reduced half time $\tau_h(Tn)$ decreases, the more the quenched temperature rises (Fig.1-12a). Curve III in Fig.1-12a represents the change in ξ or the apparent temperature of inclusion water when the fluid inclusion is cooled very fast (= rapid cooling). From curve III it is recognized that the quenching occurs at 600K (in the beginning of the cooling process).

Fig.1-11b and Fig.1-12b show the results for the isotropic diffusion model which correspond to Fig.1-11a and Fig.1-12a for anisotropic model, respectively.

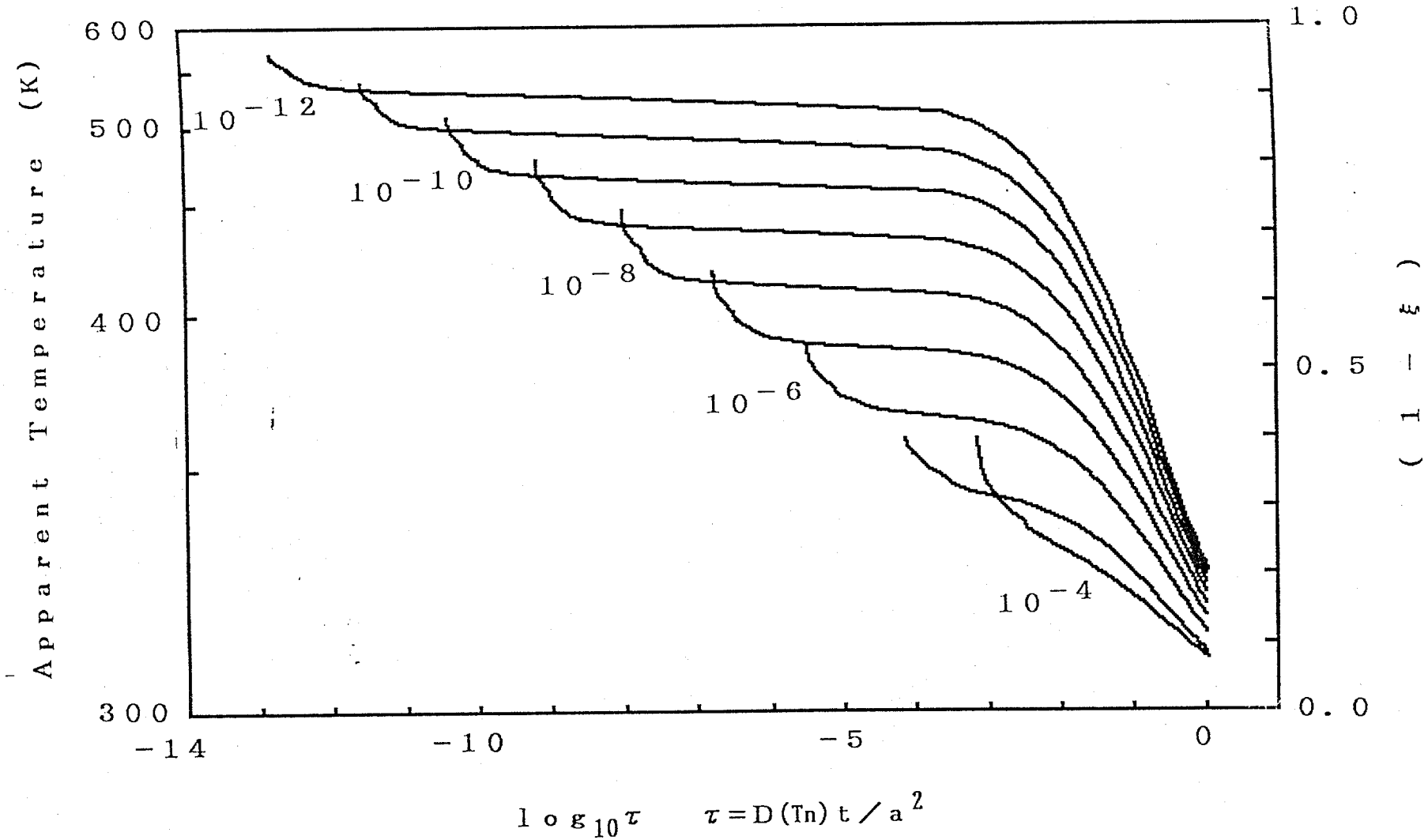

Fig.1-12a Change in ξ by the slow cooling with different reduced half times for the anisotropic diffusion model. (The numbers near the lines are the reduced half times.)

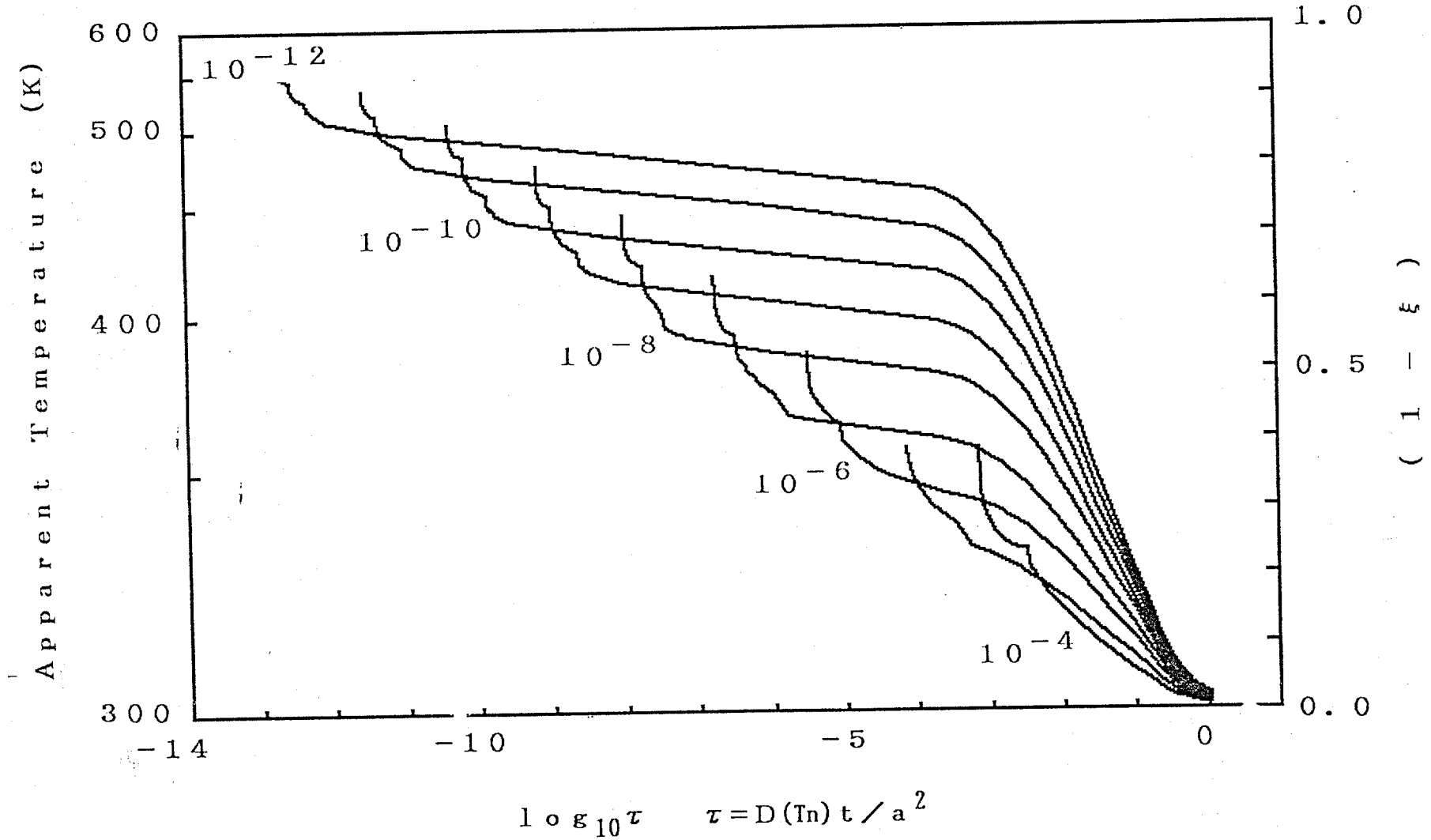

Fig.1-12b Changes in ξ by the slow cooling with different reduced half times for the isotropic diffusion model. (The numbers near the lines are the reduced half times.)

<1-5-2-4> Relation between ξ and the radius of fluid inclusion

In this section, the relation between the radius of fluid inclusion and ξ will be derived from the results obtained in the preceding section. Let us consider two different fluid inclusions 1 and 2 with the radius of a_1 and a_2, respectively. The relation between a_1 and a_2 is taken to be,

$$a_2 = \sqrt{10}\, a_1 \qquad (89),$$

and other geometric parameters for two types of inclusions are the same and that both inclusions are assumed to be cooled with the same actual half time being $\tau h(Tn) = 10^{-7}$ for the inclusion 1.
Here the actual half time t_h is,

$$t_h = 10^{-7} a_1^2 / D(Tn) \qquad (90).$$

While for the inclusion 2, the reduced half time of cooling is,

$$\tau_h(Tn) = D(Tn) t_h / a_2^2 \qquad (91).$$

Substituting (89) and (90) into (91)

$$\tau_h(Tn) = D(Tn)[10^{-7} a_1^2 / D(Tn)]/(10 a_1^2) = 10^{-8} \qquad (92)$$

is obtained.
The reduced time of the inclusion 2 is one tenth of that of the inclusion 1 for the same actual half time.

In Fig.1-13a, the change in ξ by the cooling with the reduced

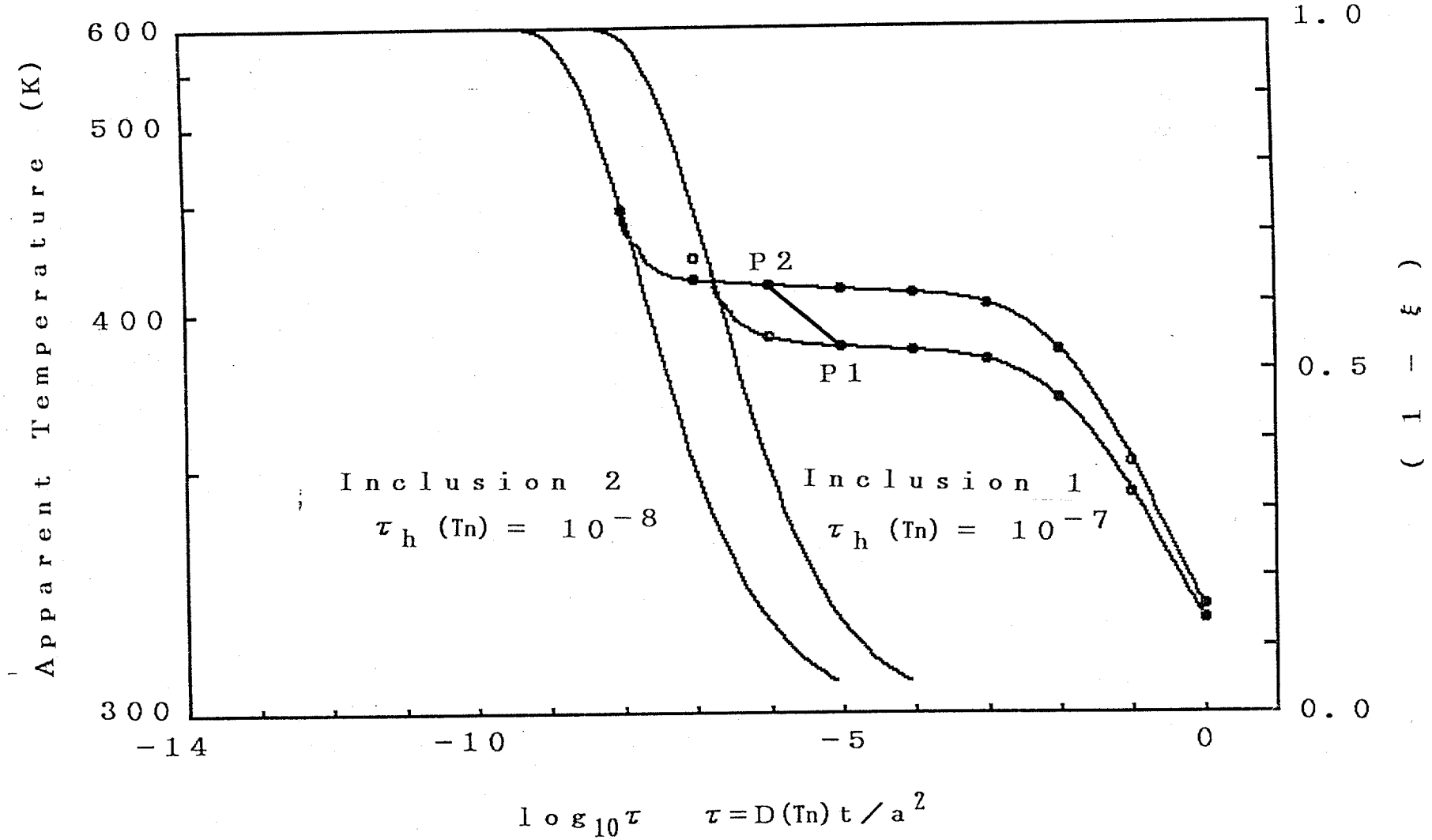

Fig.1-13a Change in ξ of fluid inclusions with different radii for the anisotropic diffusion model.

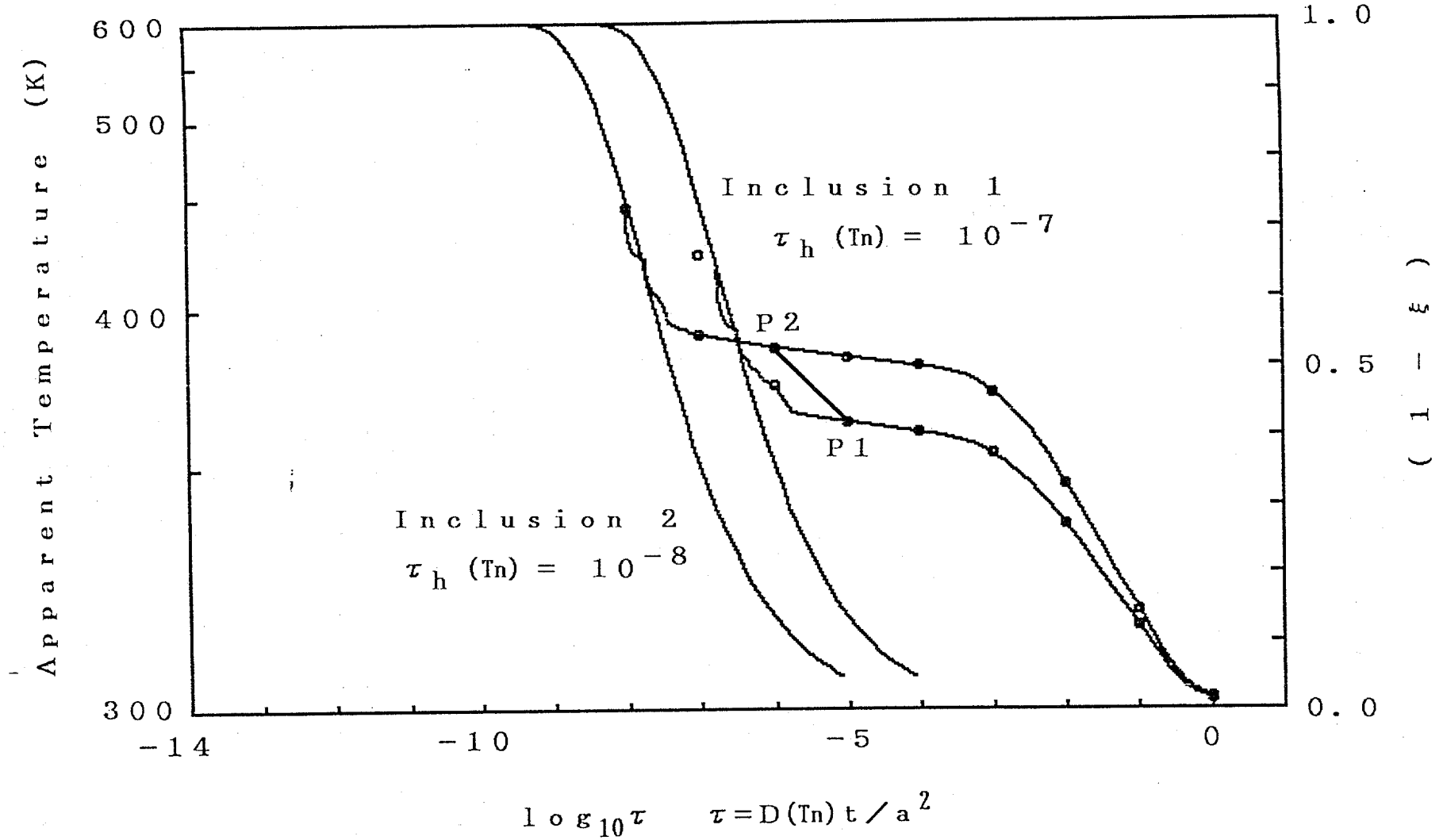

Fig.1-13b Change in ξ of fluid inclusions with different radii for the isotropic diffusion model.

half time $\tau_h(Tn) = 10^{-7}$ and 10^{-8} is shown for anisotropic diffusion model. The points P1 and P2 in Fig.1-13a show the ξ values of the inclusion 1 and 2 after elapsing one hundred times of the half time. The ξ value at P1 is higher than that of P2, which means that the $^{18}O/(^{16}O+^{18}O)$ ratio of the inclusion water with smaller radius is more changeable than that with larger radius. The difference in $\log_{10}\tau(Tn)$ (horizontal axis) between P1 and P2 just corresponds to the difference in radii. Consequently, the line connecting P1 and P2 is a part of the curve which represents the relation between the radius of inclusion and the ξ value of inclusion water after one hundred times of the half times.

For the actual half time, $t_h = 10^{-7}a_1^2/D(Tn)$, the reduced half time for the inclusions with the radius of

$10a_1$, $10^{3/2}a_1$, 10^2a_1 ,.. $10^{-1/2}a_1$, $10^{-1}a_1$, $10^{-3/2}a_1$,...

are

10^{-9}, 10^{-10} , 10^{-11} ,.. 10^{-6}, 10^{-5}, 10^{-4},...

,respectively.

In Fig.1-14a, the change in ξ due to the cooling with different reduced half time of $\tau_h(Tn) = 10^{-12} \sim 10^{-4}$ are shown.

Curve Ⅳ in Fig.1-14a is the tie line connecting the points where the reduced time is one hundred times of the reduced half time. Curve Ⅳ also represents the relation between the ξ value and the rsdius of inclusion, under the cooling condition with the ratio of $t_n/t_h = 100$.

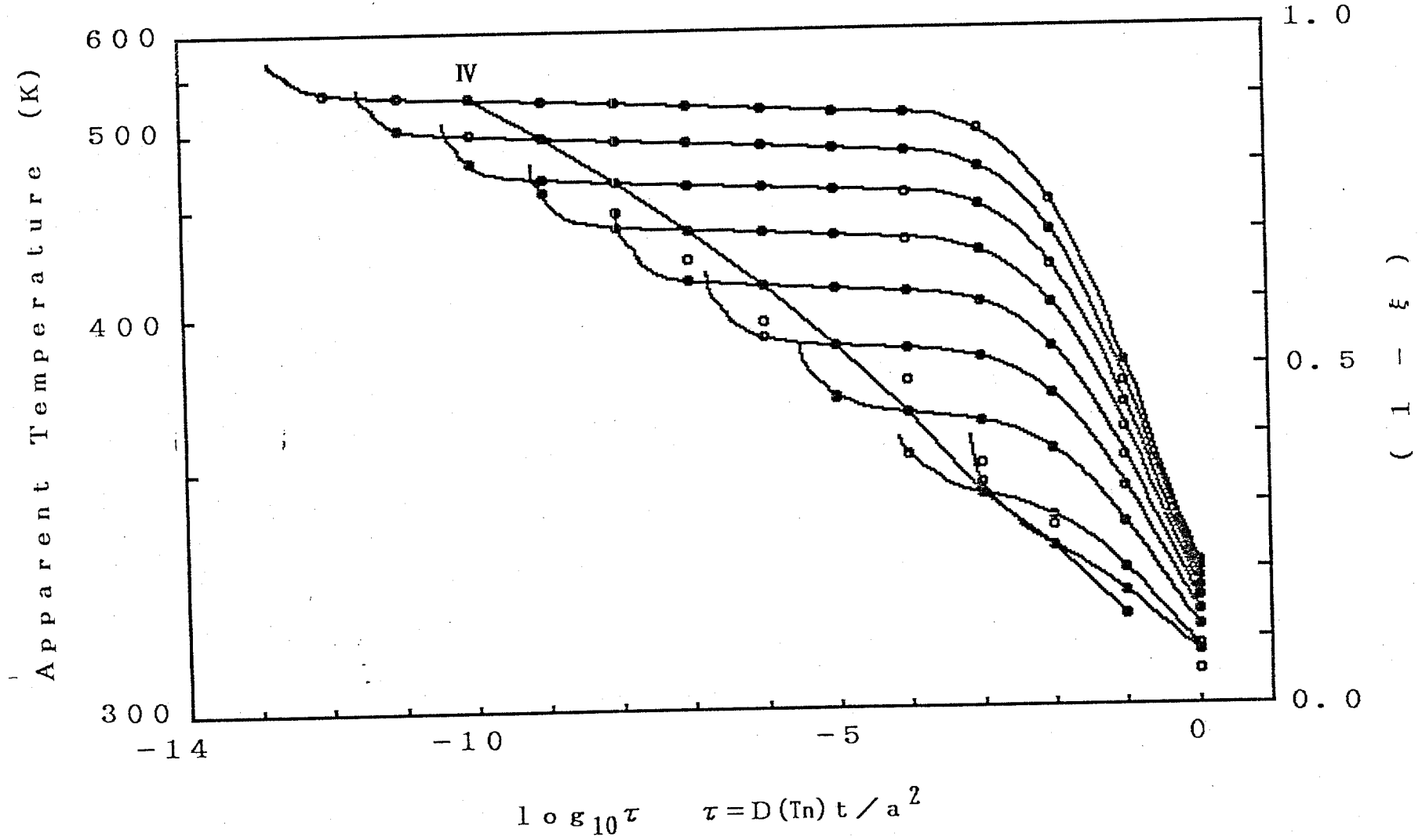

Fig.1-14a Tie line curve IV connecting the points with the ratio, $\tau_n(Tn)/\tau_h(Tn)$, of 100 for the anisotropic diffusion model.

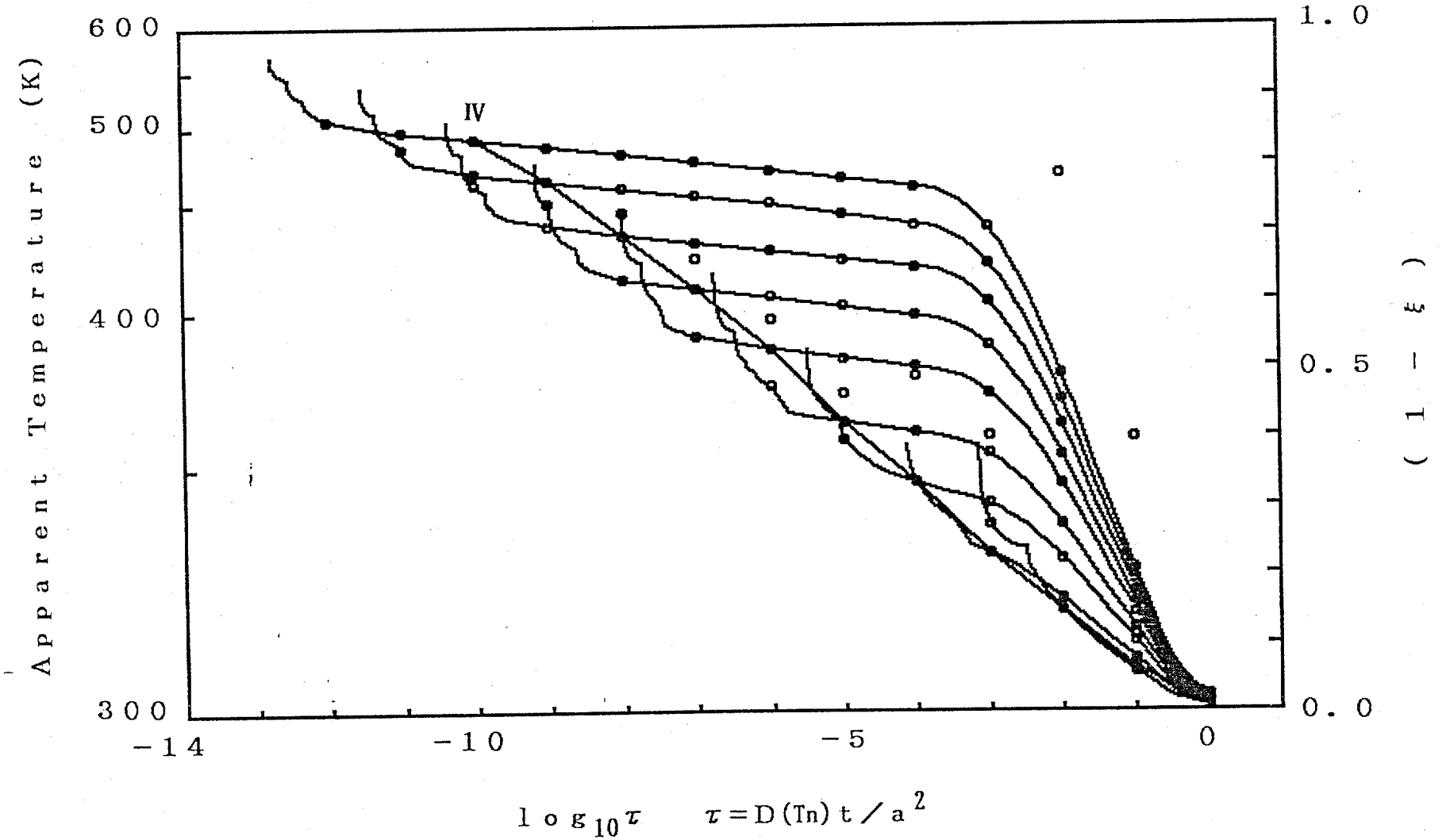

Fig.1-14b Tie line curve IV connecting the points with the ratio, $\tau_n(Tn)/\tau_h(Tn)$, of 100 for the isotropic diffusion model.

In Fig.1-15a, curves like curve IV in Fig.1-14a, with different $\tau n(Tn)/\tau h(Tn)$ ratios are shown. It is found that the slope of the curve becomes steeper and close to the line of the rapid-cooling with the increase in the $\tau n(Tn)/\tau h(Tn)$ ratios. Fig.1-13b, 1-14b, 1-15b are the results for the isotropic diffusion model which corresponds to Fig.1-13a, 1-14a and 1-15a of anisotropic diffusion model, respectively.

<1-5-2-5> Comparison with the results of measurements

The analytical results obtained by Kayahaya (1986) can be compared with the lines of Fig.1-15a and 1-15b. The quartz samples analyzed by Kazahaya are taken from the restricted part of the Kaneuchi mine. Then t_m, the time elapsed since the start of cooling is considered to be the same for all the samples.

Unfortunately the diffusion coefficient at the temperature Tn (300K), D(Tn), of the sample quartz has not yet been measured. Nevertheless, since there is no reason to put a difference for the D(Tn) value of each sample, the D(Tn) value is assumed to be common for all the samples. As D(Tn) is unknown, $\log_{10}\tau(Tn)$ on the horizontal axis can not be determined for each measured value of fluid inclusions. However, the range of diameters of inclusions for each sample is known, then the relative positions of the measured values of fluid inclusions on the horizontal axis can be determined.

The ξ value of inclusion water for the Kaneuchi quartz is calculated according to the equation, (81) in the section <1-5-2-3> where,

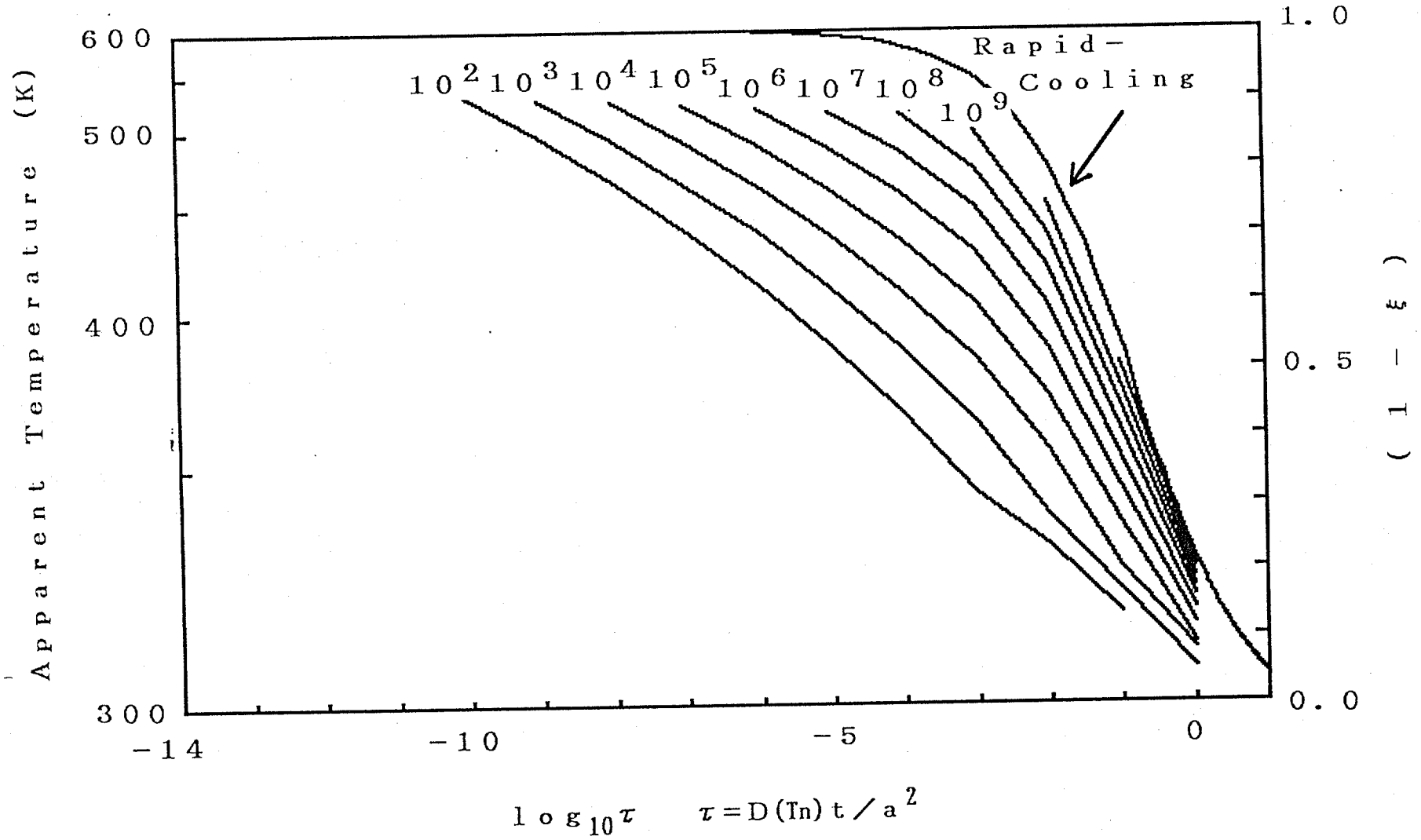

Fig.1-15a Lines representing the relations between the ξ value and the radius of fluid inclusion with different $\tau_n(Tn)/\tau_h(Tn)$ ratios for the anisotropic diffusion model. (The numbers on the top of the lines are the $\tau_n(Tn)/\tau_h(Tn)$ ratios. The line for the rapid-cooling is shown in addition.)

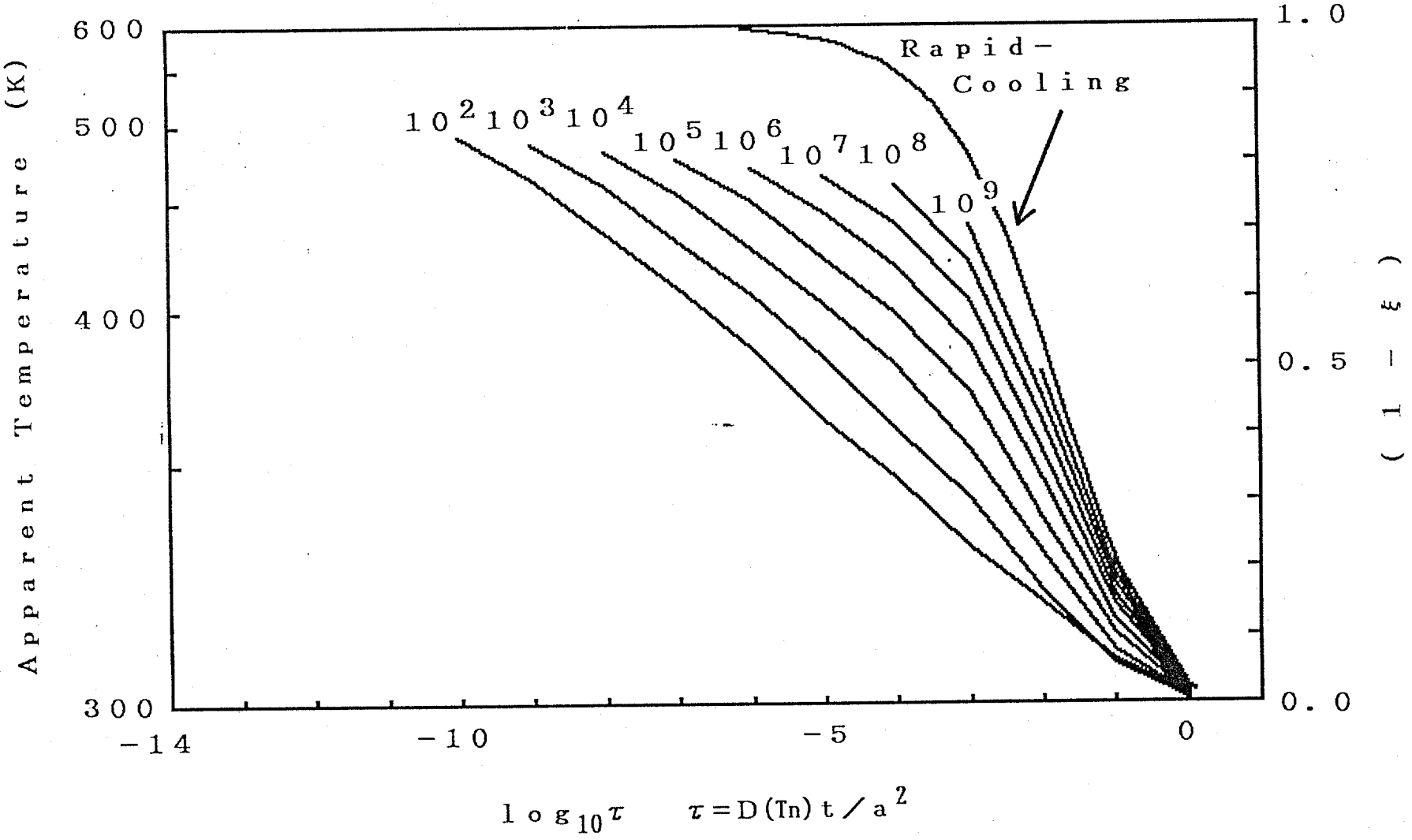

Fig.1-15b Lines representing the relations between the ξ value and the radius of fluid inclusion with different $\tau_n(Tn)/\tau_h(Tn)$ ratios for the isotropic diffusion model. (The numbers on the top of the lines are the $\tau_n(Tn)/\tau_h(Tn)$ ratios. The line for the rapid-cooling is shown in addition.)

$$W = [Ci/\alpha(T0)] + [\{Ci/\alpha(T0)\} - \{Cf/\alpha(Tn)\}]\xi \quad (93).$$

Dividing both sides with Ci,

$$W/Ci = 1/\alpha(T0) + [\{1/\alpha(T0)\} - \{(Cf/Ci)\alpha(Tn)\}]\xi \quad (94).$$

(Cf/Ci) can be calculated by (85) and (87) in the section <1-5-2-3> for the anisotropic and the isotropic diffusion models, respctively. For T0=600K, Tn=300K, γ=10 and β^* ($=\beta_{fu}Dw/Dq$) = 0.5,

Cf/Ci = 1.0013014 (for the anisotropic diffusion model)
Cf/Ci = 1.0000137 (for the isotropic diffusion model)

are given.
The left side of (94) is,

$$W/Ci = (\delta^{18}O_{inclusion\ water} + 1000)/(\delta^{18}O_{quartz} + 1000) \quad (95),$$

where $\delta^{18}O_{inclusion\ water}$ is the value on the Talbe 1-2 and $\delta^{18}O_{quartz}$ was measured by Matsuhisa (personal communication) to be +14.5‰ relative to SMOW.

$$\because \quad \delta^{18}O_{inclusion\ water} = [(W/S) - 1] \times 1000, \quad (96)$$
$$\delta^{18}O_{quartz} = [(Q/S) - 1] \times 1000, \quad (97)$$

where S is the $^{18}O/^{16}O$ ratio of Standard Mean Ocean Water (Gonfiantini,R. 1978) and W and Q are the $^{18}O/^{16}O$ ratio of the inclusion water and the host quartz, respectively.

The range of ξ value for each quartz sample is shown in Table 1-5a and 1-5b for the anistropic and isotropic diffusion model, respectively.

In Fig.1-16a and 1-16b, the measured values of fluid inclusions are plotted on the $\log_{10}\tau(Tn)$ versus $(1-\xi)$ diagram. In these figures, some lines which fit with the measured values can be selected by comparing the distribution of the measured values (quadrangle marks) with the lines representing the relation between the diameter of inclusion and the ξ. In both cases of anisotropic and isotropic diffusion models, the t_n/t_h ratio of the line fitting well with the measured values is more than 10^7.

[20] Table. 1-5 (ab)

Table 1-5a　　ξ value of inclusion water in the Kaneuchi quartz
-for the anisotropic diffusion model

sample	ξ value
-90mL	0.317 ～ 0.427
-150mL#1	0.517 ～ 0.665
-150mL#2	0.355 ～ 0.408
-420mL#2	0.741 ～ 0.961

Table 1-5b　　ξ value of inclusion water in the Kaneuchi quartz
-for the isotropic diffusion model

sample	ξ value
-90mL	0.302 ～ 0.407
-150mL#1	0.494 ～ 0.635
-150mL#2	0.338 ～ 0.389
-420mL#2	0.707 ～ 0.917

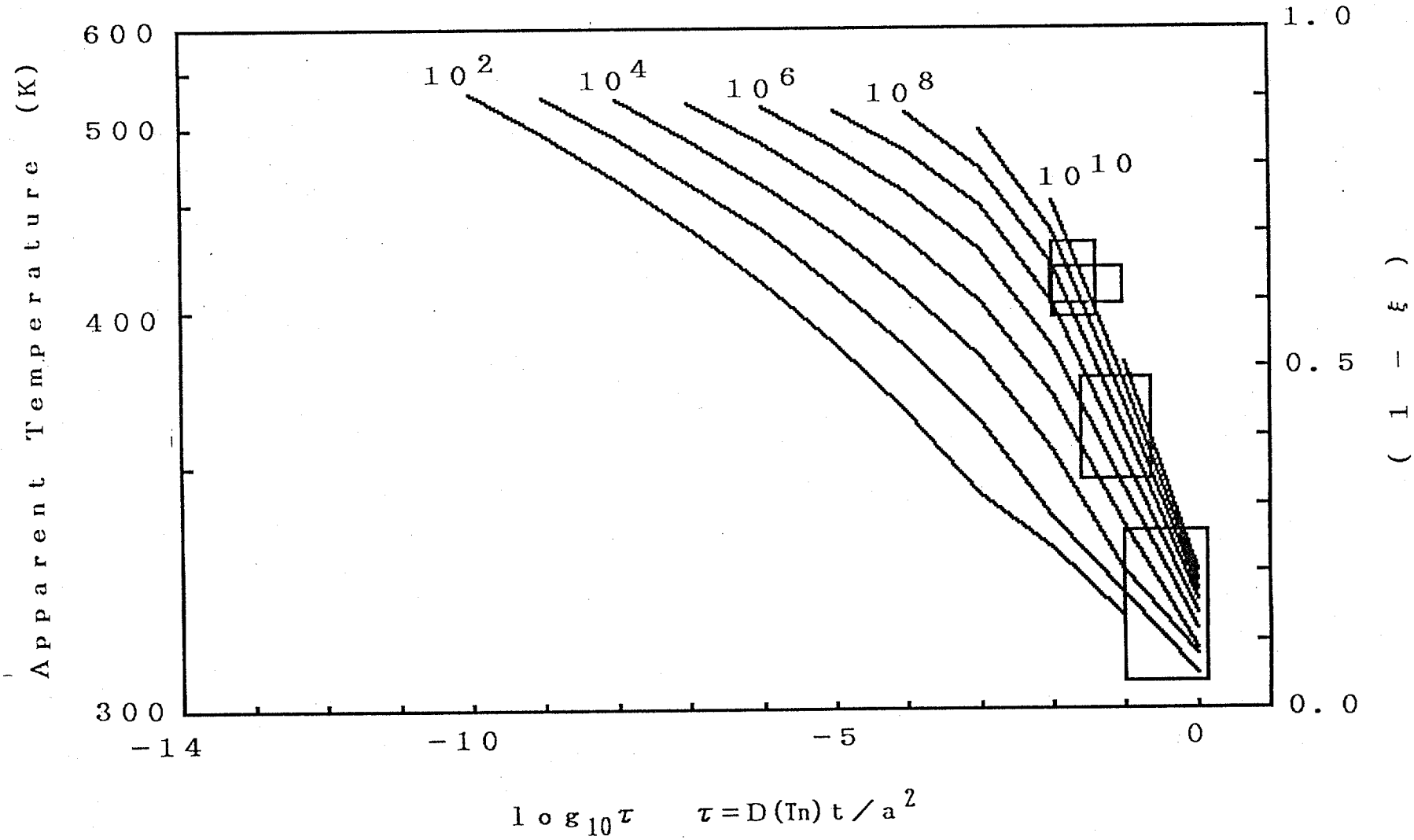

Fig.1-16a Comparison of the measured values on the Kaneuchi quartz with the lines with different $\tau_n(Tn)/\tau_h(Tn)$ ratios for the anisotropic diffusion model. (The quadrangles show the measured values.)

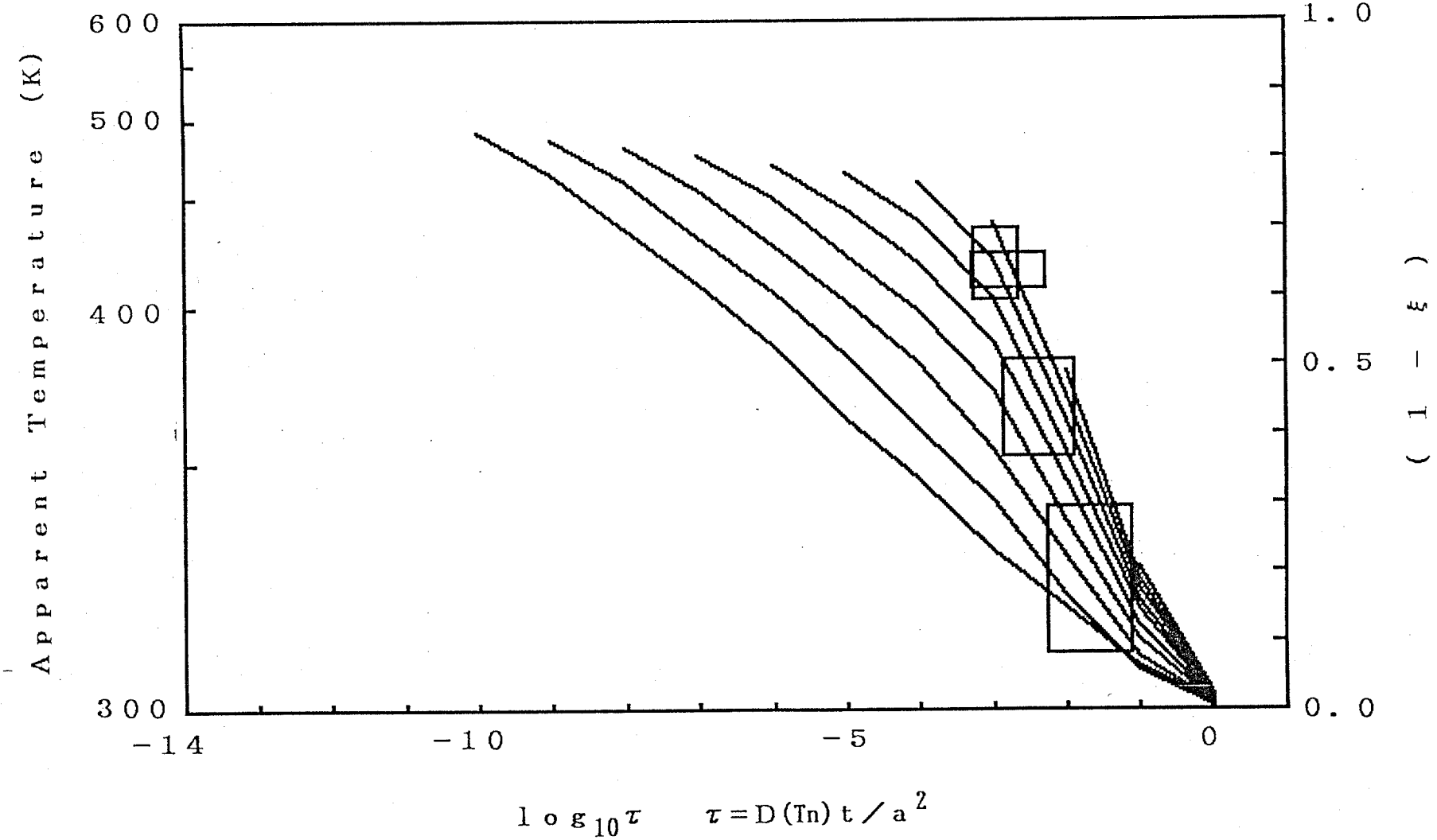

Fig.1-16b Comparison of the measured values on the Kaneuchi quartz with the lines with different $\tau_n(Tn)/\tau_h(Tn)$ ratios for the isotropic diffusion model. (The quadrangles show the measured values.)

< 1-6 > Discussion

In the preceding section, the t_n/t_h ratio of line which fits well with the measured values is determined to be more than 10^7 ,

i.e., $t_n/t_h \geqq 1\times10^7$ (98).

The K-Ar age of the Kaneuchi deposit is about 1×10^8 years (Shibata and Ishihara, 1974), which implies that 1×10^8 years has elapsed since Ar is retained and that the temperature at which the diffusive loss of Ar ceased can not be determined by the age determination itself. If the retention of Ar started at the filling temperature of fluid inclusion of 600K, then we may take t_n to be 1×10^8 years.

Then $t_n = 1\times10^8$ (years) (99).

From (98) and (99),

$t_h \leqq 10$ (years) (100),

is given. In other words, the temperature drop of the quartz vein of the Kaneuchi mine from 600K to 450K occurred within less than 10 years. This result may indicate that the major heat source of the mine at the time of quartz vein formation was the hydrothermal solution. When the supply of the hydrothermal solution declined, quartz veins were subjected to conduction cooling without a heat source.

As described in the section on the cooling of quartz vein, the half time of the temperature drop can be calculated to be,

$$4\kappa t_h/h^2 = 4.3908 \qquad (101),$$

where κ is the thermal diffusivity of quartz vein and the wall rock, and h is the half thickness of quartz vein. The thermal conductivity of slate which is the wall rock of the Kaneuchi quartz vein is 1.9×10^{-2} ($Jcm^{-1}s^{-1}K^{-1}$) and the density is 2.8 (gcm^{-3}) (Birch 1946). The specific heat of slate is about 0.8 ($Jg^{-1}K^{-1}$) (International Critical Tables 1927). The thermal diffusivity κ can be calculated from the thermal conductivity k , density ρ and specific heat c to be,

$$\kappa = kc^{-1}\rho^{-1} \qquad (102).$$

Substituting the numerical values into (102),

$$\kappa = 8.6 \times 10^{-7} \quad (m^2s^{-1}) \qquad (103),$$

is obtained.

In order to satisfy (100), the maximum value of h is calculated by the use of (101) and (103) to be 16m, being the width of 32m. As the thickness of quartz vein is about 30cm on an average, this result suggests that the thickness of high temperature plate was consistently larger than that of the vein quartz.

References

Birch,F and H.Clark (1940)
The thermal conductivity of rocks and its dependence upon temperature and composition (part I)
Am.J.Sci., 238, (1940), 529-558

Birch,F and H.Clark (1940)
The thermal conductivity of rocks and its dependence upon temperature and composition (part II)
Am.J.Sci., 238, (1940), 613-635

Choudhury,A., D.W.Palmer, G.Amsel, H.Curien and P.Baruch (1965)
Study of oxygen diffusion in quartz using the nuclear reaction $^{18}O(p,\alpha)^{15}N$.
Solid State Commum.,3,119-122,(1965)

Crank,J. (1956)
The mathematics of diffusion, Oxford, Clarendon Press 1956

Elphick,S.C., P.F.Dennis and C.M.Graham (1986)
An experimental study of the diffusion of oxygen in quartz and albite using an overgrowth technique
Contrib.Mineral.Petrol.,92, (1986), 322-330

Giletti,B.J. and R.A.Yund (1984)
Oxygen diffusion in quartz
J.Geophys.Res., 89,B6, (1984), 4039-4046

Gonfinatini, R. (1978)
Standards for stable isotopes measurements in natural compounds
Nature, 217,543-536,(1978)

Hattori,K. and H.Sakai (1979)
D/H ratios, origins, and evolution of the ore-forming fluids for the Neogene veins and Kuroko deposits of Japan
Econ.Geol., 74, (1979), 535-555

Imai,H., M.S.Kim and Y.Fujiki (1972)
今井　秀喜、金　炆栄、藤木　良規 (1972)
京都府大谷および鐘打鉱山地域の地質構造と鉱化作用
鉱山地質、22, (1972), 371-381

Kazahaya,K. and S.Mastuo (1985)
A new ball-milling method for extraction of fluid inclusions from minerals
Geochem.J., 19, (1985), 45-54

Kazahaya, K (1986)
Doctoral thesis, Tokyo Institute of Technology, Tokyo, Japan.

Kim,M.S., Y.Fujiki, S.Takenouchi and H.Imai (1972)
金　炆栄、藤木　良規、竹内　寿久祢、今井　秀喜 (1972)
京都府大谷および鐘打鉱山産鉱物中の流体包有物
鉱山地質、22, (1972), 449-455

Kita,I. (1981)
A new type ball mill made of pyrex glass
Geochim.J., 15, (1981), 289-291

Kita,I., S.Taguchi and O.Matsubaya (1985)
Oxygen isotope fractionation between amorphous silica and water at 34-93℃
Nature, 314, (1985), 83-84

Komura,R., S.Sakamaki and M.Bunno (1984)
小村　良二、坂巻　幸雄、豊　遥秋 (1984)
鐘打鉱山の閉山－61年の歴史をふりかえって－
地質ニュース、No.358, (1984), 53-60

Rye,R.O. and J.R.O'Neil (1968)
The O^{18} content of water in primary fluid inclusions from Providencia, north-central Mexico
Econ.Geol., 63, (1968), 232-238

Shibata,K. and S.Ishihara (1974)
K-Ar ages of the major tungsten and molybdenum deposits in Japan
Econ.Geol., 69, (1974), 1207-1214

Watanabe,T. (1956)
渡辺　武男 (1956)
「鉱床学の進歩」、富山房（東京）

Chapter-II

Influence of adsorption on the isotope ratios of inclusion fluid extracted using a vacuum ball mill

< 2-1 > Abstract

A ball mill made of Pyrex glass equipped with a cold finger trap cooled with liquid nitrogen is devised to extract volatiles from fluid inclusions in minerals. A special feature of the crushing mode is a horizontal oscillation of the mill, and the fragility of the mill made of Pyrex glass can be overcome. The crushing of minerals is carried out mostly by rubbing. This ball mill can reduce the influence of adsorption of once extracted volatiles onto mineral grains by trapping them during the crushing process. Furthermore, the crushing efficiency is better than that of the ball mill with a pounding mode.

Amounts and isotope ratios have been determined for water and carbon dioxide extracted from the fluid inclusions of halite and quartz. The influence of adsorption on amounts and isotopic ratios of volatiles has been evaluated by comparing the results of repeated extractions with and without the liquid nitrogen trap during the crushing process.

As for the fluid inclusions in a hydrothermal quartz sample, the method for estimating the original $\delta^{18}O$ and δD values for the water in inclusions can be established by a set of data on amount and isotope ratios with the help of material balance equations. In the case of halite samples, however, the estimation of the original $\delta^{18}O$ and δD values is much difficult, because the adsorption of vapor onto the surface of halite powder is much more than that in the case of quartz, and the presence of Mg and Ca ions in the brine disturbs the $\delta^{18}O$ value of water released during the post-heating process.

However, in a special case where the brine in inclusions is a pure NaCl solution, it is pointed out that the estimation of the original $\delta^{18}O$ and δD values is simple and possible.

The precise method for estimating the original $\delta^{18}O$ and δD values of the water in fluid inclusions is presented together with the problems to be solved in future.

For halite and quartz, the adsorption of CO_2 during the crushing process does not affect appreciably the results on the amount as well as $\delta^{13}C$ and $\delta^{18}O$ values.

Introduction

Isotope analysis of fluid inclusions in minerals has been developed for estimating the origin of the fluids responsible for the formation of the host minerals. The low temperature vacuum crushing method is suitable for extracting volatiles from fluid inclusions without altering their compositions. The press method by which a mineral sample is crushed in a collapsible metal tube has been used first for the extraction of volatiles in samples containing relatively large fluid inclusions (e.g.,Roedder et al., 1963). However, a large amount of sample is required for this method to collect volatiles with sufficient amount for a variety of analyses. In contrast to the press method, the ball milling method gives a definitely higher efficiency of extraction. Kita (1981) devised a ball mill made of Pyrex glass with an alumina ball. Kazahaya and Matsuo (1985) and Horita and Matsuo (1986) applied this ball mill to extract volatiles from inclusions in quartz and halite, respectively for isotope analyses. However, the Kita's mill has a defect that the bottom of the mill is easily broken during the pounding process by the vertical motion of the alumina ball. In addition, adsorption on the fine grains of mineral during the crushing process is inevitable whenever one uses conventional ball mills, which is serious when the amount of volatiles is small (Barker and Torkelson 1975). The adsorption and/or reaction of water vapor with the radicals formed on the fresh surfaces of mineral (Kita et al.,1982) results in significant changes in amounts, chemical compositions and isotope ratios of volatiles extracted. We devised a new ball mill in order to reduce the influence of adsorption and overcome the

fragility of the Kita's ball mill. In this study, an emphasis is laid on the technical side of extraction and analysis of volatiles in fluid inclusions, and no geochemical discussion associated with the obtained results is made.

< 2-3 > Apparatus

Perspective and cross section views of the ball mill are shown in Fig.2-1 and Fig.2-2, respectively. Body of the mill is made of Pyrex glass. The mill is composed of the upper part with a Pirani gauge sensor, Rugby-ball shaped lower part and a cold finger. The lower part contains an alumina ball 56g in weight and 30mm in diameter. Both ends of the lower part are installed with protectors made of stainless steal wire to prevent the glass walls from breaking by the collision of the ball. Thickness of the bottom wall is 4mm. The upper and lower parts are connected through Viton O-ring. Inside of the mill can be evacuated through stopcock 1. The total volume of the mill is about 300 cm^3 .

The mill containing the alumina ball and mineral sample assembled as shown in Fig.2-1 is mounted to a shaker (Fig.2-3). Shaking with linear motion parallel to the longer axis of the lower part of the mill is carried out with the frequency of 3 Herz and the 4cm amplitude of oscillation. As the alumina ball can not follow the motion, the ball moves back and forth on the bottom. The crushing of mineral sample is carried out mainly by rubbing between the ball and the bottom.

Although the inner wall of the bottom is scratched in the process of crushing quartz, the lower part can be used repeatedly, and then renewed separately. The thickness of the bottom has decreased from 4mm to 2.5mm after about 50 runs. According to Kazahaya and Matsuo (1985), the adsorption of water vapor by the powder of Pyrex glass is negligible.

Function of the cold finger is to reduce the amount of volatiles adsorbed on the fresh mineral surface generated by crushing.

By cooling the cold finger with liquid nitrogen *during the crushing*, a large portion of the water and carbon dioxide is condensed as they liberated. The pressure inside the mill can be kept at 1×10^{-3} torr during the blank run.

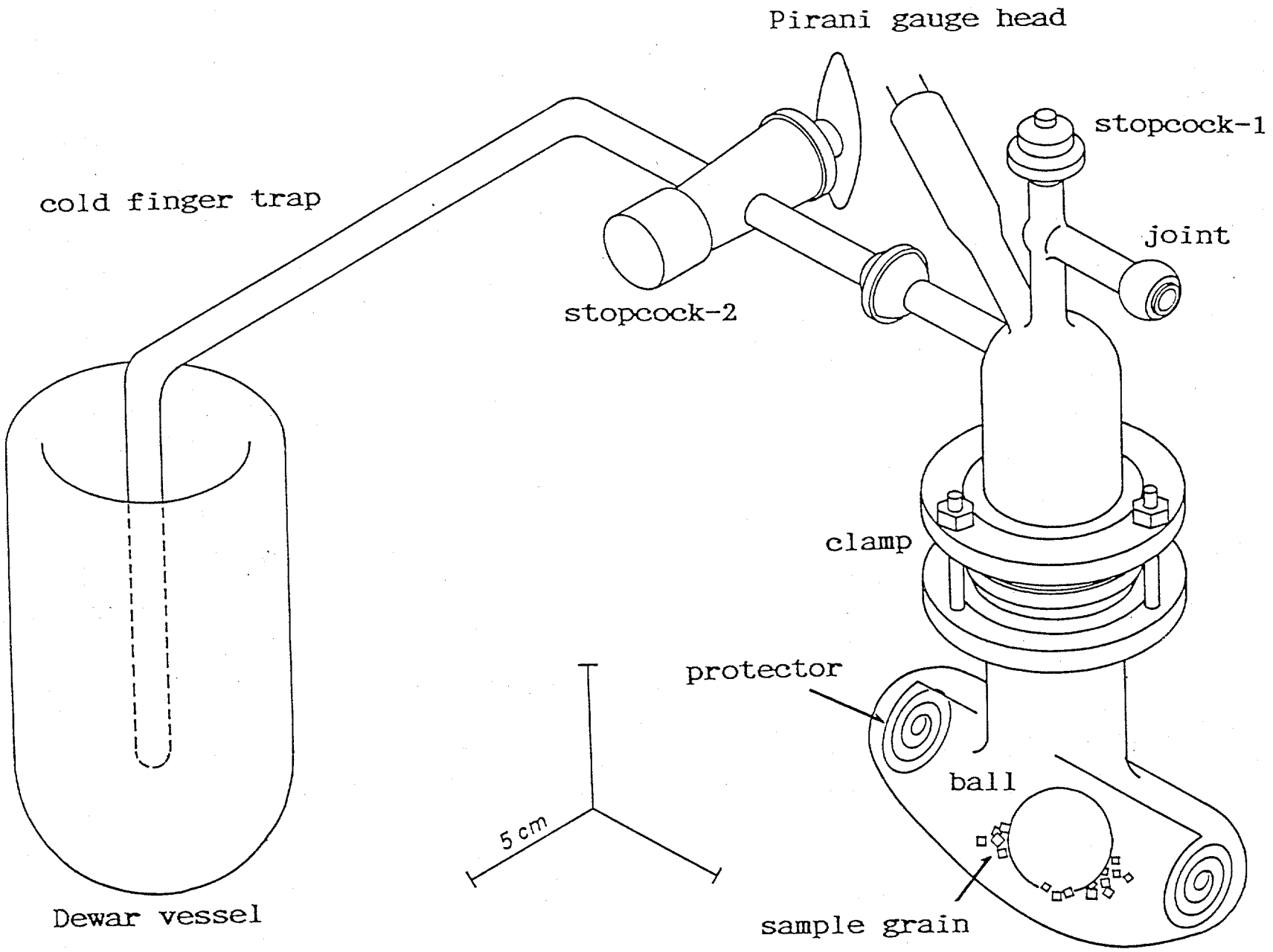

Fig.2-1. Perspective view of the ball mill.

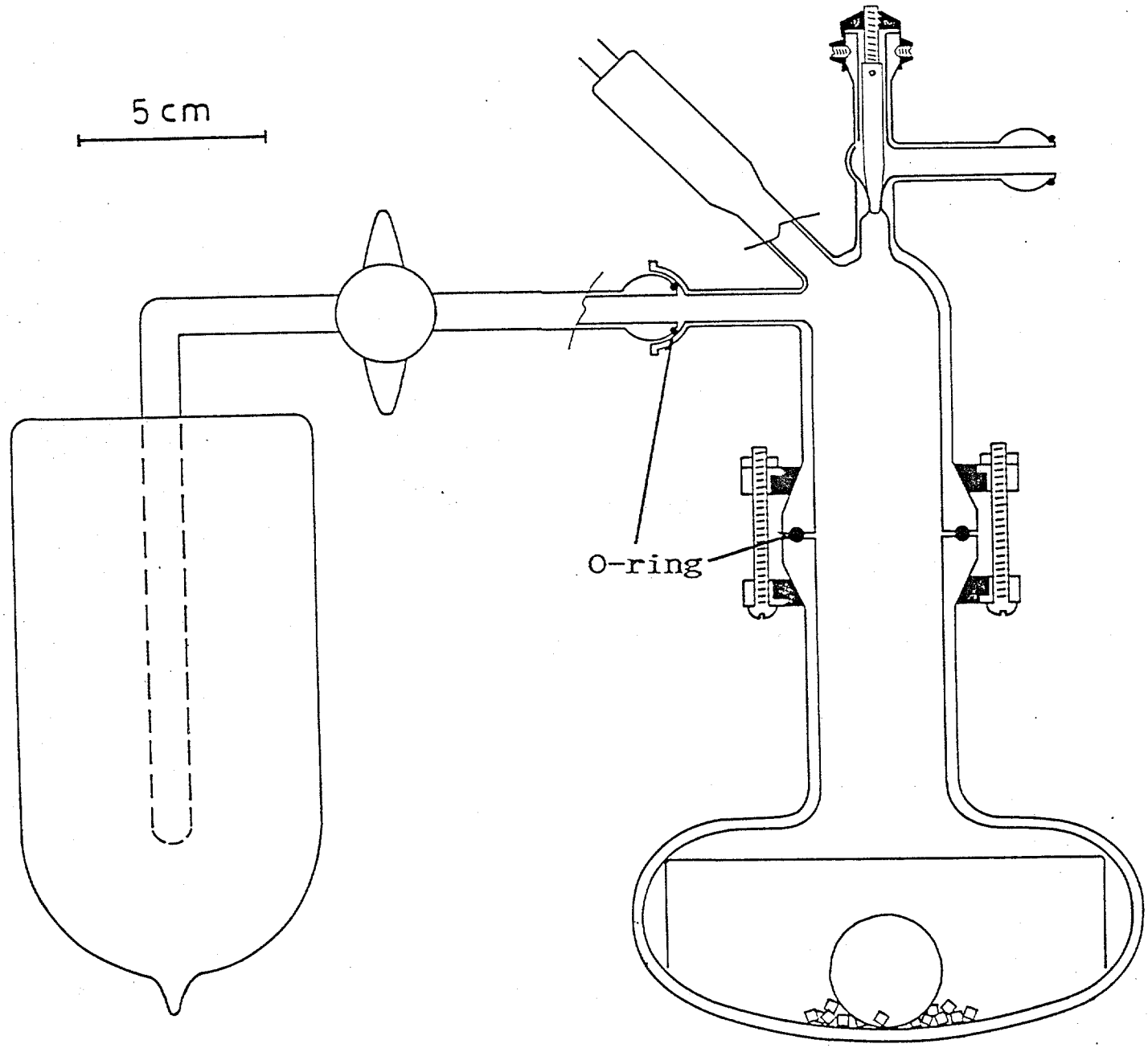

Fig.2-2. Cross section of the ball mill.

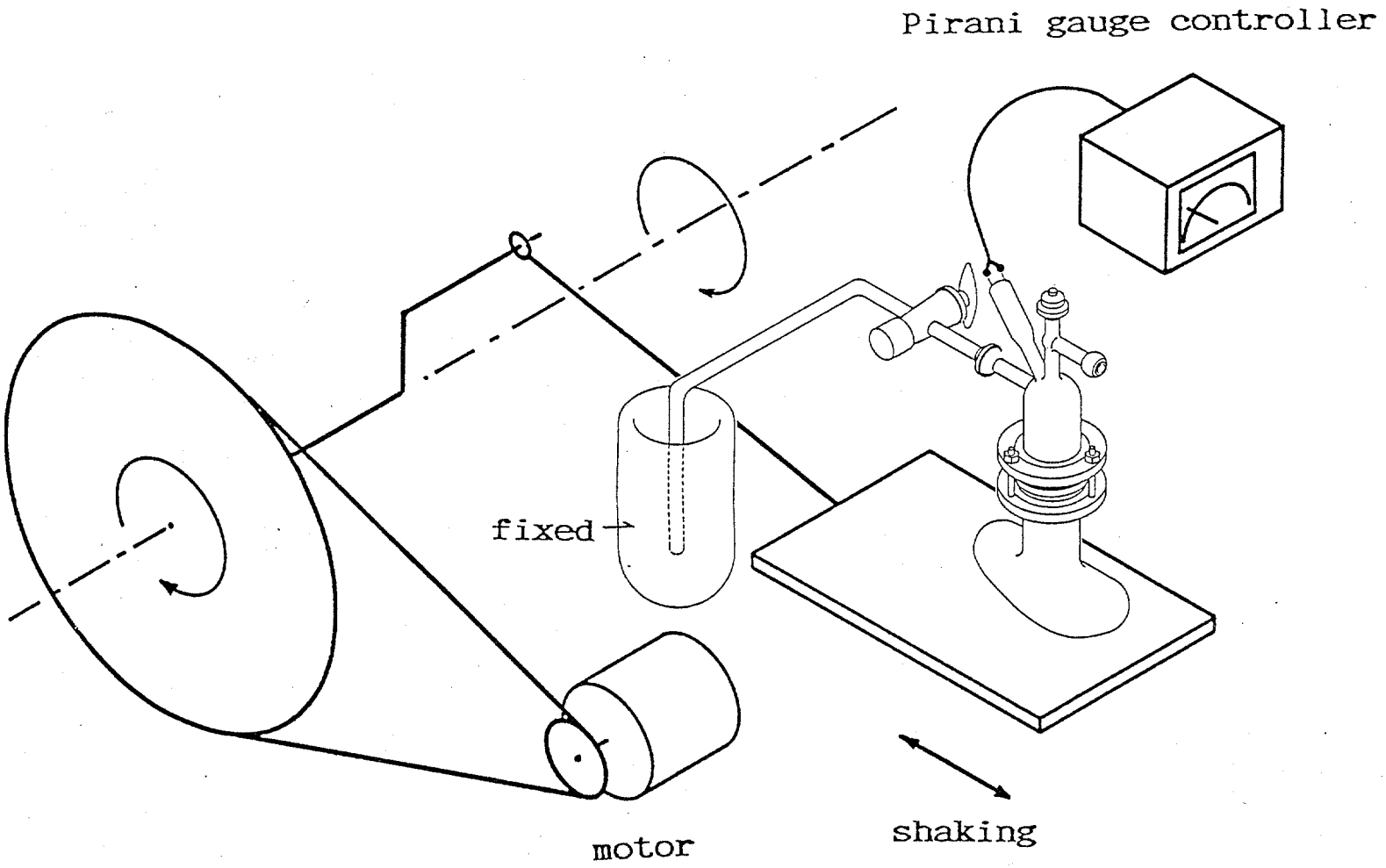

Fig.2-3. Shaking mechanism of the ball mill.
A Dewar vessel is fixed.

< 2-4 > Samples used in the extraction experiment

<2-4-1> Halite

Halite samples were collected from Mt.Sedom, close to the south end of Dead Sea, Israel. H-1, H-2, H-5 were collected at a quarry of Mt.Sedom, while H-3, H-4 were from the borehole of Amiaz 1 (Mazor *et* al.,1969). Fluid inclusions are dense in population outlining the cubic hopper growth stage, with vapor-liquid two phases. The diameter of the inclusions are less than 100 μm. In general, the shape of large inclusions is irregular and that of small inclusions less than 10 μm is spherical. Isolated inclusions are rare. Grain size of the samples prepared for crushing was 6 ~10 mesh. Halite samples were not pretreated according the the suggestion given in Horita and Matsuo (1985). Foreign matters were removed by hand-picking.

<2-4-2> Quartz

Q-1 ~Q-5 are milky white quartz collected from veins in the Kuga skarn-type tungsten deposit, Yamaguchi Prefecture, Japan (Sato 1980). Q-6 is a clear quartz collected from a vein at the Takemori rock crystal deposit, Yamanashi Prefecture, Japan. Diameters of fluid inclusions range from 5 to 100 μm for Q-1 through Q-6. All the inclusions consist of gas-liquid two phases. All the samples were washed in conc. HCl solution and rinsed in distilled water prior to the fractional separation by size distribution. During the washing of Q-1~Q-5, gas bubbling occurred vigorously due to the decomposition of calcium carbonate which fills cracks in the quartz. Grain size of the samples prepared for crushing was 10~20 mesh.

< 2-5 > Extraction experiment

<2-5-1> Pre-heating

The mineral sample was put into the mill together with the alumina ball. The amount of sample loaded was 10g and 5～6g for halite and quartz, respectively. The initial mesh sizes of halite and quartz samples were 6 ～10 mesh and 10～20 mesh, respectively, which are the maximum grain sizes to be able to crush by this mill. After having been assembled, the mill was evacuated through stopcock-1 while heating the lower part by ribbon heater over 12h. The heating temperature was set to 150℃ for halite to remove adsorbed water on the surface. For quartz samples the heating temperature was 280 ℃ to remove waters trapped in cracks and adsorbed on the surface. This heating procedure is called as *pre- heating* hereafter. In the pre-heating process, decrepitation may occur to some extent especially for the secondary inclusions.

<2-5-2> Crushing

After the pre-heating, stopcock-1 was closed and the mill was separated from the vacuum line. Then the mineral sample was crushed as described in the previous section. The crushing was carried out at room temperature, 15 ℃. Since fine powder of mineral adsorbs the mechanical energy of the ball, there is a limit for the size distribution of a sample even after a prolonged crushing period. The end of the effective crushing can be indicated by a Pirani gauge attached to the mill. In this study,

the duration of crushing was set to 1 hour. The effective crushing required less than 1 hour for most of the samples. After the crushing, the mill was left standing on the shaker for 1 hour to ensure the collection of volatiles at the cold finger trap. Volatile components collected in the cold finger trap during the crushing and standing period is called as *main-component* hereafter.

<2-5-3> Post-heating

After the crushing and standing, stopcock-2 (Fig.1) was closed and then the mill was connected again to the vacuum line. The lower part was heated up to 150 ℃ and 280℃ for 1 hour for halite and quartz, respectively. This heating procedure is called as *post-heating*. Volatiles released in this procedure were collected into a reservoir by condensation at liquid nitrogen temperature. This fraction of volatiles is called as *sub-component*. The main-component stored in the cold finger of the mill was subsequently collected into another reservoir.

<2-5-4> Procedure-1 and procedure-2

In order to obtain a dual set of data for the purpose of facilitating the interpretation of results, procedures with and without the use of the cold finger traps during the crushing process were carried out for the identical sample. The extraction procedures with and without the use of the cold trap during the crushing process are called as *procedure-1* and *procedure-2*, respectively, hereafter.

<2-5-5> Chemical and isotope compositions of volatiles in fluid inclusions.

Volatiles of inclusions from the halite samples consisted mostly of water and carbon dioxide. Only the amount and isotope ratios of water were measured because the amount of carbon dioxide was too small to measure the isotope ratios. Volatiles extracted from fluid inclusions of the quartz samples consisted mainly of water, carbon dioxide and methane. In this study, we measured the amounts and isotope ratios of water and carbon dioxide. $\delta^{18}O$ and δD values were measured for the extracted waters by an improved method of the micro carbon dioxide-water equilibration technique presented by Kishima and Sakai(1980). The lower limits of the sample size of water were 20 μmol and 5 μmol for δD and $\delta^{18}O$ measurements, respectively. When the amount of water is less than 20 μmol, the measured δD values remarkably lower than the original value were resulted by the use of uranium for reduction (refer to Chapter-Ⅲ). Other details of the measurement of amounts and isotope ratios of water and carbon dioxide are referred to Kazahaya and Matsuo (1985).

<2-5-6> Blank test

The extraction procedure-1 was carried out without a mineral sample to obtain the amount and composition of the blank of main- and sub-components. The blank material was consisted entirely of water. The amounts of water in main- and sub-components were 0.4 and 0.2 μmol, respectively, which are sufficiently low enough to affect the isotope ratios of the extracted water.

< 2-6 > Results

<2-6-1> Size distribution of the crushed samples

The size distribution of the crushed samples is shown in Table 2-1. The result obtained by the Kita's mill is also shown for comparison. Duration of the crushing process by the pounding mode using the Kita's mill was 0.5h, since a crushing period longer than 0.5h did not give better results (Kita 1981). It is clear in Table 2-1 that the rubbing mode gives better crushing efficiency than the pounding mode.

<2-6-2> Symbols to be used

In order to discuss the analytical results, we define the following symbols;

Wm (μmol) : Amount of water in the main-component.
δ Dm (‰) : $\delta D_{(SMOW)}$ of water in the main-component.
$\delta\,^{18}Om$ (‰) : $\delta\,^{18}O_{(SMOW)}$ of water in the main-component.
Cm (μmol) : Amount of carbon dioxide in the main-component.
$\delta\,^{13}Cm$ (‰) : $\delta\,^{13}C_{(PDB)}$ of carbon dioxide in the main-component.
$\delta\,^{18}Omc$(‰) : $\delta\,^{18}O_{(SMOW)}$ of carbon dioxide in the main-component.

The same symbols with the subscript s are defined for the sub-component.

Wt (μmol) : Wm+Ws
δD_{WM} (‰) : Weighted mean of δ Dm and δ Ds.

Table 2-1. Size distribution of crushed samples.

mesh size	quartz		halite
	Q-2	KITA	H-5
6− 10	−	−	12.6%
10− 20	43.6%	59.3%	11.9
20− 50	27.2	26.0	7.0
50−100	9.2	5.0	9.9
100−150	3.5	1.5	9.3
150−200	4.0	1.5	12.3
200−270	2.5	1.2	6.1
270～	10.0	5.5	30.9
sum	100.0	100.0	100.0

The initial grain size are 10-20 mesh for quartz and 6-10 mesh for halite. The amount of the samples loaded is always exactly 6.0g for quartz and 10g for halite. "KITA" refers to the result by the Kita's mill.

$\delta^{18}O_{WM}$ (‰) : Weighted mean of $\delta^{18}Om$ and $\delta^{18}Os$.

The symbols with subscript, (1) or (2) refer to the procedure-1 or -2, respectively. For example, Wm(1) and Wm(2) mean Wm by procedure-1 and -2, respectively.

<2-6-3> Quartz

In Table 2-2, the amounts and isotope ratios of the extracted water from different aliquots of Q-6 by both procedure-1 and -2 are shown. The results clearly indicate that there is an influence of the adsorption of water onto the surface of pulverized quartz on the amount and isotope ratios. First of all Wm(2) is smaller than Wm(1), on the other hand Ws(2) is larger than Ws(1). There is a only small difference by 1.8 μmol between averaged Wt(1) and Wt(2). $\delta^{18}Om(2)$ is higher than $\delta^{18}Om(1)$ being opposite to the trend for halite. However, $\delta^{18}Os(2)$ is also higher than $\delta^{18}Os(1)$. A significant difference between $\delta^{18}O_{WM}(2)$ and $\delta^{18}O_{WM}(1)$ is found, which is in contrast to the good agreement found in the case of halite.

The $\delta^{18}O$ value of quartz sample is measured only for Q-6 using the conventional oxidization method by Clayton and Mayeda (1963). The result is also give in Table 2-2.

In Table 2-3, the amounts and isotope ratios of the extracted water from quartz samples Q-1 ~Q-5 by procedure-1 are shown. It is noted that δDm values of Q-1 through Q-5 are almost the same. The uniformity in δD values is not a mere coincidence but indicates that the δD value of hydrothermal solution related to the quartz samples produced in the Kuga tungsten deposit is uniform. Ws/Wm ratios are much smaller than those of halite samples

Table 2-2. Amount and isotope ratios of the water extracted from different aliquots of sample Q-6.

run	Wm (μmol)	δ Dm (‰)	δ^{18}Om (‰)	Ws (μmol)	δ^{18}Os (‰)	Wt (μmol)	$\delta^{18}O_{WM}$ (‰)	Ws/Wm
Procedure-1								
1	23.7	-54	-6.0	3.6	-3.6	27.3	-5.7	0.15
2	28.5	-51	-6.4	4.9	-6.4	33.4	-6.4	0.17
3	25.3	-44	-6.8	4.3	-7.6	29.6	-6.9	0.17
4	25.5	-45	-6.2	4.5	-5.7	30.0	-6.1	0.18
5	22.7	-41	-7.0	3.1	-7.1	25.8	-7.0	0.14
av.	25.1	-47	-6.5	4.1	-6.1	29.2	-6.4	0.16
σ_{n-1}	2.2	5.3	0.41	0.72	1.56	2.9	0.54	0.016
Procedure-2								
6	17.1	-52	-2.5	8.9	+2.6	26.0	-0.8	0.52
7	21.1	-59	-4.0	10.0	+1.5	31.1	-2.7	0.47
8	18.6	-52	-3.0	8.8	+0.7	27.4	-1.8	0.47
9	17.0	-55	-2.8	8.2	+0.7	25.2	-1.7	0.49
av.	18.5	-55	-3.1	9.0	+1.4	27.4	-1.8	0.49
σ_{n-1}	1.9	3.3	0.65	0.75	0.90	2.6	0.78	0.024

$\delta^{18}O_{quartz}$ = +12.0‰ (to SMOW)

av.; average σ_{n-1} ; standard deviation

Runs 1～5 and runs 6～9 were carried by procedure-1 and -2, respectively. Wt is the sum of Wm and Ws. Amount of loaded samples is exactly 5.0g for each run. Ws was too small to give accurate values for δ Ds.

Table 2-3. Amount and isotope ratios of the water extracted from the quartz samples, Q-1～Q-5. (procedure-1)

	Wm (μmol)	δ Dm (‰)	δ ^{18}Om (‰)	Ws (μmol)	δ ^{18}Os (‰)	δ ^{18}O $_{WM}$ (‰)	Ws/Wm
Procedure-1							
Q-1	160.7	-48	-3.3	11.6	+2.0	-2.9	0.072
Q-2	126.4	-46	-7.1	11.7	+1.0	-6.4	0.092
Q-3	171.3	-49	-7.2	14.0	+1.5	-6.5	0.082
Q-4	232.6	-46	-2.3	14.1	+1.3	-2.1	0.061
Q-5	154.9	-48	-5.7	16.5	+7.2	-4.5	0.107

Amount of loaded samples is exactly 6.0g for each sample.

Amount of Ws was too small to give accurate values for δ Ds.

mentioned already. $\delta^{18}Os$ is consistently higher than $\delta^{18}Om$ for Q-1 ~Q-5, which is also the case for halite samples, whereas the difference between $\delta^{18}Om$ and $\delta^{18}Os$ is smaller when compared with that found in halite. For Q-4 sample with the smallest Ws/Wm ratio, the difference between $\delta^{18}Om$ and $\delta^{18}O_{WM}$ is in the range of analytical error.

In Table 2-4, the amount and isotope ratios of the CO_2 gas extracted from different aliquots of Q-6 are listed. Excepting for a slight difference between $\delta^{18}Omc(1)$ and $\delta^{18}Omc(2)$, the amount and isotope ratios by procedure-1 and -2 agree well each other. It is noted that Cs/Cm ratios in procedure-1 is definitely lower than Ws/Wm ratios of Q-6 in procedure-1, indicating that the degree of adsorption of the surface of pulverized samples is much less for CO_2 than H_2O.

<2-6-4> Halite

In Table 2-5, the amount and isotope ratios of different aliquots of H-5 by procedure-1 and -2 are given and in Table 2-6, those of the water extracted from H-1 ~H-4 are given.

In Table 2-5, we can see the influence of adsorption on the amounts and isotope ratios of the extracted water by comparing the amounts and isotope ratios of water obtained in procedure-1 and -2. Wm(2) is smaller than Wm(1), on the other hand, Ws(2) is larger than Ws(1). A good agreement between Wt(1) and Wt(2) is obtained. $\delta Dm(2)$ and $\delta^{18}Om(2)$ are both lower than $\delta Dm(1)$ and $\delta^{18}Om(1)$ respectively. A good agreement between $\delta^{18}O_{WM}(1)$ and $\delta^{18}O_{WM}(2)$ is noticeable. For the results in procedure-1, the standard deviation σ_{n-1} for $\delta^{18}O_{WM}$ is definitely smaller than that for $\delta^{18}Om$ and $\delta^{18}Os$.

Table 2-4. Amount and isotopic ratios of the CO_2 extracted from different aliquots of quartz sample Q-6.

run	Cm (μmol)	δ^{13}Cm (‰)	δ^{18}Omc (‰)	Cs (μmol)	Ct (μmol)	Cs/Cm
Procedure-1						
1	1.92	-9.7	+36.4	0.10	2.02	0.052
2	2.17	-9.9	+37.1	0.09	2.26	0.041
3	2.03	-9.8	+37.2	0.07	2.10	0.034
4	2.10	-9.7	+36.7	0.11	2.21	0.052
5	1.99	-9.7	+38.0	0.08	2.07	0.040
av.	2.04	-9.8	+37.1	0.09	2.13	0.044
Procedure-2						
6	1.98	-9.8	+38.8	0.07	2.05	0.035
7	2.18	-9.6	+38.6	0.10	2.28	0.046
8	2.11	-9.7	+38.9	0.05	2.16	0.024
av.	2.09	-9.7	+38.8	0.07	2.16	0.033

av.; average

Runs 1～5 and runs 6～8 were carried out by procedure-1 and -2, respectively. Ct is the sum of Cm and Cs. Amount of loaded samples is exactly 5.0g for each run.

Table 2-5. Amount and isotope ratios of the water extracted from different aliquots of sample H-5.

run	Wm (μmol)	δ Dm (‰)	δ ^{18}Om (‰)	Ws (μmol)	δ Ds (‰)	δ ^{18}Os (‰)	Wt (μmol)	δ ^{18}O $_{WM}$ (‰)	Ws/Wm
Procedure-1									
1	36.0	-54	-9.1	15.4	—	+24.8	51.4	+1.1	0.43
2	35.6	—	-11.7	16.1	—	+28.8	51.7	+0.9	0.45
3	30.9	-54	-5.8	10.8	—	+25.8	41.7	+2.4	0.35
4	32.5	-51	-7.0	12.7	—	+23.3	45.2	+1.5	0.39
av.	33.8	-53	-8.4	13.8	—	+25.7	47.5	+1.5	0.41
σ_{n-1}	2.5	1.7	2.59	2.5		2.32	4.9	0.67	0.044
Procedure-2									
5	21.7	-58	-15.8	24.3	-45	+19.4	46.0	+2.8	1.12
6	21.9	-64	-17.5	25.9	-56	+17.0	47.8	+1.2	1.18
7	21.6	—	-16.1	25.8	-48	+17.1	47.4	+2.0	1.19
av.	21.7	-61	-16.5	25.3	-50	+17.8	47.1	+2.0	1.16
σ_{n-1}	0.15	4.2	0.91	0.90	5.7	1.4	0.95	0.80	0.038

av.; average σ_{n-1} ; standard deviation

Runs 1-4 were carried out by procedure-1, while Runs 5-7 were by procedure-2 δ ^{18}O $_{WM}$ is the weighted mean of δ ^{18}Om and δ ^{18}Os. Amount of sample loaded is exactly 5.0g for each run.

Table 2-6. Amount and isotope ratios of the water extracted from the halite samples, H-1～H-4. (procedure-1)

	Wm (μmol)	δ Dm (‰)	δ ^{18}Om (‰)	Ws (μmol)	δ Ds (‰)	δ ^{18}Os (‰)	δ ^{18}O $_{WM}$ (‰)	Ws/Wm
H-1	188.1	-34	-5.1	55.0	-32	+26.6	+2.1	0.292
H-2	111.1	-41	-6.8	19.0	—	+26.8	-1.9	0.171
H-3	205.0	-38	-3.5	35.4	-26	+37.8	+2.6	0.173
H-4	217.6	-38	-4.0	36.2	-29	+32.5	+1.2	0.166

Amount of sample loaded is exactly 10.0g for each sample.

In Table 2-6, relatively large Ws/Wm ratios are found when compared with the corresponding ratios for quartz which are shown in Table 2-2. It should be noted that there are large differences about 30‰between $\delta\,^{18}Om$ and $\delta\,^{18}Os$, however, the differences between $\delta\,Dm$ and $\delta\,Ds$ are much less.

< 2-7 > Discussion

<2-7-1> Quartz

Although Ws/Wm ratios in both procedure-1 and -2 are consistently lower in the case of quartz than in halite (refer to Table 2-2 and 2-5), the mechanism of vapor adsorption onto the surface of powdered sample is quite different because of the radical formation during the crushing process in the case of quartz. The presence of radicals should enhance the trapping of water vapor. Whereas, the lower ratio of Ws/Wm in the case of quartz is certainly related to the smaller surface area of quartz grains after crushing (refer to Table 2-1).

For the convenience of following discussion, the following notations are introduced.

WM-1, WM-2: The water in main-component extracted by procedure-1 and -2, respectively.

WS-1, WS-2: The water in sub-component extracted by procedure-1 and -2, respectively.

AW: The water excessively adsorbed onto the quartz surface by the procedure-2 than by -1.

DW: The desorbed water during the post-heating by procedure-2.

In order to estimate the $\delta^{18}O$ value of the original water contained in fluid inclusions ($\delta^{18}Oo$) of Q-6, the following four equations are necessary,

$$\delta^{18}Oo \times Wt(1) = \delta^{18}Om(1) \times Wm(1) + \delta^{18}O_{Aw}(1) \times [Wt(1)-Wm(1)] \quad (1)$$

$$\delta^{18}O_o \times Wt(2) = \delta^{18}O_m(2) \times Wm(2) + \delta^{18}O_{Aw}(2) \times [Wt(2)-Wm(2)] \quad (2)$$

and $$\delta^{18}O_{Aw}(1) = \delta^{18}O_o \times (1 - f_1^{\alpha})/(1 - f_1) \quad (3)$$

and $$\delta^{18}O_{Aw}(2) = \delta^{18}O_o \times (1 - f_2^{\alpha})/(1 - f_2), \quad (4)$$

where f_1 and f_2 correspond to $Wm(1)/Wt(1)$ and $Wm(2)/Wt(2)$ respectively and α denotes the $^{18}O/^{16}O$ fractionation factor during the adsorption process at 288K. Equations (1) and (2) are respectively the material balance equations of oxygen isotopes for procedure-1 and -2. Equations (3) and (4) are Rayleigh distillation equations for the isotopic fractionation of during the adsorption process.

In the above four equations, the unknowns are $\delta^{18}O_o$, $\delta^{18}O_{Aw}(1)$, $\delta^{18}O_{Aw}(2)$ and α. By solving the equations (1),(2),(3) and (4) simultaneously, after substituting the numerical data given in Table 2-2, we obtain a following set of values:

$$\delta^{18}O_o : -9.2 \text{ ‰},$$
$$\delta^{18}O_{Aw}(1) : -26.0 \text{ ‰},$$
$$\delta^{18}O_{Aw}(2) : -19.9 \text{ ‰},$$
and $$\alpha : 0.9817 .$$

In the above calculations, all the $\delta^{18}O$ values are converted to $1+10^{-3}\delta^{18}O$, and $Wt(1)=Wt(2)=29.2\ \mu mol$, so that $Wt(2)-Wm(2)$ is put to be equal to $10.7\ \mu mol$.

By the same way, another set of values for hydrogen isotopes

are obtained using the data given in Table 2-2.

δD_o : -43.0 ‰ ,
$\delta D_{Aw}(1)$: -13.2 ‰ ,
$\delta D_{Aw}(2)$: -22.0 ‰ ,
and α : 1.028 .

In the case of hydrogen isotopes, the situation is much simpler. However, there is no measured data for $\delta D_s(1)$ and $\delta D_s(2)$ due to the small amount of the extracted water for both Ws(1) and Ws(2), and we can not compare the relation between $\delta D_{Aw}(1)$ versus $\delta D_s(1)$ and δD_{Aw} versus $\delta D_s(2)$.

In order to obtain the original δD and $\delta^{18}O$ values, a set of data for Wm, Ws, δD_m and $\delta^{18}O_m$ for both procedure-1 and -2, altogether 8 data, together with the corresponding data of amounts, is definitely necessary.

δD_s and $\delta^{18}O_s$ values in addition give a key to elucidating the isotopic behavior in the adsorption-desorption process. Most of the previous results on isotopic data of fluid inclusions in quartz have dealt with what are obtained by procedure-2 (without a cold trap). Therefore, the obtained δD values give only a sort of the lower limit, and $\delta^{18}O$ values the upper limit when the correct original values are compared with the data obtained in Table 2-2. In this respect, the isotopic data for the main component obtained by procedure-1 are closer to those of the original values as seen in Table 2-2.

When the results obtained for $\delta^{18}O_o$, $\delta^{18}O_{Aw}(1)$ and $\delta^{18}O_{Aw}(2)$ are compared, it is clear that the adsorbed water is much depleted in ^{18}O, indicating that the uptake process of water vapor by powdered quartz is not a simple adsorption process.

It is interesting to note that the $\delta^{18}O$ value of water vapor in isotope exchange equilibrium with the host quartz ($\delta^{18}O$: +12.0 ‰) at 288K is calculated to be -25.8 ‰ by the equation,

$$10^3 \ln \alpha = 3.52 \times 10^6 T^{-2} - 4.35 \qquad (5),$$

given by Kita (1985) for amorphous quartz in the temperature range from 30-100 ℃. For AW-1 where the extent of adsorption is 14%, $\delta^{18}O_{AW}(1)$ is -26‰, indicating the released water vapor is in near exchange equilibrium with the host quartz before being uptaken (adsorbed) by fresh surface of quartz powder. when the extent of adsorption proceeds, like in the case of AW-2 (36.6% adsorbed), $\delta^{18}O_{AW}(2)$ comes closer to the original value of -9.2 ‰ due to the Rayleigh process. The situation is graphically presented in Fig.2-4.

According to Arends et al., (1963) and Schrader et al., (1969), Si and SiO radicals are formed by mechanical crushing of quartz. By the reaction of water vapor with those radicals, silanol radicals (-SiOH) may form according to the reaction,

$$H_2O + \text{-Si}\cdot + \text{-SiO}\cdot \rightarrow 2\text{-SiOH} \qquad (6).$$

In this process, one of the oxygen atoms of two silanol radicals is derived from the water vapor. Then the $\delta^{18}O$ values of silanol group for procedure-1 and -2 are calculated respectively to be -7.0‰ [(12.0 - 26.0)/2] and -4.0 ‰ [(12.0 - 19.9)/2]. Even if the complete recovery of water from the silanol group is guaranteed during the post-heating process, one of the two oxygen atoms contained in the silanol group should be left behind during the decomposition (dehydration) process, for

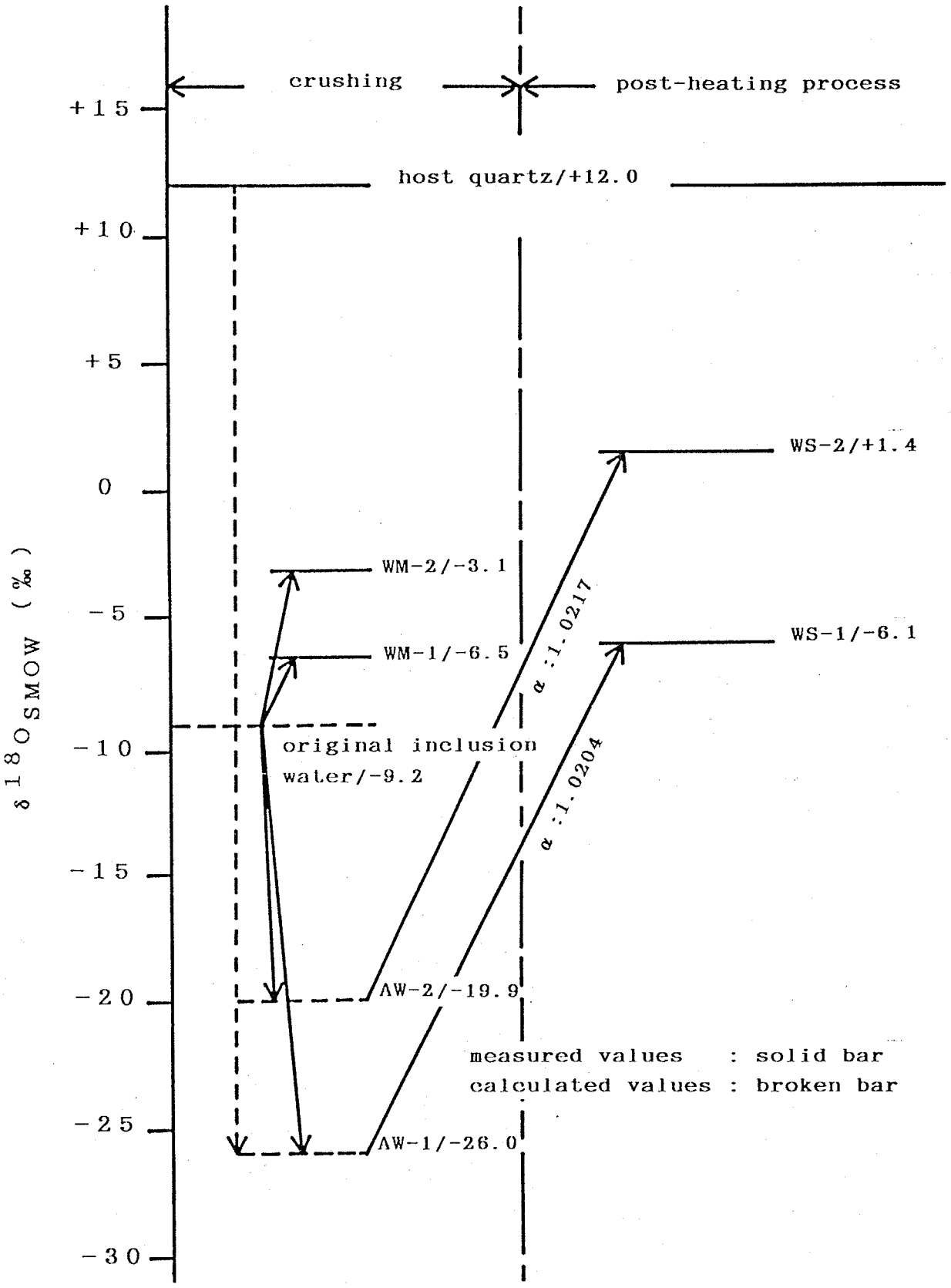

Fig.2-4. Relation among the $\delta^{18}O$ values of water and quartz

which we know nothing about the isotope fractionation especially under kinetic condition at 280℃ (the temperature of post-heating). Note that the nominal fractionation factors corresponding to AW-1 → WS-1 and AW-2 → WS-2 are close each other, 1.0204 and 1.0217, respectively, as shown in Fig.2-4. At least qualitatively, however, the fact that $\delta^{18}Os(1)$, -6.1 ‰, and $\delta^{18}Os(2)$, +1.4 ‰ are always higher than the corresponding values for the silanol group of -7.0‰ and -4.0 ‰ respectively, suggests that during the post-heating process,

1) ^{18}O is enriched in the desorbed (dehydrated) water rather than in SiO_2 formed from the silanol group, or
2) further incorporation of oxygen atoms of the host quartz takes place by exchange during the desorption or dehydration process;

the later case being more plausible.

In Table 2-3, it should be noted that the difference between $\delta^{18}Os(1)$ and $\delta^{18}Om(1)$ for Q-1 through Q-5 is much larger than that for Q-6 seen in Table 2-2. This contradiction may be attributed to the difference in the water content between the Q-1 ～Q-5 group and Q-6. When the amount of water released during the crushing process by procedure-1 for the former group is more than 100 μmol, the amount of water adsorbed on the surface of quartz increases considerably, and in the process of the post-heating the isotope exchange with quartz to give the water of sub-component more enriched in ^{18}O.

However, the disagreement in the difference between $\delta^{18}Os(1)$ and $\delta^{18}Om(1)$ between Q-6 and Q-1 ～Q-5 group may be attributed to another reason, e.g., the nature of quartz. As mentioned in the section of sample-description, the appearance of Q-1 ～Q-5 is different from that of Q-6, i.e., Q-1～Q-5 are milky white, whereas Q-6 is transparent. Kazahaya and Matsuo

(1985) found that a milky white quartz contains a species of water released in vacuum over 700 ℃, which is not contained in a transparent quartz. The water contained in other than fluid inclusions of milky white quartz may also be a source to raise the $\delta^{18}Os(1)$ value.

In Table 2-4, the amount and isotope ratios of CO_2 extracted from Q-6 are shown. The amounts and isotope ratios by both procedures agree well within the analytical error except for a small difference between $\delta^{18}Omc(1)$ and $\delta^{18}Omc(2)$. The difference by 1.6 ‰ between $\delta^{18}Omc(1)$ and $\delta^{18}Omc(2)$ is out of the range of analytical error. $\delta^{18}Omc(2)$ seems to be lowered through an isotope exchange with the adsorbed water on quartz surface depleted in ^{18}O as mentioned in the previous paragraphs. Excepting for a small shift in $\delta^{18}O$, it is concluded that the influence of adsorption on amounts and isotope ratios of CO_2 gas is not detected within the present analytical precisions.

In Table 2-7, differences between $\delta^{18}Omc(1)$ and $\delta^{18}Om(1)$, $\Delta^{18}O$, obtained for all the quartz samples are given. The values of $\Delta^{18}O$ range from 38.1 to 42.9 ‰. $\Delta^{18}O$ can be compared directly with the oxygen isotope fractionation factor between CO_2 and water. Neglecting the salt effect, the isotope exchange equilibrium temperature for each sample are calculated using the equation presented by O'Neil and Adami (1969). The results are also shown in Table 2-7. The calculated temperature seems reasonable, however, the temperatures for Q-1 ~Q-5 are somewhat higher than 288K of room temperature. The higher temperatures can be attributed to a salts effect on the fractionation factor or an incomplete attainment of the equilibrium between CO_2 and water at room temperature within the period from the end of pre-heating to the start of crushing.

Table 2-7. Differences between $\delta^{18}O$ values of the CO_2 and water extracted from quartz samples Q-1～Q-6

	$\delta^{18}Om$ (‰)	$\delta^{18}Omc$ (‰)	$\Delta^{18}O$ (‰)	T (K)
Procedure-1				
Q-1	-3.3	+38.0	40.6	298
Q-2	-7.1	+31.5	38.1	311
Q-3	-7.2	+34.1	40.8	296
Q-4	-2.3	+39.2	40.8	296
Q-5	-5.7	+35.1	40.2	300
Q-6 [a)]	-6.5	+37.1	42.9	286

$\Delta^{18}O = 10^3 \ln[(\delta^{18}Omc + 1000)/(\delta^{18}Om + 1000)]$

a); Averaged values are used.

$10^3 \ln \alpha_{(carbon\ dioxide\ -\ water)} = 16.60(10^3 T^{-1}) - 15.19$, given by O'Neil and Adami (1969) is used for the calculation of the equilibrium temperature.

<2-7-2> Halite

As seen in Table 2-5 (results on the H-5 halite), the adsorption of water vapor affects significantly the results on the amount and isotope ratios of the extracted water.

Smaller Wm(2) than Wm(1) indicates that the adsorption of water vapor onto the surface of halite powder during the crushing process under vacuum takes place. On the other hand, larger Ws(2) than Ws(1) indicates that the use of a cold trap during the crushing process reduces the amount of adsorption. A good agreement between Wt(1) and Wt(2) means an effective recovery of the adsorbed water by the post-heating.

δ Dm(2) and $\delta\,^{18}$Om(2) are lower than δ Dm(1) and $\delta\,^{18}$Om(1) respectively, which suggests that an enrichment in heavier isotopes in the adsorbed water occurs in the adsorption process. Relatively large isotope fractionation for oxygen than hydrogen in the adsorption process is inferred. Large difference between $\delta\,^{18}$Om and $\delta\,^{18}$Os by both procedures are found for all the samples H-1 ~H-5 (Tables 2-5,2-6) however, the difference between δ Dm(2) and δ Ds(2) is as large as 10‰ as seen in Table 2-5.

Again the same notations such as WM-1, WM-2, WS-1, WS-2, AW and DW used in the case of halite are introduced for the following discussion.

Let us first assume that the adsorption-desorption process is reversible and the adsorbed water can be recovered completely during the post-heating process. Then the following material balance equations are independently possible for the estimation of $\delta\,^{18}$Oo,

$$\delta\,^{18}\mathrm{Oo} \times \mathrm{Wt}(1) = \delta\,^{18}\mathrm{Om}(1) \times \mathrm{Wm}(1) + \delta\,^{18}\mathrm{Os}(1) \times [\mathrm{Wt}(1) - \mathrm{Wm}(1)] \quad (7)$$

$$\delta^{18}O_o \times Wt(2) = \delta^{18}O_m(2) \times Wm(2) + \delta^{18}O_s(2) \times [Wt(2)-Wm(2)] \quad (8)$$

Substituting numerical values for the H-5 sample in Table 2-5 into the above equations, $\delta^{18}O_o$ is calculated to be +1.4 ‰ from (7) and +2.1‰ from (8). A good agreement between the two values may be concluded when the accumulation of errors in the process of calculation, and +1.8 ‰ as an average is taken for $\delta^{18}O_o$. However, δD_o can be calculated to be -55‰ only by a similar equation to eq.(8), due to the lack of data on $\delta^{18}O_s(1)$.

According to Horita (1987), $\delta^{18}O$ and δD values of the Dead Sea brine are in the ranges from +2 to +5 ‰ and +2 to +10‰, respectively, depending on the density of the brine. The calculated value of $\delta^{18}O_o$ of +1.8‰ agrees marginally with the Dead Sea brine value, but that of δD_o of -55 ‰ is by far the lower. The direct comparison of fluid inclusions in the H-5 halite and the Dead Sea brine without considering the "evolution" of fluid inclusions after the entrapment due to the recrystallization of the host halite and other factors is not reasonable.

In the above calculation for estimating the $\delta^{18}O_o$ and δD_o values, $\delta^{18}O_s$ and δD_s data of the sub-component obtained during the post-heating process are involved. The fact that the H-5 halite is marine in origin and a large amount of Mg^{2+} (Ca^{2+}) is contained in the brine in fluid inclusions should be considered (Horita and Matsuo, 1986), because some hydrate salts containing Mg^{2+} may form when the vesicles are broken to evaporate the brine during the crushing process.

Hydrate salts, such as $KMgCl_3 6H_2O$ (carnallite), $MgCl_2 6H_2O$ (bischofite), $CaSO_4 2H_2O$ (gypsum), $CaMg_2Cl_6 12H_2O$ (tachhydrite) never release all the oxygen atoms

of the water of crystallization contained at the temperature of post-heating of 280 ℃, e.g.,

$$MgCl_2 6H_2O \rightarrow MgO + 5H_2O + 2HCl \qquad (9).$$

Therefore, the complete recovery of water from hydrate salts is impossible. Besides, there is a possibility of oxygen isotope exchange between the water vapor and carbonates of sulfates during the dehydration process in the post-heating.

The use of the data on the sub-component such as $\delta^{18}Os$ and δDs in order to estimate the original values, $\delta^{18}Oo$ and δDo, is not recommended. Then the material balance equations using only the data on the main-component as done in the case of quartz is the reliable way to estimate the original values. However, the halite of fresh water origin such as the halite from Searles Lake, California, contains fluid inclusions with overwhelming concentrations of Na^+ as cation and Cl^- and HCO_3^- as anion (Horita, 1987). In such a case, no admission of dehydrated water from hydrate salts is expected in the process of post-heating. Hence the reversible adsorption-desorption assumption with the use of data on the sub-component can be applied to such a type of halite.

In the following simultaneous equations using only the data on the main-component, it is assumed that the dehydration of hydrate salts occurs only in the process of post-heating.

$$\delta^{18}Or \times Wt(1) = \delta^{18}Om(1) \times Wm(1) + \delta^{18}O_{Aw}(1) \times [Wt(1)-Wm(1)] \qquad (10)$$

for procedure-1,

$$\delta^{18}Or \times Wt(2) = \delta^{18}Om(2) \times Wm(2) + \delta^{18}O_{AW}(2) \times [Wt(2)-Wm(2)] \quad (11)$$

for procedure-2,

$$\delta^{18}O_{AW}(1) = \delta^{18}Or \times (1 - f_1^{\alpha})/(1 - f_1) \quad (12),$$

and $$\delta^{18}O_{AW}(2) = \delta^{18}Or \times (1 - f_2^{\alpha})/(1 - f_2), \quad (13),$$

where $\delta^{18}Or$ denotes the $\delta^{18}O$ values of released water during crushing process (excluding the water taken to form by hydrate salts), and the other notations are the same as those discussed in the case of quartz. Substituing the average values for H-5 halite given in Table 2-5, a following set of results in obtained,

$$\delta^{18}Or : -2.1 \text{ ‰},$$
$$\delta^{18}O_{AW}(1) : +13.3 \text{ ‰},$$
$$\delta^{18}O_{AW}(2) : +9.9 \text{ ‰},$$
$$\text{and} \quad \alpha : 1.0185 .$$

Another set of results for hydrogen isotopes is also obtained by the same way,

$$\delta Dr : -47 \text{ ‰},$$
$$\delta D_{AW}(1) : -32 \text{ ‰},$$
$$\delta D_{AW}(2) : -35 \text{ ‰},$$
$$\text{and} \quad \alpha : 1.0192 .$$

A schematic presentation of the concept of a variety of water

species of halite dealt with in this study is given below.

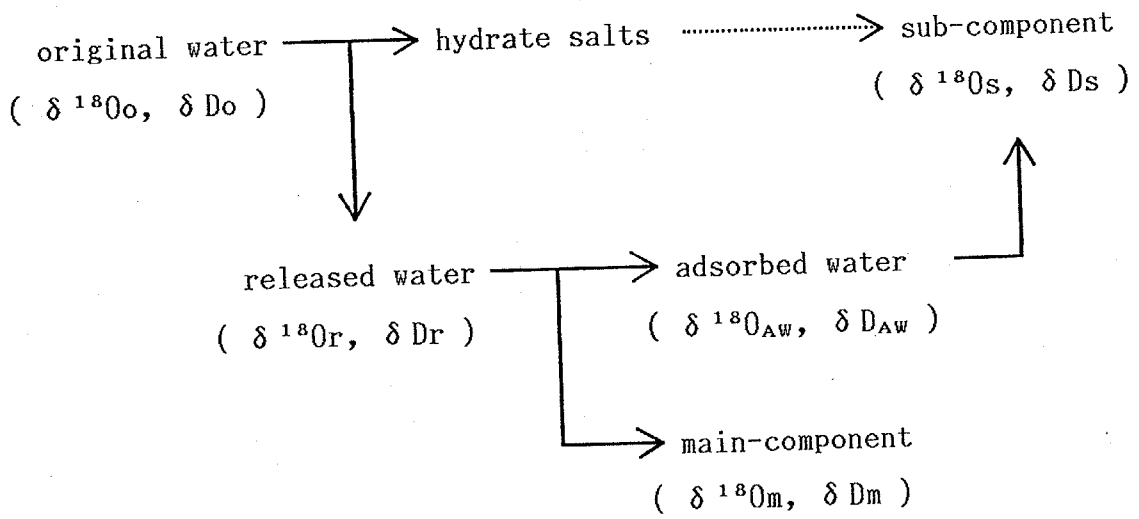

where the dotted line indicates the partial recovery. As seen in the above diagram, the isotope data on hydrate salts are necessary in order to estimate the original values of $\delta\,^{18}O_o$ and δD_o. For the reason mentioned already, the isotope data on hydrate salts is impossible to estimate in this study. The acquisition of the data is, however, possible only when the average chemical composition of brine in halite is known, together with the experimental information for the kinetic isotope effect on the decomposition process of hydrate salts containing Mg^{2+} (Ca^{2+}).

If the amount of water contained in hydrate salts is negligible compared with that of the released water, then $\delta\,^{18}O_r$ and δD_r obtained above can represent the $\delta\,^{18}O_o$ and δD_o values.

When $\delta\,^{18}O_{AW}(1)$ of +13.3‰ is compared with $\delta\,^{18}O_s(1)$ of +25.7 ‰ and $\delta\,^{18}O_{AW}(2)$ of +9.9 ‰ with $\delta\,^{18}O_s(2)$ with +17.8‰, it is clear that the water derived from hydrate salts is definitely more enriched in ^{18}O than the adsorbed water, which seems to be reasonable. Similarly when $\delta D_{AW}(2)$ of -35‰ is compared with $\delta D_s(2)$ of -50‰, the trend is just opposite, i.e., deuterium

is more enriched in the adsorbed water than hydrate salt, which seems also plausible.

Since, ^{18}O is always enriched in the water of crystallization of hydrate salts than the coexisting saturated solutions (e.g., Fontes and Gonfiantini, 1967 for gypsum; Kamegai and Matsuo for sulfate hydrates, unpublished). On the other hand, deuterium is always depleted in the water of crystallization (e.g., Matsuo et al., 1972 for saline minerals; Horita, 1987 for carnallite and tachhydrate) except for rare cases of $Na_2SO_4 10H_2O$ and $Na_2CO_3 10H_2O$ (Pradhananga and Matsuo, 1985).

< 2-8 > Concluding Remarks

By the use of a new type ball mill with a cold finger, the operation for crushing mineral samples (halite and quartz) was carried out by a rubbing mode. With and without the use of a cold finger, a set of data on the amount and isotope ratios of the extracted water was obtained.

In order to obtain the original (true) values for δ Do and $\delta\,^{18}$Oo of the water in inclusions, the set of data is definitely necessary. Previous data published on isotope ratios of fluid inclusions in minerals need be redetermined by the present method.

Decrepitation or melting by heating gives wrong results (Kazahaya and Matsuo, 1985 for quartz, Horita and Matsuo, 1986 for halite) though not mentioned in this paper.

The major problem in the case of halite is the salt effect on the evaporation of brine and the decomposition of hydrate salts formed after the opening of fluid inclusions, which has been pointed out already by Horita (1987) when Mg^{2+} and/or Ca^{2+} with high concentrations are present in the brine, oxide and/or hydroxide remain even after the post-heating to retain a part of oxygen atoms included in the water of crystallization of hydrate salts.

On the other hand, the major problem in the case of hydrothermal quartz is the incorporation of oxygen atoms of the host quartz during the adsorption-desorption process of water.

However, the present method offers a paradigm in order to obtain the original δ D and $\delta\,^{18}$O values of water contained in fluid inclusions of quartz, though the trial to reach the original values of halite is not perfect, due to the lack of the method for chemical analysis of brine in inclusions of halite.

Finally, the amount and isotope ratios of water in fluid inclusions in general are much uniform, as exemplified by the data in Table 2-2 and 2-6 in a chunk of mineral sample, in contrast to the apparent heterogeneity in size and number density of fluid inclusions by visual observations.

References

Arends,J., A.J.Dekker and W.G.Perdok (1963)
Color centers in quartz produced by crushing
Phys.Status Solid, 3, 2275-2279 (1963)

Barker,C. and Torkelson,B.E. (1975)
Gas adsorption on crushed quartz and basalt.
Geochim.Cosmochim.Acta 39, 212-218.

Clayton,R.N. and T.Mayeda (1963)
The use of bromine pentafluoride in the extraction of oxygen from oxides and silicates for isotopic analysis
Geochim.Cosmochim.Acta, 27, (1963), 43-52

Horita,J. (1987)
Doctoral thesis , Tokyo Institute of Technology, Tokyo, Japan

Horita,J. and Gat,J.R.
Stable isotope analysis of water from concentrated brines.
Chem.Geol.(Isot.Geosci.) (submitted)

Horita,J. and Matsuo,S. (1986)
Extraction and isotopic analysis of fluid inclusions in halites.
Geochem.J. 20, 261-272.

Kazahaya,K. and Matsuo,S. (1985)
A new ball-milling method for extraction of fluid inclusions from minerals.
Geochem.J. 19, 45-54.

Kishima,N. and Sakai,H. (1980)
Oxygen-18 and deuterium determination on a single water sample of a few milligrams.
Anal.Chem. 52, 356-358.

Kita,I. (1981)
A new type ball mill made of pyrex glass.
Geochem.J. 15, 289-291.

Kita,I., Matsuo,S. and Wakita,H. (1982)
H_2 generation by reaction between H_2O and crushed rock; An experimental study on H_2 degassing from the active fault zone.
J.Geophys.Res. 87, 10789-10795.

Mazor,E., Rosenthal,E. and Ekstein,J. (1969)
Geochemical tracing of mineral water sources in the south western Dead Sea basin, Israel.
J.Hydrol. 7, 246-275.

O'Neil,J.R. and Adami,L.H. (1969)
The oxygen isotope partition function ratio of water and the structure of liquid water.
J.Phys.Chem. 73, 1553-1558.

Roedder,E., Ingram,B. and Hall,W.E. (1963)
Studies of fluid inclusions Ⅲ: Extraction and quantitative analysis of inclusions in the milligram range.
Econ.Geol. 58, 353-374.

Roedder,E. (1984)

The fluids in salt.

Am.Mineral. 69, 413-439.

Sato,K. (1980)

Tungsten skarn deposit of the Fujigatani Mine, southwest Japan.

Econ.Geol. 75, 1066-1082.

Schrader,R., R.Wissing and H.Kubsch (1969)

Zur Oberflachenchemie von mechanisch activiertem Quarz

Z.Anorg.Allg.Chem., 365,191-198,(1969)

Truesdell,A.H. (1974)

Oxygen isotope activities and concentrations in aqueous salt solution at elevated temperatures —Consequences for isotope geochemistry.

Earth Planet.Sci.Lett. 23, 387-396.

Chapter-Ⅲ

$^{18}O/^{16}O$ and D/H ratio determinations for water samples of several micro moles

Abstract

This paper describes an improved procedure for D/H and $^{18}O/^{16}O$ ratio analyses presented originally by Kishima and Sakai (1980). A sealed glass tube for the isotope exchange equilibration between water and CO_2 gas was employed instead of a conventional container with a greased stopcock. The use of the sealed tube enabled us to handle 5~6 μmol of water for accurate and precise $\delta^{18}O$ measurement, with precision of 0.42‰($1\sigma_{n-1}$). However, for precise δD measurement more than 40 μmol of water was required.

< 3-2 > Introduction

Simultaneous analyses of $^{18}O/^{16}O$ and D/H for a few milligrams of water are important in the field of geochemistry. Suzuoki and Itoh (1974) presented a method utilizing the oxygen isotope equilibration between water vapor and CO_2 gas catalyzed by a hot platinum filament. Kishima and Sakai (1980) described a more reliable equilibration method between liquid water and CO_2 gas under a CO_2 pressure higher than 1 atm in a container equipped with a greased stopcock. The CO_2 gas, however, sometimes may leak out through the greased stopcock, and contamination and/or loss of sample water through the grease may also occur. A sealed Pyrex glass capillary tube was used in this work for the reaction vessel to eliminate the greased stopcock. Thus the lower limit of the amount of a sample required for a reliable analysis was reduced. A simple procedure was shown for the preparation of a series of water samples of small amounts with constant $^{18}O/^{16}O$ and D/H ratios.

Experimental

D/H and $^{18}O/^{16}O$ ratios of water are expressed in this report by the δ-notation:

$$\delta D \text{ or } \delta^{18}O = \left(\frac{R_{sample}}{R_{standard}} - 1 \right) \times 1000,$$

where R_{sample} is the D/H or $^{18}O/^{16}O$ ratio of the sample water and $R_{standard}$ is that of the Vienna Standard Mean Ocean Water (V-SMOW) (Gonfiantini,1978).

Two series of water samples, A and B, were prepared to check the accuracy of the isotope ratio measurements, The amount of each water sample in A series ranged from 5 to 51 μmol and that in B series from 43 to 1.1×10^{5} μmol.

The A series samples were made from moist air collected into an air bag on the roof of a building of Tokyo Institute of Technology, where the air temperature, the relative humidity and the atmospheric pressure were 9.5℃ ,53% and 1,016mb, respectively. The volume of the air bag was about 4 *l*. The air temperature in the laboratory was always kept higher than on the roof where the air was sampled to prevent the condensation of moisture in the bag. The amount of the water vapor in the air bag was estimated to be 1.1×10^{-3}mol. The vacuum line shown in Fig.3-1 was used for the preparation of A series samples. First, trap-1 (T1) was cooled with liquid nitrogen and the air was leaked from the air-bag (AB) through a needle valve(N), while stopcock S1, S2, S3 and S5 were open. I adjusted the needle valve to control

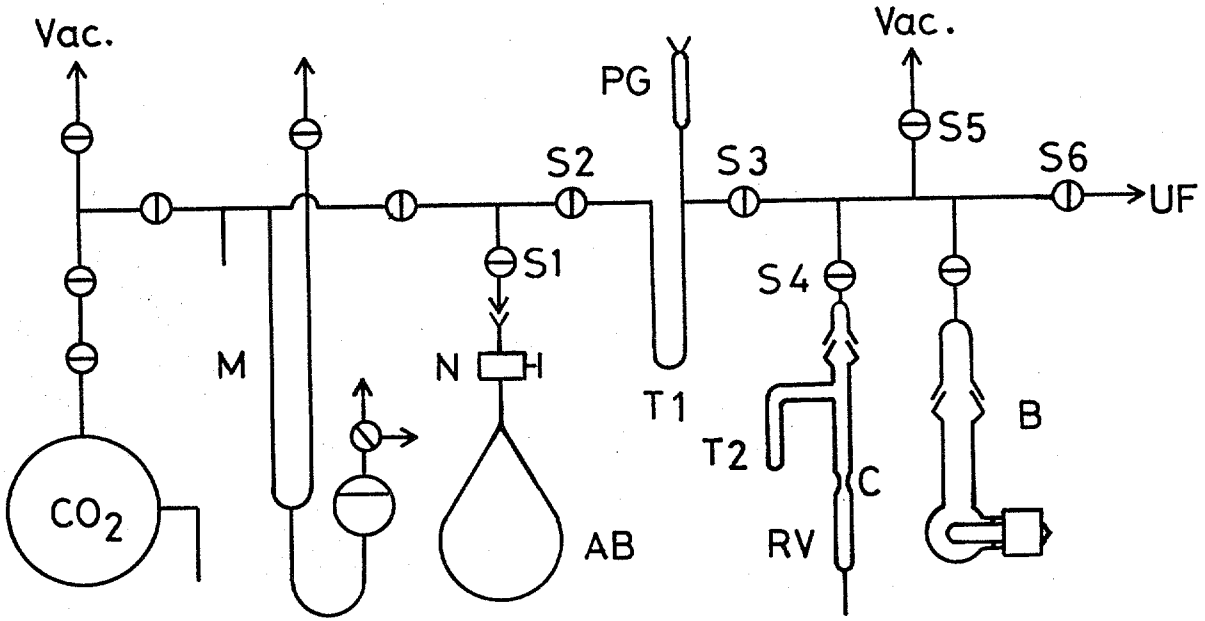

Fig.3-1

Vacuum line for the preparation of a small amount water sample: (M) constant volume mercury manometer; (N) needle valve; (AB) air bag; (PG) Pirani gauge sensor; (RV) Pyrex glass tube for the container; (C) constriction; (B) breaker for a container and a glass capillary; (UF) uranium furnace for the reduction of water to H_2 gas.

and monitor the flow rate of the air by the pressure reading of a Pirani gauge (PG). Then, the amount of water sample collected in T-1 was strictly proportional to the duration of pumping. Under the particular condition of this experiment, 11 μmol of water was collected per one minute when the pressure at PG was 4 torr. An aliquot of air moisture and the carbon dioxide contained in the air were condensed into trap-1 after a desired time of pumping. The condensate was repeatedly processed by the procedures described below.

If a significant isotope fractionation had taken place between the moisture in the air bag and that flowing out from the bag, the isotope ratio of A series samples would change systematically. Such a systematic change was not observed for the $\delta^{18}O$ value as will be shown later. The isotope ratios of A series water samples ,however, may not show the true value of the moisture in the collected air, because a part of the moisture may be adsorbed on the inner surface of the air bag and the trapping efficiency of moisture at trap-1 may not be 100 %. Even if the isotope ratios of the trapped water is different from the original value of the moisture, the constancy in the isotope ratios of each aliquot of the trapped water (see below) is important for the purpose of the preparation of small quantities of water samples with constant isotope ratios.

The CO_2 gas in trap-1 trapped with water was removed by changing the coolant to acetone slush, and the water remained was transferred into trap-2. A complete recovery of the adsorbed water on the inner wall of trap-1 was assured by gentle heating trap-1. Purified CO_2 gas from a tank was introduced into trap-2 and stopcock-4 was closed. The amount of the introduced CO_2 gas was measured manometrically in advance within an accuracy of 1%.

A part of the container (RV) below the constriction (C) was immersed into liquid nitrogen up to the middle, and the H_2O and CO_2 in trap-2 were transferred to the lower half of RV, and the glass tube was sealed off at C by the sharp flame of a hand torch. The outer and inner diameters of RV made of Pyrex glass were 3 mm and 1.7 mm, respectively. The inside of the tube had been cleaned with the chromic acid mixture. During the sealing, the lower half of RV was kept immersed in liquid nitrogen. The sealed container was kept at 25.0℃ in a thermostat over five days.

The advantages of this greasless container is that gas leakage, contamination and memory effect due to greased stopcocks do not practically exist. The container was about 30 mm long to make the inner pressure to be about 1 atm for 3-4 μmol of CO_2 used in this experiment. A small volume is desirable for the container, because the rate of exchange reaction increases with increasing CO_2 pressure and because amount of water vapor relative to that of liquid water reduces.

The oxygen isotope exchange reaction between water and CO_2 proceeded to 50% equilibrium in 9 hours when 6 and 4 μmol of H_2O and CO_2 , respectively, were used. After equilibration, the container was broken in a breaker (B) to recover water and CO_2 . The CO_2 was separated from water, transferred into a reservoir, and subjected to the $\delta^{18}O$ measurement on a VG-Micromass 602C. The $\delta^{18}O$ of the water was calculated in consideration of the mass balance between CO_2 and water. The details for the calculation were the same as that in Kishima and Sakai(1980). A value of 1.04120 (Gonfiantini,1984) was used for the oxygen isotope fractionation factor between CO_2 and water at 25℃.

The water remained in trap-2 was reduced to H_2 gas by metallic uranium in furnace (UF) at 700℃ (Bigeleisen et al.,1952). The

H_2 gas was collected by a Toepler pump, and the amount of the H_2 gas was measured manometrically within an accuracy of 1 %, which is necessary for the material balance calculation mentioned above. The D/H ratio was measured on a Hitachi mass spectrometer, type D2MS.

Series B samples, distilled Tokyo tap water, were subjected to the cross-check between the $\delta^{18}O$ values obtained by the present technique and that by the method of Yoshida and Mizutani(1986). For the measurement of the $\delta^{18}O$ by the present technique, 43～70 μmol of water, designated as B-1 in Table 1, was introduced into the vacuum line (Fig.1) by breaking a Pyrex glass capillary tube containing the water, whose both ends were sealed with epoxy resin. This method was not successful for 5-6 μmol of water samples, i.e., the measured $\delta^{18}O$ of samples were not reproducible. However, it was successful for samples of 43 μmol or more. The subsequent procedure was the same as described before. The $\delta^{18}O$ value of series B water was measured for a large amount of water sample (0.11mol) and by the method of Yoshida and Mizutani(1986). The result is given as B-2, in Table 3-1.

< 3-4 > Results and discussion

Figure 3-2 shows the analytical results on $\delta^{18}O$ for A series. A reasonable reproducibility are found among 15 samples with different sample sizes. The results of $\delta^{18}O$ analyses of A and B series samples are listed in Talbe 3-1. The $\delta^{18}O$ values of B-1 and B-2 agree well with each other, which indicates that the accuracy of B-1 is satisfactory. This in turn implies that the results on A series have an accuracy similar to that of B-1, because A series contains some components with a sample size similar to that of B-1.

As shown in Figure 3-2 and Table 3-1, a water sample with several micro moles can be handled by the present technique for $\delta^{18}O$ measurement within a precision of $0.42‰(1\sigma_{n-1})$, and for a sample with amount more than 43μmol within $0.16‰(1\sigma_{n-1})$. The standard deviation for A series is inferior to that of B-1, which seems to reflect a possible fluctuation in the preparation of A series samples.

Figure 3-3 shows the results of δD measurements for A series samples versus amount of water used. The δD values diverge in the lower amount range, in contrast to the constancy of $\delta^{18}O$ over the entire range. This suggests that the scatter in δD values certainly arises from the reduction process of sample water into H_2 gas by hot uranium. It is seen in Fig.3-2 that the δD measurement with a good precision needs at least 40μmol of water. The minimum amount of water may depend on the amount of uranium and/or uranium oxide in the reduction furnace. The average δD of A series (Tokyo air moisture) was -118.3‰, excluding the samples less than 40μmol, and the standard deviation ($1\sigma_{n-1}$) was 0.4‰ (n=5). Of course, a water sample larger than 70μmol can be handled by the present technique, using containers of correspondingly larger volumes.

[30]

Table 3-1. Measurements of $\delta^{18}O$ of A and B series water samples

sample	amount of water (μ mol)	number of preparations	averaged $\delta^{18}O_{(SMOW)}$ (‰)	standard deviation ($1\sigma_{n-1}$)
A	5～51	15	−16.77	0.42
B-1	43～70	5	−11.53	0.16
B-2[a]	1.1×10^5	6	−11.55	0.13

[a] Measurement by the method of Yoshida and Mizutani (1986).

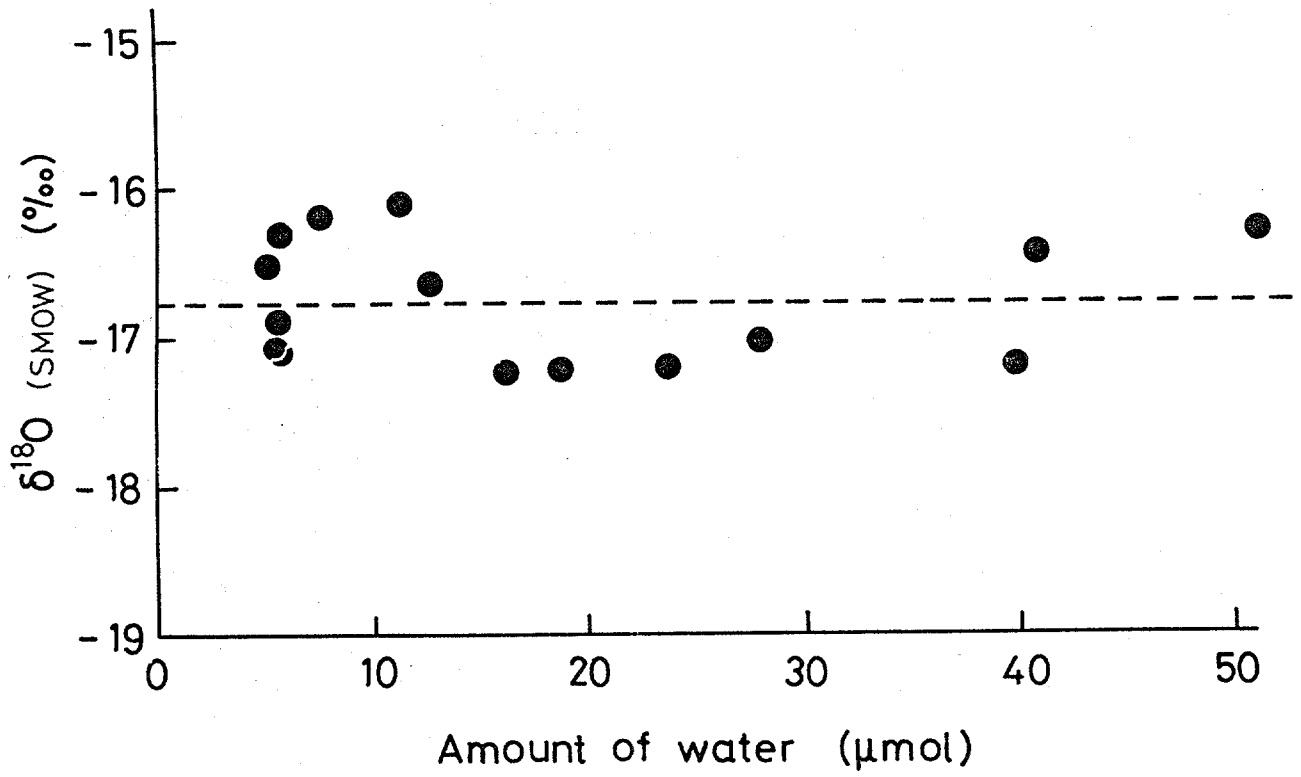

Fig.3-2

Relationship between the $\delta^{18}O$ value and the water amounts of the A series. Broken line represents the averaged $\delta^{18}O$ values.

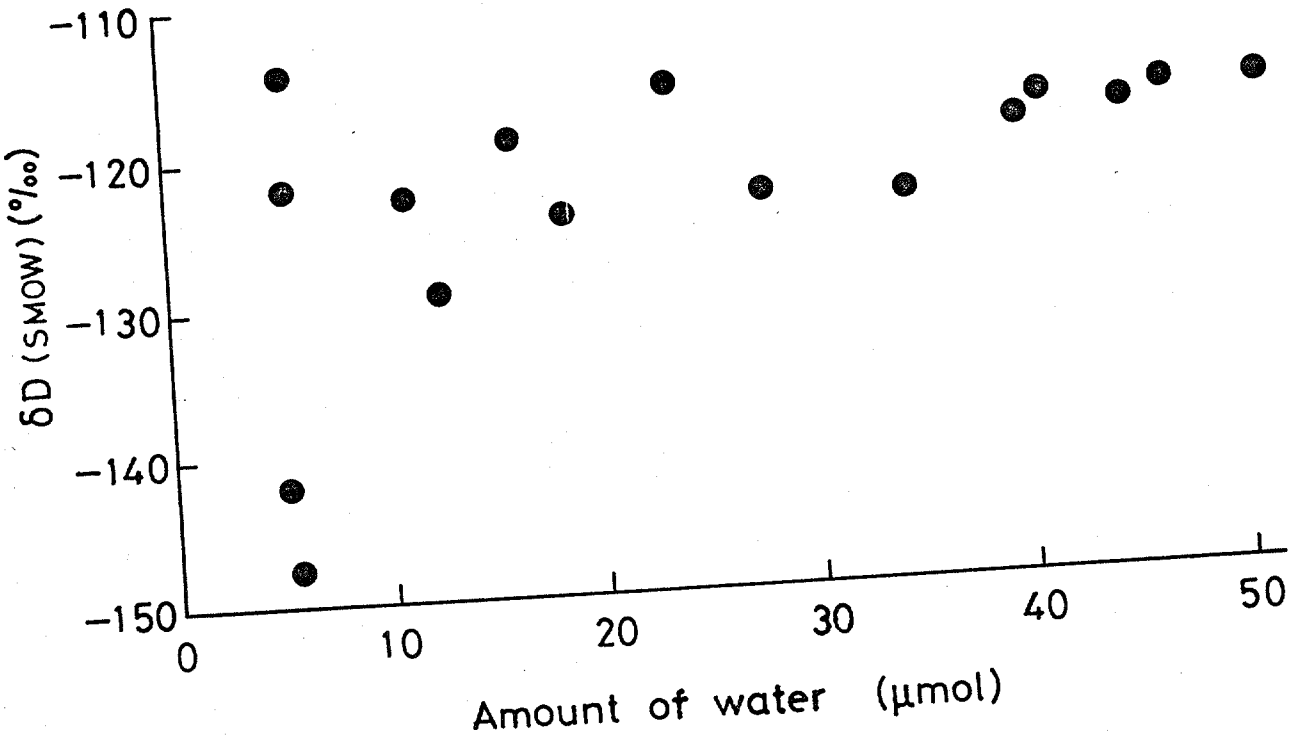

Fig.3-3

Relationship between the δD value and the water amounts of the A series.

< 3-5 >

Conclusions

δD and $\delta^{18}O$ of water prepared from an air moisture were measured simultaneously by the micro CO_2-water equilibration technique, in which a Pyrex glass container was used instead of a conventional container with a greased stopcock. A reproducibility of 0.42 ‰($1\sigma_{n-1}$) for $\delta^{18}O$ was obtained using 5-51 μmol of water. For δD, 0.4‰($1\sigma_{n-1}$) was obtained using 40-51 μmol of water, however, using the water lower than 40 μmol, δD did not show a fixed value.

The results of δD measurement on water samples smaller than 40 μmol seems to be due to the reduction process of water by the uranium furnace, because the isotope ratios were disturbed in a process after breaking the container.

References

Bigeleisen,J., Perlman,M.L. and Prosser,H.C.(1952).
Conversion of hydrogenic materials to hydrogen for isotopic analysis.
Anal.Chem. 24, 1356-1357.

Gonfiantini,R.(1978).
Standards for stable isotope measurements in natural compounds.
Nature 271, 534-536.

Gonfiantini,R.(1984).
Advisory group meeting on stable isotope reference samples for geochemical and hydrological investigations. IAEA, Vienna (1983).

Kishima,N. and Sakai,H.(1980).
Oxygen-18 and deuterium determination on a single water sample of a few milligrams.
Anal. Chem. 52, 356-358.

Suzuoki,T. and Itoh,T.(1974).
A method of oxygen isotope analysis of milligram quantities of water using CO_2-H_2O equilibration.
Mass Spectrosc. 22, 135-141.

Yoshida,N. and Mizutani,Y.(1986).
Preparation of carbon dioxide for oxygen-18 determination of water by use of a plastic syringe.
Anal.Chem. 58, 1273-1275.

Appendix－ I

The following partial differential equations is solved using the Laplace transformation

$$\frac{\partial C}{\partial t} = D(T)\left[\frac{\partial^2 C}{\partial r^2} + \frac{2}{r}\times\frac{\partial C}{\partial r}\right] \qquad \begin{matrix} t>0 \\ a<r<\gamma a \end{matrix} \qquad (1)$$

$$4\pi a^2 Dq D(T)\frac{\partial C}{\partial r} = (4/3)\pi a^3 \beta_{ru} Dw \left[\frac{\partial W}{\partial t}\right] \qquad \begin{matrix} t>0 \\ r=a \end{matrix} \qquad (2)$$

$$\frac{\partial C}{\partial r} = 0 \qquad \begin{matrix} t\geqq 0 \\ r=\gamma a \end{matrix} \qquad (3)$$

$$C = Co \times \frac{\alpha(Tn)}{\alpha(To)} \qquad \begin{matrix} t=0 \\ r=a \end{matrix} \qquad (4)$$

$$C = Co \qquad \begin{matrix} t=0 \\ a<r\leqq\gamma a \end{matrix} \qquad (5)$$

where C: $^{18}O/(^{16}O+^{18}O)$ of the oxygen atoms in the quartz neglecting the precence of ^{17}O,
r: the distance from the center of the fluid inclusion,
t: the time elapsing from the start of the cooling,
Dw: the number of oxygen atoms in a unit volume of the water,
Dq: the number of oxygen atoms in a unit volume of the quartz,
D(T): the self diffusion coefficient of the oxygen atoms in the quartz at temperature T(K),
β_{ru}: the filling rate of the fluid inclusions, $0<\beta_{ru}\leqq 1$,
a: the radius of the fluid inclusions,
γa: the radius of the surrounding quartz,
$\alpha(T)$: the oxygen isotope fractionation factor between quartz and water at T °K,
Ti: the temperature of the system before the start of the cooling,
Tf: the temperature of the system after the system have cooled down,
W(t): the $^{18}O/(^{16}O+^{18}O)$ ratio of inclusion water, $W = C/\alpha(Tf)$.

In order to eliminate the dimensions in the equations (1)-(5), the following variables and a functions are introduced.

$$x=(r-a)/a \quad (6), \qquad \tau = D(Tn)t/a^2 \quad (7)$$

$$F(x,\tau) = (r/a)[\{C(r,t)/Co\} - 1]/[\{\alpha(Tf)/\alpha(Ti) - 1] \qquad (8)$$

Using (6)-(8), (1)-(5) are transformed into,

$$\frac{\partial F}{\partial \tau} = \frac{\partial^2 F}{\partial x^2} \qquad \begin{matrix} \tau>0 \\ 0<x<\gamma-1 \end{matrix} \qquad (9)$$

$$\frac{\beta\,\partial F}{\partial \tau} - \frac{\partial F}{\partial x} + F = 0 \qquad \begin{matrix} \tau>0 \\ x=0 \end{matrix} \qquad (10)$$

$$\frac{\partial F}{\partial x} - \frac{F}{\gamma} = 0 \qquad \begin{matrix} \tau\geqq 0 \\ x=\gamma-1 \end{matrix} \qquad (11)$$

$$F = 1 \qquad \tau = 0,\ x = 0 \qquad (12)$$

$$F = 0 \qquad \tau = 0,\ 0 < x \leqq \gamma - 1 \qquad (13)$$

where $\beta = \beta_{ru} Dw / [\, 3Dq\, \alpha\, (Tn)\,]$ (14).

The Laplace transformation are applied to the eqations (9)-(13). The following expressions are defined.

$$\mathfrak{L}\,[F\,] = f(s) = \int_0^{\infty} F(x,\tau)\, \exp(-s\tau)\, d\tau \qquad (16)$$

$$\frac{\partial f}{\partial t} = f_t\ ,\ \frac{\partial^2 f}{\partial x^2} = f_{xx},\quad \frac{\partial f}{\partial x} = f_x \qquad (17)$$

(9) is transformed to,

$$sf(x,s) - F(x,0) - f_{xx}(x,s) = 0$$

$$sf(x,s) - f_{xx}(x,s) = 0 \quad (\because F(x,0) = 0) \qquad (18).$$

(10) is transformed to,

$$\beta\, \{sf(0,s) - F(0,0)\} - f_x\,(0,s) + f(0,s) = 0$$

$$\{\, s\beta + 1\,\}\, f(0,s) - f_x\,(0,s) - \beta = 0 \quad (\because F(0,0) = 0) \qquad (19).$$

(11) is transformed to,

$$f_x\,(\gamma - 1, s) - f(\gamma - 1, s)/\gamma = 0 \qquad (20).$$

The fundamental solution for equation (18) is,

$$f(x,s) = K_1 \exp(\sqrt{s}\, x) + K_2 \exp(-\sqrt{s}\, x) \qquad (21)$$

where K_1 and K_2 are constants.

at $x = 0$, (21) is,

$$f(0,s) = K_1 + K_2 \qquad (22).$$

(21) is differentiated with respect to x,

$$f_x\,(x,s) = K_1 \sqrt{s} \exp(\sqrt{s}\, x) - K_2 \sqrt{s} \exp(-\sqrt{s}\, x) \qquad (23).$$

at $x = 0$, (23) is,

$$f_x\,(0,s) = K_1 \sqrt{s} - K_2 \sqrt{s} \qquad (24).$$

(23) and (24) are substituted into (19).

$$\{ s\beta + 1 \} (K_1 + K_2) - (K_1 \sqrt{s} - K_2 \sqrt{s}) - \beta = 0 .$$

The above equation is changed to,

$$\{ s\beta + 1 - \sqrt{s} \} K_1 + \{ s\beta + 1 + \sqrt{s} \} K_2 - \beta = 0 \quad (25).$$

At $x = \gamma - 1$, (21) is,

$$f(\gamma - 1, s) = K_1 \exp \{\sqrt{s} (\gamma - 1)\} + K_2 \exp \{-\sqrt{s} (\gamma - 1)\} \quad (26).$$

At $x = \gamma - 1$, (23) is,

$$f_x (\gamma - 1, s) = K_1 \sqrt{s} \exp \{\sqrt{s} (\gamma - 1)\} - K_2 \sqrt{s} \exp \{-\sqrt{s} (\gamma - 1)\} \quad (27).$$

(26) and (27) are substituted into (20),

$$K_1 (\gamma \sqrt{s} - 1) \exp \{\sqrt{s} (\gamma - 1)\} + K_2 (-\gamma \sqrt{s} - 1) \exp \{-\sqrt{s} (\gamma - 1)\} = 0 \quad (28)$$

A simultaneous equation on the two unknown, i.e., K_1 and K_2 is made of (26) and (28),

$$\begin{bmatrix} A & B \\ C & D \end{bmatrix} \begin{bmatrix} K_1 \\ K_2 \end{bmatrix} = \begin{bmatrix} \beta \\ 0 \end{bmatrix} \quad (29)$$

where,

$$A = s\beta + 1 - \sqrt{s} \quad (30),$$

$$B = s\beta + 1 + \sqrt{s} \quad (31),$$

$$C = (\gamma \sqrt{s} - 1) \exp \{\sqrt{s} (\gamma - 1)\} \quad (32),$$

$$D = (-\gamma \sqrt{s} - 1) \exp \{-\sqrt{s} (\gamma - 1)\} \quad (33).$$

The solution of (29) is,

$$\begin{bmatrix} K_1 \\ K_2 \end{bmatrix} = \begin{bmatrix} \frac{D\beta}{AD - BC} \\ \frac{-C\beta}{AD - BC} \end{bmatrix} \quad (34).$$

For the the calculation of $AD - BC$, the following expressions are introduced,

$$A = a_1 - a_2 \qquad a_1 = s\beta + 1$$

$$B = a_1 + a_2 \qquad a_2 = \sqrt{s}$$

$$C = (b_1 + b_2) c_+ \qquad b_1 = -1 \qquad c_+ = \exp \{\sqrt{s} (\gamma - 1)\}$$

$$D = (b_1 - b_2) c_- \qquad b_2 = \gamma \sqrt{s} \qquad c_- = \exp \{-\sqrt{s} (\gamma - 1)\}$$

$$AD-BC=(a_1 b_1 + a_2 b_2)(c_- - c_+) - (a_1 b_2 + a_2 b_1)(c_- + c_+)$$

$$a_1 b_1 + a_2 b_2 = (\gamma - \beta)s - 1$$

$$a_1 b_2 + a_2 b_1 = \gamma \beta s\sqrt{s} + (\gamma - 1)\sqrt{s}$$

$$c_- - c_+ = -2\sinh\{\sqrt{s}(\gamma - 1)\}$$

$$c_- + c_+ = 2\cosh\{\sqrt{s}(\gamma - 1)\}$$

Then,

$$AD-BC=-2\{(\gamma - \beta)s - 1\}\sinh\{\sqrt{s}(\gamma - 1)\} - 2\{\gamma \beta s\sqrt{s} + (\gamma - 1)\sqrt{s}\}\cosh\{\sqrt{s}(\gamma - 1)\} = G(s) \quad (35)$$

(21) can be expressed as a function of s,

$$f(x,s) = K_1(s)\exp(\sqrt{s}\,x) + K_2(s)\exp(-\sqrt{s}\,x) \quad (36)$$

In order to obtain the $F(x, \tau)$ function, the inverse Laplace transformation is applied to (36).

In order to obtain the "résidu" of the function (36), points of essential singularity of the function are calculated.

$$AD-BC = 0 \quad (37)$$

$\sqrt{s} = iq$ ($i=\sqrt{-1}$, q is real and positive) is substituted into the equation (37),

$$-2\{-(\gamma - \beta)q^2 - 1\}\,i\sin\{q(\gamma - 1)\}$$

$$-2\{-\gamma \beta q^3 + (\gamma - 1)q\}\,i\cos\{q(\gamma - 1)\} = 0$$

is given.

Then,

$$\frac{\sin\{q(\gamma - 1)\}}{\cos\{q(\gamma - 1)\}} = \frac{-\gamma \beta q^3 + (\gamma - 1)q}{(\gamma - \beta)q^2 + 1}$$

$$\tan\{q(\gamma - 1)\} = \frac{-\gamma \beta q^3 + (\gamma - 1)q}{(\gamma - \beta)q^2 + 1} \quad (38).$$

The q value satisfying (38) is the points of essential singularity of the function (36).

$$f(x,s) = \frac{\beta}{G(s)}[(-\gamma\sqrt{s} - 1)\exp\{-\sqrt{s}(\gamma - 1)\}\exp(\sqrt{s}\,x) - (\gamma\sqrt{s} - 1)\exp\{\sqrt{s}(\gamma - 1)\}\exp(-\sqrt{s}\,x)]$$

$$f(x,s) = \beta \frac{H(s)}{G(s)}$$

where, $H(s) = (-\gamma\sqrt{s}-1)\exp\{-\sqrt{s}(\gamma-1)\}\exp(\sqrt{s}\,x) - (\gamma\sqrt{s}-1)\exp\{\sqrt{s}(\gamma-1)\}\exp(-\sqrt{s}\,x)$

$$H(s) = -2\gamma\sqrt{s}\cosh\{\sqrt{s}(x-\gamma+1)\} - 2\sinh\{\sqrt{s}(x-\gamma+1)\}$$

$$F(x,\tau) = \beta\,\mathcal{L}^{-1}\left[\frac{H(s)}{G(s)}\right]$$

where $\mathcal{L}$ is the operator of the Laplace transformation,

$$= \beta\sum \lim_{q\to q_n}\left[(q-q_n)\frac{H(q)}{G(q)}\exp(q\tau)\right]$$

$$= \beta\sum\left[\lim_{q\to q_n}\left\{\frac{(q-q_n)}{G(q)}\right\}\lim_{q\to q_n}\{H(q)\exp(q\tau)\}\right]$$

$$= \beta\sum\left[\lim_{q\to q_n}\frac{1}{G(p)^*}\lim_{q\to q_n}\{H(q)\exp(q\tau)\}\right] \qquad (39)$$

where, $G(q)^* = \frac{d}{dq}\{G(q)\}$

$$G(s)^* = \{-(1/s)-1+\beta-\gamma^2+\gamma-\beta(\gamma^2-\gamma)s\}\sinh\{\sqrt{s}(\gamma-1)\} + \{(\gamma-1)/\sqrt{s}-(\gamma-\beta)(\gamma-1)-(2\beta)s\sqrt{s}\}\cosh\{\sqrt{s}(\gamma-1)\} \qquad (40)$$

Substitute $s=-q_n^2$ and $s\sqrt{s}=-q_n^3 i$ into $H(s)$ and $G(s)^*$,

$$H(q_n) = -(2\gamma q_n i)\left[(1/\gamma)q_n^{-1}\sin\{q_n(x-\gamma+1)\} + \cos\{q_n(x-\gamma+1)\}\right] \qquad (41)$$

$$G(q_n)^* = (\gamma q_n i)\left[(1/\gamma)q_n^{-3} - \{(1/\gamma)+\gamma-1-\beta\gamma\}q_n^{-1} + (\gamma-1)\beta q_n\right]\sin\{q_n(\gamma-1)\} + (\gamma q_n i)\left[-\{(\gamma-1)/\gamma\}q_n^{-2} - (1-\beta\gamma)(\gamma-1) - 2\beta\right]\cos\{q_n(\gamma-1)\} \qquad (42)$$

Substitute (41) and (42) into (39),

$$F(x,\tau) = \beta\sum_{n=1}^{\infty}\frac{H(q_n)}{G(q_n)^*}\exp(-q_n^2\tau) \qquad (43),$$

is obtained.

$$F(x,\tau) = 2\beta \sum_{n=1}^{\infty} \left[\frac{q_n \sin\{q_n(x-\gamma+1)\} + \gamma q_n^2 \cos\{q_n(x-\gamma+1)\}}{A_n \sin\{q_n(\gamma-1)\} + B_n \cos\{q_n(\gamma-1)\}} \times \exp(-q_n^2 \tau) \right] + (x+1)3\beta / (\gamma^3 + 3\beta - 1) \quad (44)$$

Where q_n (n=1,2,3...) is the solution of the following equation.

$$\tan\{\sqrt{s}(\gamma-1)\} = \frac{(\gamma - 1 - \gamma\beta q_n^2) q_n}{1 + (\gamma - \beta) q_n^2} \quad (45)$$

A_n and B_n are,

$$A_n = -\beta\gamma(\gamma-1)q_n^3 + (\gamma^2 - \gamma + 1 - \beta)q_n \quad (46)$$

$$B_n = -\{\gamma^2 + (\beta-1)\gamma + \beta\} q_n^2 + (\gamma-1) \quad (47).$$

Appendix-2

Based on the discussion in Chapter-Ⅱ, the following material balance equations are put up,

$$\delta^{18}O_o \times Wt(2) = \delta^{18}O_m(2) \times Wm(2) + \delta^{18}O_{AW}(2) \times Ws(2) \quad (1),$$

and

$$\delta^{18}O_{WM}(2) \times Wt(2) = \delta^{18}O_m(2) \times Wm(2) + \delta^{18}O_{DW}(2) \times Ws(2) \quad (2),$$

where the notations are the same as those in Chapter-Ⅱ.

(2) is subtructed from (1), then,

$$\delta^{18}O_o \times Wt(2) - \delta^{18}O_{WM}(2) \times Wt(2) =$$

$$\delta^{18}O_{AW}(2) \times Ws(2) - \delta^{18}O_{DW}(2) \times Ws(2) \quad (3),$$

which is rearranged into,

$$\delta^{18}O_o =$$

$$\delta^{18}O_{WM}(2) + [\ \delta^{18}O_{AW}(2) - \delta^{18}O_{DW}(2)\ ] \times [Ws(2)/Wt(2)] \quad (4).$$

Here, a factor k_1 is introduced,

$$k_1 = [\ \delta^{18}O_{DW}(2) + 1000\ ]/[\ \delta^{18}O_{AW}(2) + 1000\ ], \quad (5).$$

(5) is transformed into,

$$\delta\,^{18}O_{AW}(2) - \delta\,^{18}O_{DW}(2) =$$

$$\delta\,^{18}O_{AW}(2)(\,1 - k_1\,) - 1000(\,k_1 - 1\,) \qquad (6).$$

Here, another factor k_2 is introduced,

$$k_2 = [\,\delta\,^{18}O_{AW}(2) + 1000\,]/[\,\delta\,^{18}O_{WM}(2) + 1000\,] \qquad (7),$$

(7) is transformed into,

$$\delta\,^{18}O_{AW}(2) = \delta\,^{18}O_{WM}(2)k_2 + 1000(\,k_2 - 1\,) \qquad (8).$$

(8) is substituted into (6),

$$\delta\,^{18}O_{AW}(2) - \delta\,^{18}O_{DW}(2) =$$

$$\delta\,^{18}O_{WM}(2)\,\alpha_2(\,1 - k_1\,) - 1000(\,k_1 - 1\,)k_2 \qquad (9),$$

(9) is substituted into (4), to obtain the relation between $\delta\,^{18}O_o$ and $\delta\,^{18}O_{WM}(2)$,

$$\delta\,^{18}O_o = \delta\,^{18}O_{WM}(2)\times[\,1 + k_2(\,1 - k_1\,)\{Ws(2)/Wt(2)\}\,]$$

$$+ 1000k_2(\,1 - k_1\,)\{Ws(2)/Wt(2)\} \qquad (10).$$

For the numerical values of k_1 and k_2 the results on the quartz sample Q-6 (in Table 2-2) is used, which are calculated as,

$$k_1 = (\,+1.4 + 1000\,)/(\,-19.9 + 1000\,) = 1.02173 \qquad (11),$$

$$k_2 = (-19.9 + 1000)/(-1.8 + 1000) = 0.98187 \qquad (12).$$

As seen in Table 2-2, Ws(1) do not depend on Wm(1), which suggests that Ws(1) is controlled by the adsorption-desorption process of water on the quartz surface.
Then it is assumed that Ws(2) is constant for the measured values of Kazahaya (1986) to be 22 μmol, where as Ws(1) in Table 2-3 is 17 μmol at most. The difference between Ws(2) and Ws(1) of 4.9 μmol for Q-6 sample (in Table 2-2) and the Ws(2) value mentined above are used.
Substituting above numerical values into (10),

$$\delta^{18}O_o = \delta^{18}O_{WM}(2) \times [\, 1 - \{0.469/Wt(2)\} \,] - 469/Wt(2) \qquad (13).$$

where the unit of Wt(2) is μmol.